Fall 2018

MEASUREMENT OF DYNAMIC PRESSURE GRADIENTS ON THE SURFACE OF SHORT CYLINDERS

Stephanie Gilooly
University of New Hampshire, Durham

MEASUREMENT OF DYNAMIC PRESSURE GRADIENTS ON THE SURFACE OF SHORT CYLINDERS

BY

STEPHANIE GILOOLY

BS, Mechanical Engineering, University of New Hampshire, 2016

THESIS

Submitted to the University of New Hampshire
in Partial Fulfillment of
the Requirements for the Degree of

Master of Science

in

Mechanical Engineering

September 2018

This thesis has been examined and approved in partial fulfillment of the requirements for the degree of Master of Science in Mechanical Engineering by:

Advisor, Dr. Diane Foster,
Professor of Mechanical Engineering
and Ocean Engineering

Dr. Thomas Lippmann,
Professor of Oceanography
and Ocean Engineering

Dr. Barry Fussell,
Professor of Mechanical Engineering

on 06/22/2018.

Original approval signatures are on file with the University of New Hampshire Graduate School.

ACKNOWLEDGMENTS

I would like to thank the Strategic Environmental Research and Development Program for funding this research. I would like to thank my adviser and my committee members for their guidance and encouragement. I'd also like to thank everyone who helped me with my research, including Kara Koetje, Meagan Wengrove, Jon Hunt, John Ahern, Paul Lavoie, Jim Irish, Todd Jones and the UNH Space Science Center, Sital Khatiwada, Corina Gudinas, Sam Lippmann, Ian Lander, and the rest of the UNH ME and OE graduate students. Finally, I'd like to thank my friends and family for all their support.

TABLE OF CONTENTS

LIST OF FIGURES

Figure **Page**

ABSTRACT

Measurement of Dynamic Pressure Gradients on the Surface of Short Cylinders

by

Stephanie Gilooly

University of New Hampshire, September, 2018

As a result of military testing and training around the United States, the property potentially containing military weapons in underwater environments exceeds 10 million acres. The weapons, called munitions, are difficult to locate, can move suddenly, and are a danger to marine life and the public. Before safe and cost-effective munition recovery efforts can be developed, a better understanding of their mobility in underwater environments is needed. Specifically, this research looks to resolve the role of dynamic pressure gradients surrounding the munition that can impact its position or orientation. To do so, a pressure-mapped model munition (PMM) has been designed, fabricated, and tested in laboratory and field settings. The PMM is an untethered instrument, containing all electronics necessary to retrieve, time, and store data. The PMM is capable of detecting and measuring surface pressure gradients and orientation and positional changes and uses an acoustic tracker for retrieval purposes after a deployment.

The surface pressure mapping was accomplished with an array of 16 small diaphragm pressure sensors. The instrument also contains an Inertial Measurement Unit (IMU) to record orientation changes. All data is stored to an on-board microSD card and recorded on the same time stamp. After wiring and constructing the PMM, the instrument was evaluated through several laboratory experiments to determine its accuracy in detecting hydrostatic pressure changes, orientation changes, passing waves, and environment changes, such as being submerged in a sand bed.

The diaphragm pressure sensors were sampled at 13 Hz with battery and disk storage of up to 3 days. Individual pressure sensors can experience drift up to 1 mbar/hour, which is the hydrostatic equivalent of 1 cm of water per hour, and showed offsets of up to 50 mbar, or 50 cm of hydrostatic pressure. The rolling experiment and the overnight drift experiment proved that a reference pressure sensor, in combination with the orientation data from the IMU on board the instrument, can

be used to recreate the steady state pressures. While the pressure sensors have an internal temperature measurement, a reference temperature sensor installed on the surface would allow for better characterization of the instrument's response to environment changes.

The pressure sensors accurately recorded changes in pressure due to hydrostatic changes and passing waves with a noise rms of only 0.25 mbar, or 2.5 mm of hydrostatic pressure. This result was promising for this research because the interest is in recording dynamic pressure gradients due to passing waves and local vortices. The instrument resolved wave motions as accurately as standard field instruments.

Horizontal pressure gradients across the PMM were in phase with the local acceleration as measured with an acoustic Doppler velocimeter as would be predicted by linear wave theory. However, the pressure gradients across the munition were larger than the local acceleration, providing evidence for the influence of vortex shedding. Additional evidence for vortex shedding was evident in the local deviations of pressure surrounding the munition during a passing wave. The observations show that during 100% exposure, the offshore face of the munition experiences a magnified signal as the crest passes, while the onshore side experiences a pressure deficit. Moreover, spectra of the PMM pressure observations showed significant energy at the first harmonic frequency that was not present in the nearby free stream pressure measured by the Vector. The largest KC value for the flow in the laboratory experiments was 3.1, meaning that, if the cylinder were in the freestream, there would be vortices shedding twice a wave period. However, comparisons with theory are challenging due to vortex growth limitations due to the percent exposure of the short cylinder.

The laboratory experiments have demonstrated the current PMM's capabilities to capture passing waves or vortex shedding schemes causing dynamic pressure gradients on the surface of the cylinder. To date, full scale laboratory and field conditions have been limited to wave environments that do not exceed the threshold for momentary liquefaction. Planned field studies will provide for observations in the higher energy conditions that can lead to significant positional state change of the short cylinder. This instrument will allow for quantitative measurements of vortices in controlled, laboratory experiments and in nearshore environments, improving the understanding of fluid around a cylinder.

CHAPTER 1

INTRODUCTION

1.1 Motivation

The Strategic Environmental Research and Development Program (SERDP) is part of the United States' Department of Defense (DOD) in partnership with the Department of Energy (DOE) and the Environmental Protection Agency (EPA). One of their areas of interest is to locate military weapons, called munitions, that have been lost in testing and training exercises since the 18^{th} century. As a result of this military testing and training, the property potentially containing munitions in underwater environments exceeds 10 million acres. Locating munitions is more complicated in dynamic, corrosive, underwater environments where current technologies are rather limited. There are over 400 active and former military installations that have tested munitions in water or near water environments, such as rivers or estuaries. These munitions vary in size and mainly consist of unexploded ordnance (UXO) and discarded military munitions (DMM). Unexploded munitions cause a threat to the public and marine life and must therefore be safely identified, removed, and detonated in a controlled manner. However, in dynamic underwater environments, access is more limited and it is difficult to characterize the motion of munitions. As a result, SERDP is funding projects relating to Wide Area Assessments, Detailed Surveys, Recovery and Disposal, Munitions Mobility, and Underwater Phenomenology [10]. This research at the University of New Hampshire (UNH) looks to contribute to knowledge on munition mobility in underwater environments.The forcus of this research is to understand the effects of dynamic pressure gradients, such as those created by passing wave fields and possibly vortices, on changes to the munition's position or orientation. These concepts will be further explained in the subsequent sections.

1.2 Linear Wave Theory

Linear wave theory describes the propagation of free surface gravity waves, assuming a homogeneous, incompressible, irrotational, inviscid fluid, a mostly-horizontal fixed bed, and a uniform atmospheric pressure at the free surface. Linear wave theory gives predictions for wave-induced velocity and pressure in the water column.

$$u(x,z,t) = \frac{HgT}{2L}\frac{cosh(2\pi(d+z)/L)}{cosh(2\pi d/L)}sin(\frac{2\pi x}{L} - \frac{2\pi t}{T}) \tag{1.1}$$

$$v(x,z,t) = \frac{HgT}{2L}\frac{sinh(2\pi(d+z)/L)}{cosh(2\pi d/L)}cos(\frac{2\pi x}{L} - \frac{2\pi t}{T}) \tag{1.2}$$

$$P(x,z,t) = \rho g\eta\frac{cosh(2\pi(d+z)/L)}{cosh(2\pi d/L)} \tag{1.3}$$

where

$$\eta(x,z,t) = \frac{H}{2}cos(\frac{2\pi x}{L} - \frac{2\pi t}{T}) \tag{1.4}$$

Above, u and v are horizontal and vertical velocities, respectively, H is the wave height, g is the gravitational constant, T is the wave period, L is the wavelength, d is the depth of the water, and η is the surface elevation [14]. According to these equations, wave-induced velocity and pressure are attenuated deeper in the water column. These three equations are true for any wave condition, although if the wave has certain characteristics, simplifications can be made. A wave is considered to be traveling in deep water if $h/L > 1/2$. In deep water, the wave-induced pressures and velocities are fully attenuated at half its wavelength below the free surface. On the other hand, the wave is shallow if $d/L < 1/20$.

Using linear wave theory, the orbital pressure magnitude, or the magnitude of equation 1.3, can be related to the standard deviation of the pressure signal,σ_p, by the following equation. The derivation of this equation can be found in the appendix.

$$\frac{P_o}{\rho g} = \frac{\sqrt{2}\sigma_p}{\rho g} = \frac{H}{2}\frac{cosh(2\pi(d+z)/L)}{cosh(2\pi d/L)} \tag{1.5}$$

This relationship is used in the experimental results to characterize the accuracy of the pressure sensors used on the instrument constructed. Overall, linear wave theory is useful in predicting what waves will impact the munitions on the seafloor. This research is focused on the nearshore environment so most waves will be in shallow water conditions, where the flow will impact the sediment bed and any munitions in the area.

1.3 Key Fluid Dynamics Concepts

Objects on or near the sediment bed in the nearshore will interact with the bottom boundary layer. A boundary layer is a region of a flow that is altered by the presence of another object or surface. The flow has to slow down at the fluid-object interface but is still going the same speed far away from the object, and this creates a region of velocity gradients between the surface and what is called the "freestream" environment, as seen in Figure 1.1a. The bottom boundary layer is the boundary layer created by the fluid interaction with the sediment bed and an additional boundary layer will develop on the munition if it is exposed to the fluid.

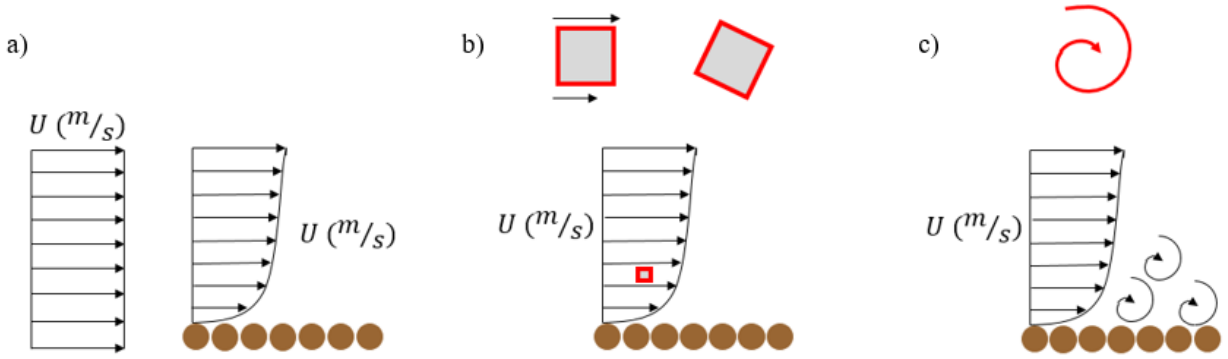

Figure 1.1: Concept sketch of a) a boundary layer, b) vorticity, and c) a vortex.

In boundary layers, fluid particles can have vorticity. Vorticity is the angular momentum of a fluid element. Visualizing a single water element in the boundary layer, it is clear that the velocity at the top of the element is faster than the velocity at the bottom, and this will cause the element to rotate. A vortex is an arrangement of several rotating fluid elements, that creates a pattern of angular motion. Vortices, discussed in detail in section 1.6, cause pressure gradients and can

spatially be on the order of the object inducing them. This research is interested in capturing the vortices created by the presence of the munition in the bottom boundary layer to relate their effects to the incipient motion of the object.

1.4 Incipient Motion

Even studying the mechanisms behind incipient motion of homogeneous sand grains under steady flow conditions can be challenging for researchers. In a coastal environment with oscillatory, steady, and turbulent flows acting on heterogeneous sediment beds, the mechanics are further complicated. Quasi-steady theories of incipient motion are paramaterized with the Shields parameter, θ, which represents the ratio between disruptive shear stresses trying to mobilize a single layer of grains and the stabilizing forces created by gravity and grain-to-grain interactions [11]. The shear stresses come from the bottom boundary layer of flow interacting with the sediment bed. The Shields parameter is given by equation 1.6,

$$\theta = \frac{\tau_b}{(\rho_s - \rho) g d_{50}} \tag{1.6}$$

where τ_b is the bed shear stress, ρ_s and ρ are the sediment and water densities respectively, g is the gravitational constant, and d_{50} is the length scale of the object of interest, meaning the median grain size diameter or the characteristic diameter of the munition.

In the case of motion on a munition, to determine if the shear stress can move the munition itself, the length scale would be the characteristic diameter of the munition. However, to determine if the sand in the surrounding sea bed is mobilized, the characteristic length scale should be the median grain size diameter. As the Shield's parameter increases for a particular system, the disruptive forces dominate the resistive forces, and motion begins. Critical values of Shield's parameter depend on bed state parameters [11]. Models and formulations for the burial and scour of munitions have generally shown good correlation to the Shields parameter based on either grain size and/or the munition's characteristic diameter. [9] Previous efforts have largely considered three mechanisms that impact munitions positional state: burial due to scour, bedform migration over

munitions, or mobility of "proud" munitions. In each of these cases, the characteristic length scale varies between the sediment grain size, the ripple height, or the munition's diameter, respectively. Previous methods have predicted munition burial due to scour and ripple migration well in deeper water but have had less success predicting the munition's state in the nearshore in depths less than 5 m.

In the nearshore region, the changes in munition positional state changes are further complicated by liquefaction. Liquefaction is when the bed becomes fluidized as a result of a strong pressure gradient with respect to the immersed weight of the sediment bed. Liquefaction can be generated by the buildup of pore-water pressure or by the upward vertical pressure gradient during the passage of a wave trough [14]. In 1990, Sleath parameterized the mobilization of a plug of sediment on the order of 100 sand grains due to pressure gradients with the equation:

$$S = \frac{-\frac{dP}{dx}}{(\rho_s - \rho)g} \tag{1.7}$$

where $\frac{dP}{dx}$ is the horizontal pressure gradient. Like the Shields parameter, the Sleath parameter is a ratio between disruptive forces and resistive forces and as the parameter increases, motion is more likely to occur [12]. Foster *et al.* (2006) found the first field evidence of bed fluidization and created a parameter, Υ, that combines the effects of shear stress and pressure gradients and predicts incipient motion as a function of bed state characteristics.

$$|\Upsilon| = |-\theta\frac{d_{50}}{h} - S| \geq KC_b \tag{1.8}$$

In equation 1.8, d_{50} is the median grain size diameter of the bed, h is the thickness of the sediment plug, K is the static coefficient of friction, and C_b is the packed bed concentration. [5] The effects of the Shields and Sleath parameters can work together to mobilize or stabilize the bed or can oppose one another, depending on the flow state, so it is important to consider the effects of the mechanisms on one another. Frank *et al.* (2015) characterized incipient motion of a single grain proud on a heterogeneous bed using acetate beads, gravel, and ping-pong-ball-like spheres

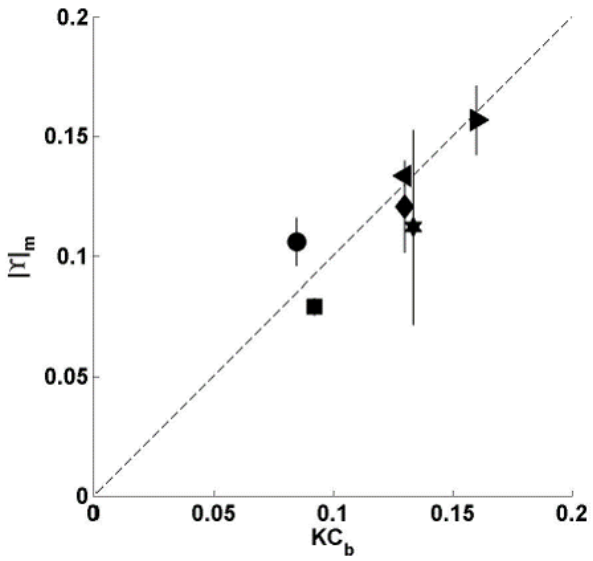

Figure 1.2: Incipient motion for acetate beads (circles), gravel (squares), and smart grains (other symbols) [6].

with good agreement, as seen in Figure 1.2 [6]. The long-term goal of the overarching project is to relate munition mobility to these incipient motion criteria used in sediment transport.

1.5 Scour

Scour is a process that occurs when the incipient motion criteria has been met for the sediment in the sea bed, and it defined as the "erosional and accretionary bedform patterns that occur in the vicinity of obstacles that are on or near a sediment bed" [7]. In simpler terms, scour is the sediment transport introduced to a system as a result of an obstacle interacting with the flow. Without the obstacle, the flow acting on the bed could already be active; this is called live bed scour. Clear bed scour describes a bed that is at rest in the absence of the obstacle. Once the obstacle is introduced, the flow will modify to meet its new boundary conditions and new flow patterns, such as vortices, are likely to form. The flow modifications will increase the bed shear stress and create new sediment transport patterns, which could be erosional or accretive. Local scour describes the effects of a structure on flow on a small scale. Global scour, on the other hand, is a result of a large obstacle or multiple objects. For example, local scour would occur if a single

pipe was in the flow, whereas global scour would occur if supports for an entire bridge were in the flow [7].

Naturally, munitions in the nearshore are objects introduced to the flow that cause scour on the bed. Vortices are generated as the flow passes over the munitions, creating disturbances immediately behind and downstream from the munition. Former studies have found that the presence of munitions can create scour pits into which munitions roll; this is one common method of munition burial [7, 9].

1.6 Vortices

While much is known about sediment transport, there is a great deal still unknown about incipient motion on larger objects, such as a munition. One area not currently considered is the effect of vortices. Vortices begin forming behind a cylinder as the Reynolds number, $Re = DU/\nu$, increases. In the previous equation, D is the diameter of the cylinder, U is the flow velocity, and ν is the kinematic viscosity of the fluid. The Reynolds number is a non-dimensional number commonly used in fluid dynamics to represent the ratio between inertial and viscous forces in a flow. Faster flows with larger spatial scales and lower viscosity will have higher Reynolds numbers. Higher Reynolds numbers indicate more turbulence present in a flow, while low Reynolds numbers could indicate laminar flow. If the flow is fully laminar, it flows in parallel layers with no mixing, so dynamic rotations like vortices would not be formed. There is a stagnation point in the front of the cylinder where the fluid comes to rest, and the other parallel layers are diverted around the cylinder. As the Reynolds number increases to $5 < Re < 40$, the flow begins to separate from the surface of the cylinder and steady vortices form to the rear of the cylinder. An instability is observed at $Re = 40$ and by $Re = 100$, the vortices shed off the cylinder in a periodic manner [15].

The vortices in a steady current away from a wall shed due to the following mechanism. A pair of unstable vortices will be formed at the rear of the cylinder; one will be larger than the other, one will be towards the top of the cylinder while the other is at the bottom, and they will be rotating in opposite directions from one another [15]. As the smaller vortex grows, it moves towards the

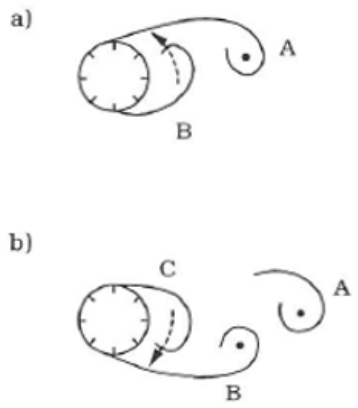

Figure 1.3: Example of vortex shedding: (a) vortex A is shed by development of vortex B, then (b) vortex C replaces vortex A on the top of the cylinder and will shed vortex B as it develops [15].

other vortex and cuts off further supply of vorticity to the larger vortex. The separated vortex is convected downstream from the flow. Then a smaller vortex forms in its place and the process repeats, now separating the originally small vortex and convecting it downstream. This concept can be seen in Figure 1.3 [15]. When $Re = 200$, three-dimensional instabilities develop. For high Re, such as $Re = 10^5$, a fully turbulent wake is obtained [3]. The development as a function of Reynolds number can be seen clearly in Figure 1.4.

So far, this summary of vortices has assumed the cylinder will be in a freestream environment under steady current. However, this research is interested in both steady and oscillatory flows, as both are present in nearshore environments. Flow surrounding a cylinder in oscillatory flow is also dominated by another non-dimensional number used to represent flow conditions: the Keulegan-Carpenter (KC) number, $KC = U_m T_w / D$. Here, U_m is the maximum velocity from the oscillatory flow and T_w is the period of the oscillatory flow. As described in Figure 1.4, vortices begin forming and turbulence increases as KC increases. Figure 1.4 represents flow with a constant Re; as expected, changes in Re directly impact the threshold KC values shown in the figure. There are also several shedding regimes that can occur based on KC. As KC increases, the flow develops from a single pair regime to a double pair regime. After the double pair regime, the number of

vortex pairs shedding in one full period increases by one each time the KC regime is increased. This is a result of the shedding frequency increasing proportionally with KC.

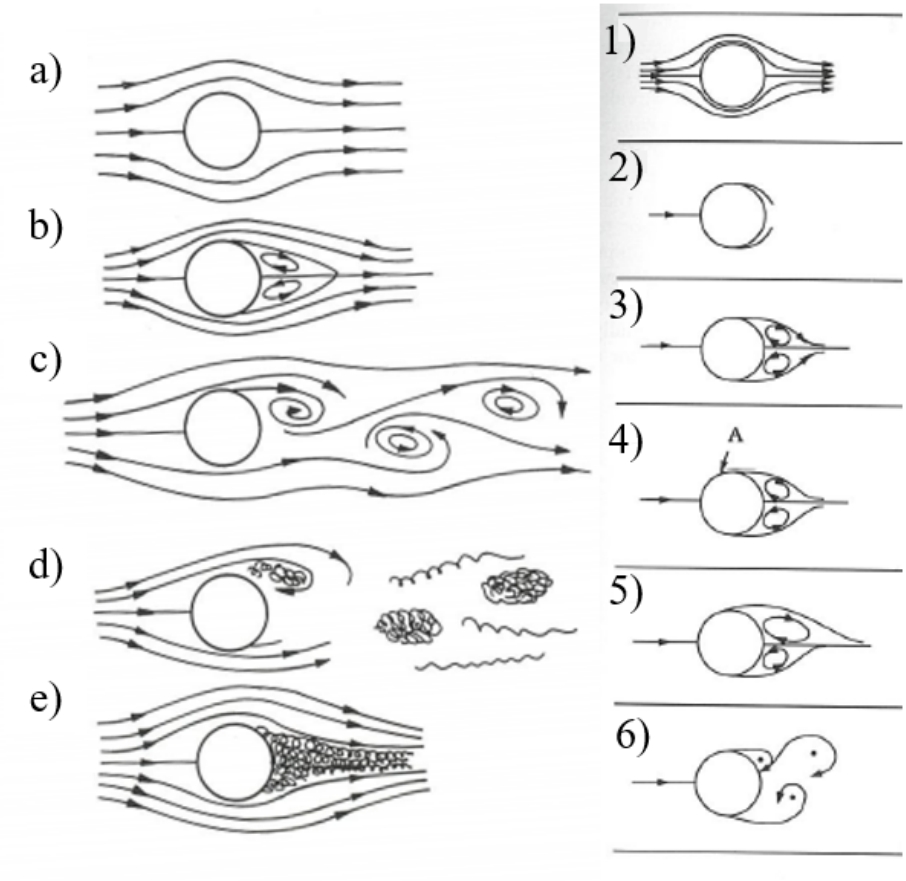

Figure 1.4: Flow developments with increasing a-e) Re or 1-6) KC: a) $Re < 1$, b) $5 < Re < 40$, c) $100 < Re < 200$, d) $Re \approx 10^4$, e) $Re \approx 10^6$ [3]. 1) $KC < 1.1$, 2) $1.1 < KC < 1.6$, 3) $1.6 < KC, < 2.1$, 4) $2.1 < KC < 4$, 5) $4 < KC < 7$, 6) $7 < KC$, all at constant $Re = 10^3$ [15]. Increasing KC and Re results in vortices and turbulence in the cylinder wake.

The effects of wall proximity on these flows must also be considered because the cylinder-like objects of interest in this research will be resting on or buried in the sediment bed. If a cylinder is placed on a bed under solely steady current, vortex shedding will be suppressed [1]. This is linked to the asymmetry in vortex development, since a vortex cannot be formed on the bottom of the cylinder and there is no interaction between vortices pairs to cause separation. A quantitative example of this is seen in Figure 1.5. However, since the cylinder in this example is only exposed

to steady flow, there are no oscillations and no vortex shedding so it cannot accurately predict pressure around the PMM in the field.

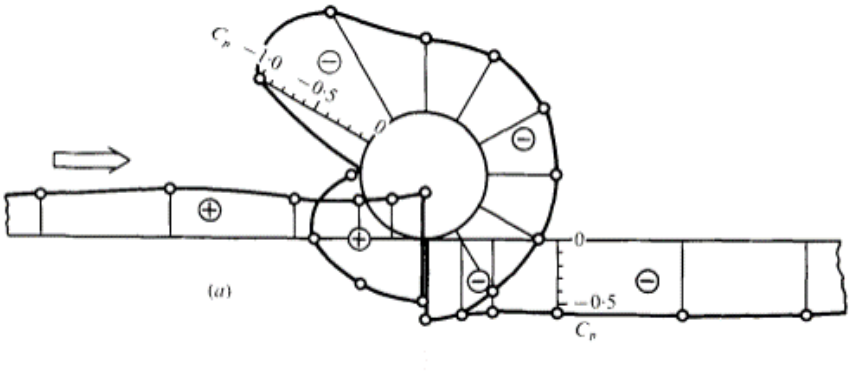

Figure 1.5: Pressure coeffients around a cylinder under steady flow for $Re = 4.5 * 10^4$. Pressure Coefficient is defined as $C_p = (p - p_o)/(\frac{1}{2}\rho U^2)$. [1].

In oscillatory flows, a vortex grows behind the cylinder each half-period, then is washed over the cylinder as the flow reverses [15]. These vortices are on the order of the diameter of the cylinder and include dynamic velocity and pressure gradients. Figure 1.6 shows clockwise and counterclockwise vortices forming on and shedding off a bottom-seeded cylinder during an experiment in a wave flume [13]. Currently, incipient motion criteria does not account for effects of vortices, and the long-term goal of this research is to resolve the role of these vortices and create a theoretical formulation including all potential forcings for incipient motion.

The Strouhal number, $St = f_v D/U$, relates the vortex shedding frequency, f_v, to the diameter of the cylinder and the passing velocity [15]. For a sensor to record a signal, the sensor must sample at least twice as fast as the maximum frequency in the signal. Therefore, using the diameter of the PMM and half of its sampling frequency, it can be calculated that the fastest velocities for which the PMM can resolve vortice signals is 4 m/s. This Strouhal number considers only a steady freestream current acting on a cylinder, so the complexities of steady and oscillatory flow in the nearshore and wall effects will complicate this prediction.

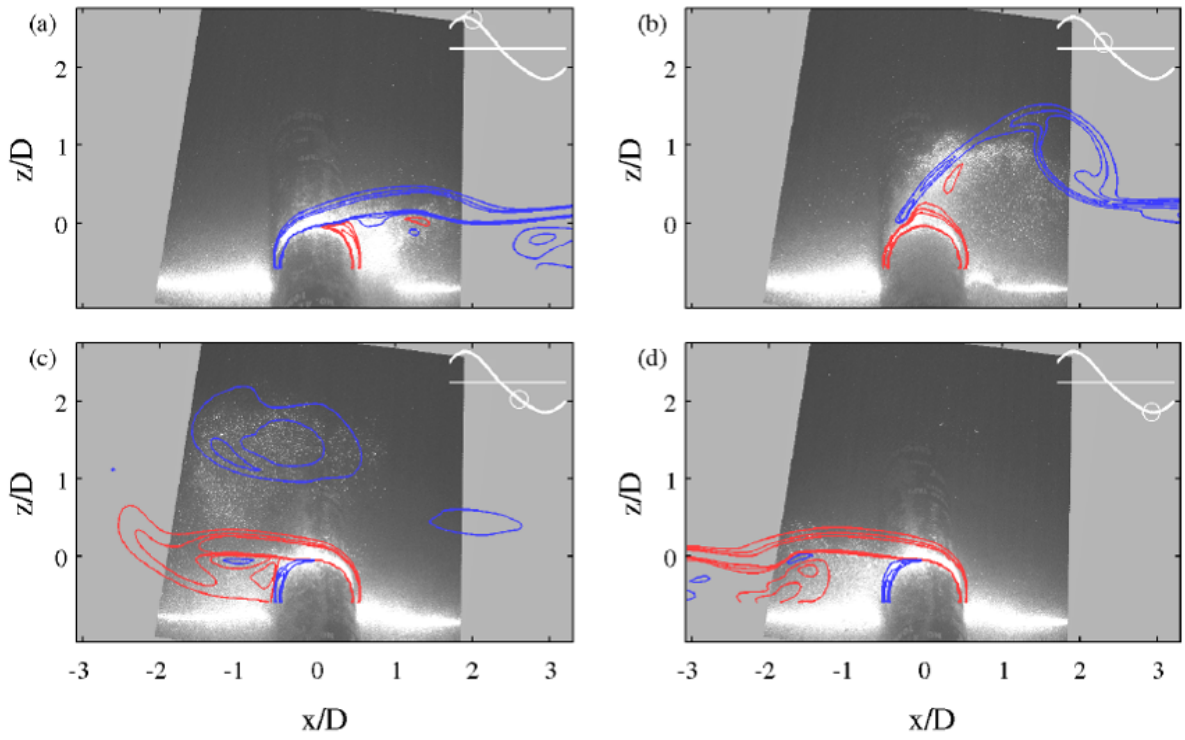

Figure 1.6: Coherent structures generated from oscillatory flow over a bottom-seeded short cylinder. Modeled y-plane vorticity contours are shown in red and blue overlaid on PIV images. Blue is negative (clockwise) vorticity and red is positive (counterclockwise) vorticity. (a-d) Phase of wave is shown in the upper right hand corner of each panel [13].

1.7 Objectives

The objectives of this work were to develop an instrument that can autonomously resolve the positional state change and surface pressure of munition-like objects. This involved evaluating pressure sensors for data reliability and ease of surface mounting, constructing a short cylinder instrument, and collecting data using the instrument to verify its accuracy and prove the concept of the Pressure-Mapped Munitions (PMMs). In future iterations of the project, fins and cones will be added to the short cylinder so it resembles a 155 mm munition.

The PMM cylinder must contain an Inertial Measurement Unit (IMU), which collects 3-axis accelerometer, gyroscope, and magnetometer data. The combined data can recreate the instantaneous angular position of the cylinder. The accelerometer data can be used to recreate an estimate

of the sensor's location as well, but accelerometers are very noisy and without an accompanying GPS signal for verification or correction, position tracking with an accelerometer is not accurate. The cylinder will be untethered when tested in the field, so it needs to internally house all the sensors, batteries, and data collection instruments it will need. The development of this instrument will allow for Eulerian and Lagrangian measurements of the flow field surrounding a munition during a positional state change, leading to a better understanding of the dynamics.

CHAPTER 2

PRESSURE SENSOR CHARACTERIZATION

2.1 Sensor Selection

Pressure sensors used to map the instrument's surface will be under pressures of 1500 mbar from hydrostatic pressure alone, considering they will be deployed in water up to 5 m deep. Additionally, dynamic pressure will be acting on the cylinder due to passing waves and vortex shedding. Ideally, drift should be minimized and the sensors should be able to accurately read steady-state pressures, but the most important attribute of these sensors is to accurately reflect changes in pressure. The two sensors considered for the pressure map were the FlexiForce sensors and the MS5837-30BA sensors, seen in Figure 2.1. The FlexiForce sensors are thin and flexible so they would be easy to wrap around the surface of the cylinder without impacting the flow. The sensing area, highlighted in Figure 2.1b, changes the sensor's resistance as a force is applied. The MS5837-30BA sensors are diaphragm pressure sensors. These sensors are small and other UNH projects have had success with them in the past but they would be harder to implement into the design [17, 16].

Figure 2.1: Considered pressure sensors: a) FlexiForce and MS5837-30BA diaphragm sensors, b) Closer image, highlighting sensing areas of both sensors.

A test apparatus was created to examine both sensors' response to changing hydrostatic pressure. The sensors are being evaluated against one another for data reliability and ease of installation. Figure 2.2 shows the test apparatus at different stages of its construction. Each sensor was placed flush to the surface of a case and held in place and waterproofed by epoxy and Scotchkote. The case contained an Arduino microcontroller, an SD card writer, and a 9 V battery to power the test apparatus. The case was then weighted so it would not float on the water surface. A rope was tied to the case handle, along with a measuring tape used to determine the depth of the case. The case was deployed in the UNH Engineering Tank in 0.3 m increments, and then was raised in the same manner. There was some human error due to the method used to deploy the pressure case and more accurate results could be attained using a traverse; however, the focus of this experiment was to compare the two sensors, which will undergo the same loading conditions regardless of the accuracy of the deployment depths.

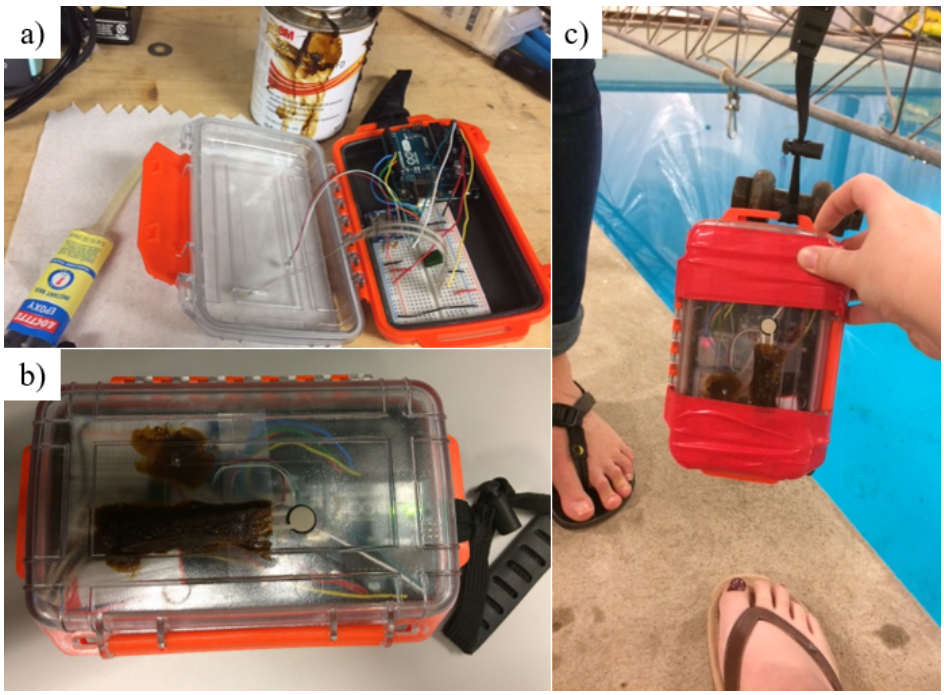

Figure 2.2: Pressure sensor test apparatus: a) sensors placed in case before epoxy and Scotchkote are added, b) case fully assembled, and c) case weighted and deployed.

The primary results are shown in Figure 2.3. The FlexiForce sensor is shown in blue and the diaphragm sensor is shown in red. The diaphragm sensor accurately reflects the pressure seen by the case, while the FlexiForce sensor severely underestimates the pressure forces even though it was calibrated in the air using scale weights. The calibration was then redone based on the ratio of maximum pressure measured by the diaphragm and FlexiForce sensors.

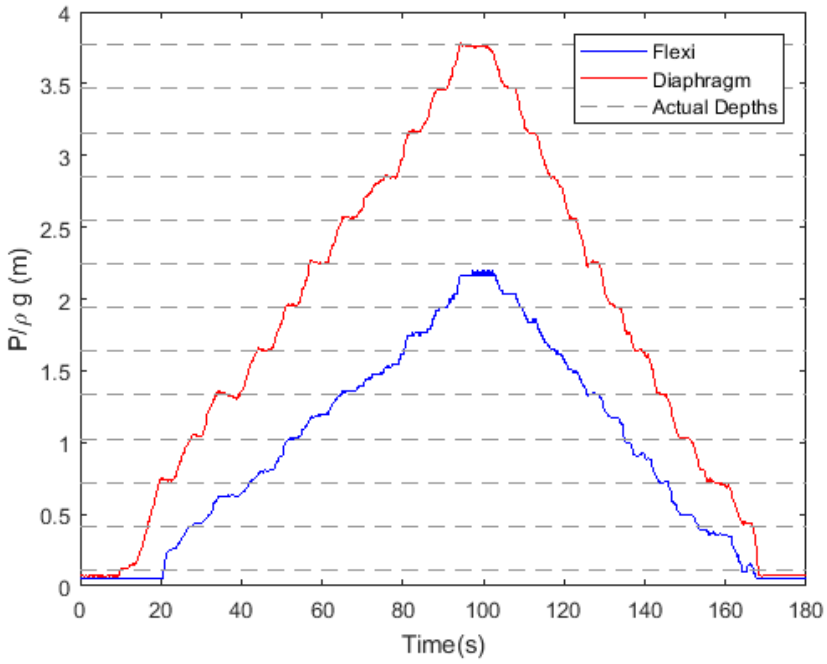

Figure 2.3: Preliminary pressure sensor deployment results. Equivalent hydrostatic pressure in meters is plotted versus time for both sensors (diaphragm sensor in red, FlexiForce sensor in blue). Grey dashed lines indicate the actual depths of the sensors in the experiment.

After re-calibration, the hysteresis in the FlexiForce data is more clear. Hysteresis is the dependence of an instrument on its history; for example, when the FlexiForce was under 1 m of hydrostatic pressure, it reported a different measurement during the descent than during the ascent [4]. The sensor is also sensitive to temperature changes and is most accurate under constant loading conditions [17]. The sensors would be experiencing dynamic loading conditions in the nearshore environment. Based on these results, only the diaphragm sensors were selected for this iteration of the project.

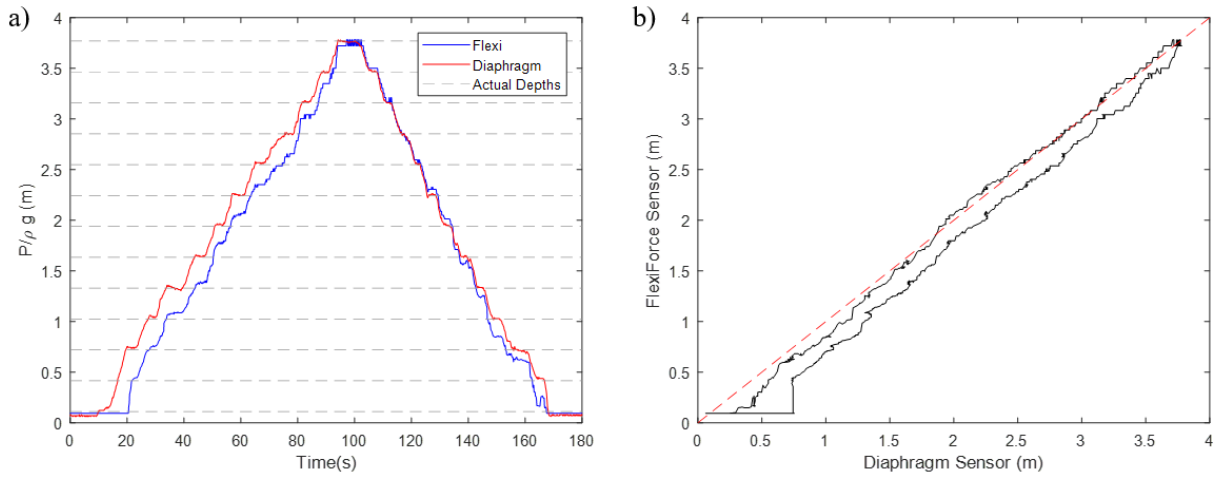

Figure 2.4: Calibrated pressure sensor deployment results. a) equivalent hydrostatic head in meters is plotted versus time for both sensors (diaphragm sensor in red, re-calibrated FlexiForce sensor in blue). Grey dashed lines indicate the actual depths of the sensors in the experiment. b) Hydrostatic calibrated FlexiForce data vs. hydrostatic diaphragm data. Red dashed line indicates the ideal relationship between the two sensors if they read the same pressures.

2.2 Preliminary Observations

To evaluate the hydrostatic response and drift of these sensors, an experiment was conducted using two of the sensors. The first sensor was potted at the bottom of a clear graduated cylinder, as seen in Figure 2.5. The second sensor was exposed to the air and was to be used as a reference sensor, measuring any atmospheric change. The experiment began with both sensors exposed to atmospheric conditions. Then water was added to the graduated cylinder to increase the hydrostatic pressure of the first sensor. Three increments of 200 mL of water were added to the graduated cylinder, each resulting in an additional 6.7 cm of water in the graduated cylinder. Pressure and temperature were recorded by both sensors at 8 Hz using an Arduino microcontroller and an SD card writer. The results can be seen in Figure 2.6.

The expectation for this data set was that the reference sensor would remain relatively constant, while the graduated cylinder sensor would begin at the reference temperature, then increase three times to a final hydrostatic pressure measurement of 0.2 m, and then remain constant. As seen in the

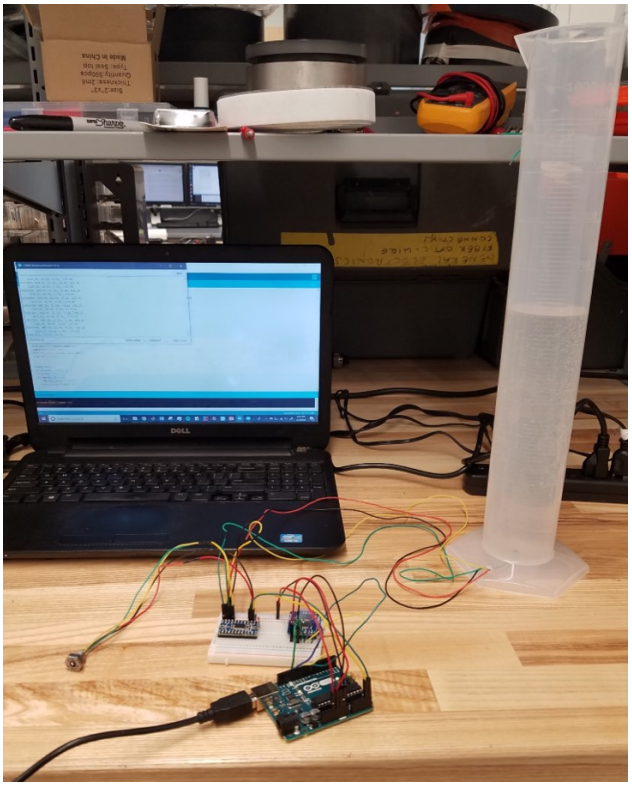

Figure 2.5: Experimental setup for graduated cylinder experiment. First sensor is potted in the center of the bottom of the graduated cylinder seen on the right. Second sensor, used as a reference, is seen to the left. Data was collected using an Arduino and SD card writer.

figure, the reference sensor's pressure reading was offset from atmospheric pressure and drifting throughout the experiment. The graduated cylinder sensor's pressure reading was slightly offset but performed well until it reached its steady-state pressure and then began to drift as well. The sensors and the water added to the graduated cylinder were room temperature and this was a relatively short experiment, so it seems unlikely that these drifts in pressure reflect the pressure in the room. To examine this further, the temperature readings from both sensors were also recorded. Again, there appears to be a great deal of offset and drift, especially in the reference sensor. According to the sensor's datasheet, the accuracy of the temperature readings is 4^{o}C and the root mean square is 0.0022^{o}C. Based on these results, the pressure sensor's temperature measurements were not considered reliable.

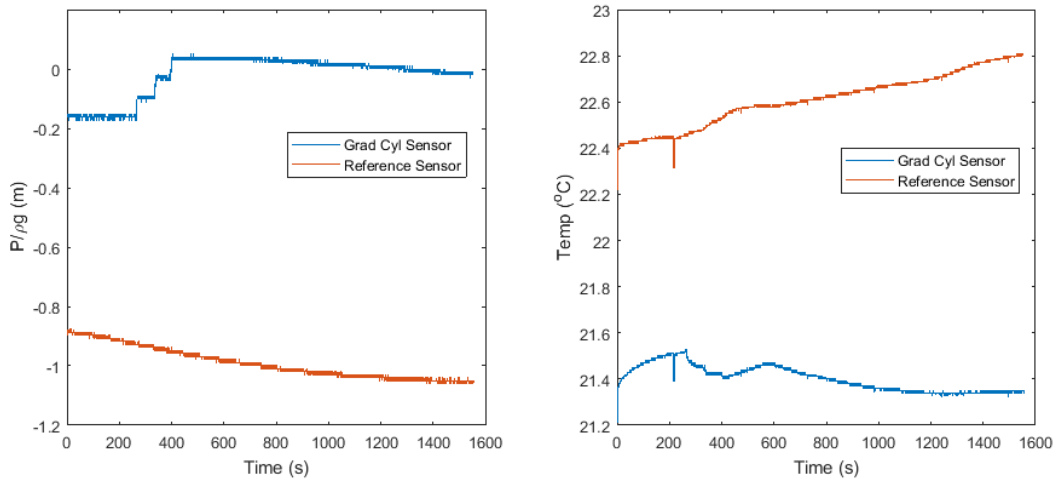

Figure 2.6: a) Pressure and b) temperature for sensors used in graduated cylinder experiment. Data from the graduated cylinder sensor is seen in blue and the atmospheric reference sensor data is seen in red. Pressure has been normalized by the density of water and the gravitational constant to give it units of length to better represent changes in hydrostatic pressure.

The reference sensor was supposed to record the temperature and pressure trends in the room during the graduated cylinder experiment so any drift would hopefully be accounted for. However, this does not appear to be the result of the experiment. Figure 2.7 shows graduated cylinder pressure first corrected by subtracting the drift estimated by the reference pressure sensor and then corrected by subtracting a constant atmospheric pressure, which removed its offset. It is clear that correcting the pressure signal only by removing its offset was the more accurate analysis. This means that the pressure sensors cannot use one another for calibration purposes.

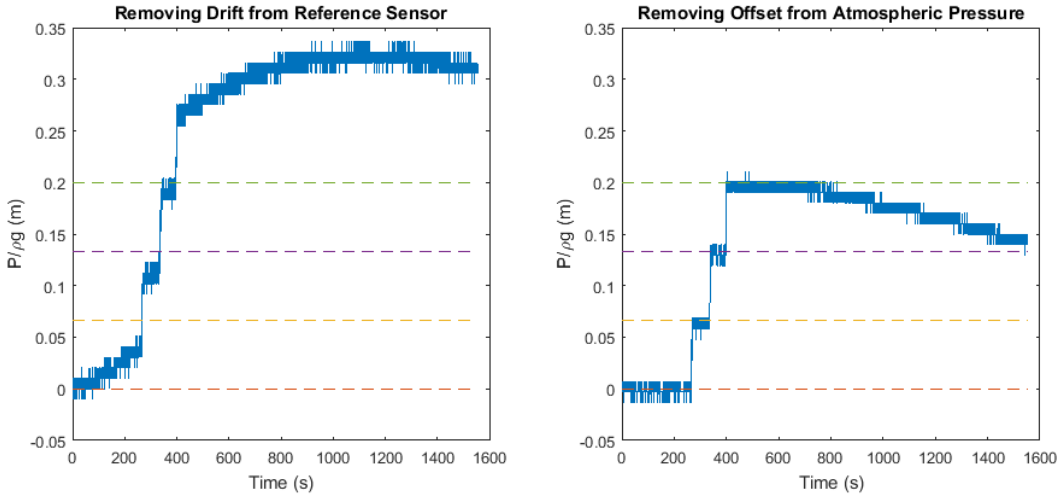

Figure 2.7: Graduated cylinder pressure corrected by a) reference pressure measurements and b) atmospheric pressure. The horizontal lines in both plots are the actual values of hydrostatic pressure the sensor underwent in the experiment.

CHAPTER 3

INSTRUMENT FABRICATION

The long-term goals of this project are to understand the role of dynamic pressure gradients on underwater munitions during their state changes, and to relate their mobility to incipient motion criteria currently used in sediment transport. The deployment of a pressure-mapped munition (PMM) with additional instruments should achieve the desired results. After choosing the appropriate pressure sensor, the base of the PMM needed to be designed and built to house all necessary electronics.

3.1 Pressure Sensor Implementation

As seen in Figure 2.1, the MS5837-30BA diaphragm sensors have a 3 mm diameter sensing area and the base of the sensor is 3 mm x 3 mm. The sensor has four 1.3 mm x 1.3 mm pads onto which wires needed to be soldered. Flexible silicone 30 AWG wires were used because they were small, sturdy, and flexible. Each wire used is color-coded: red is 3.3V power, black is ground, and green and yellow are the SCL and SDA connections needed for I^2C communication, discussed in Section 3.2. The UNH Space Science center's microscopic soldering station was used to solder the wires onto the back of the pressure sensors.

The sensing area of the diaphragm sensor needed to be flush to the surface of the PMM while simultaneously creating a waterproof seal and allowing its wires to connect to the other electronics inside the cylinder. Ideally, the sensors would be removable in case of malfunction. As a result, a custom hex head screw was designed. The 5/16"-18 thread, 1/2" long 304 Stainless Steel screw has a tapered hole through its center, allowing for the sensor's wires to access the center of the cylinder. The sensor is potted in the hole, making this part of the screw waterproof. A small area behind the screw's head was machined flat for an o-ring. The o-ring makes a piston seal with the

cylinder, making the entire screw waterproof. A socket and socket wrench are used to install each sensor securely and properly. The technical drawing of the hex screw can be seen in Appendix C.

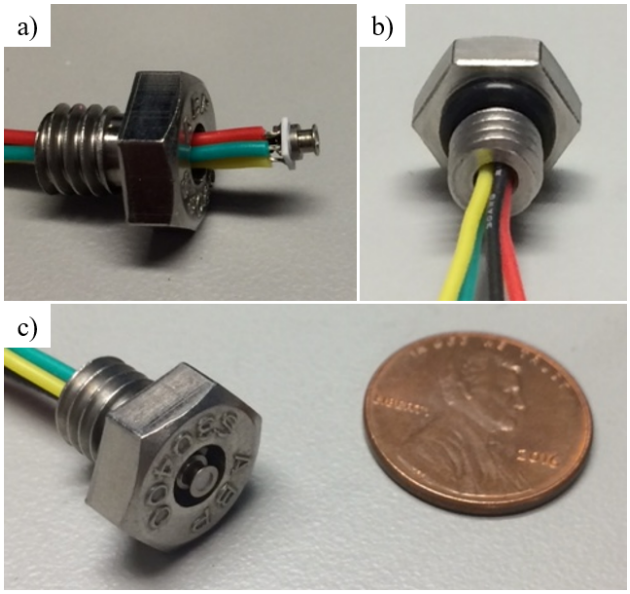

Figure 3.1: Pressure sensor and implementation screw: a) sensor's wires are threaded through the screw, as is done right before potting process, b) back of screw, showing the o-ring used to create a waterproof seal, and c) sensor with screw flush to surface next to a penny for a size reference.

The sensor was potted using Loctite EA E-60NC Epoxy, which has a low viscosity and a long hardening time. The low viscosity aloows the epoxy to settle in the small spaces around the sensor, making for a better waterproof seal. The sensing area was covered by a small, circular piece of electrical tape as a precaution during the potting process. The sensor's wires were fed through the screw, then the epoxy was added to the opening using small mixing nozzles, then the sensor was slowly lowered into its position, flush to the top of the hex head. Clay was used at the bottom of the screw while the potting hardened to ensure that the low viscosity epoxy did not flow out of the screw. The epoxy takes an entire day to fully harden.

3.2 Electronics

Since the PMM will be untethered while deployed, it must house all the technology necessary to retrieve and store data, to power itself, and to be recovered after the deployment. An Inertial

Measurement Unit (IMU) combines data from a 3-axis accelerometer, a 3-axis gyroscope, and a 3-axis magnetometer to measure orientation. This project uses a NGIMU from x-io Technologies, which is an IMU with a housing that also includes a real-time clock (RTC) and an microSD card writer. The SD card writer stores data onto an microSD card and the RTC ensures that all data recorded is on the same timestamp. The IMU alone cannot be used for position tracking due to the noise universally present in accelerometer data; however, the accelerometer data will note sudden accelerations, such as those due to incipient motion occuring.

As briefly mentioned previously, the MS5837-30BA pressure sensors use I^2C communication to collect data, convert the voltage signals to pressure measurements, and communicate them to a microcontroller. In I^2C communication, there is a "master," such as the microcontroller, that can communicate with at least one "slave," such as a pressure sensor, through a I^2C bus comprising of a Serial Clock line (SCL) and a Serial Data line (SDA). The master device can bi-directionally communicate with up to 127 different slave devices on the same two bus lines, so long as each sensor has a unique I^2C address. [2] The pressure sensors used in this project have one fixed I^2C address, so only one could be connected to the microcontroller at a time. This was addressed with a Texas Instruments TCA9548A multiplexer, which has a programmable I^2C address and allows the user to use up to eight I^2C sensors with the same address at a time. The microcontroller connects to the multiplexer, and the multiplexer can redirect it to one of its eight ports. Since the multiplexer has a programmable address, up to eight multiplexers at a time can be connected to the same I^2C bus lines. This means the project can use up to 64 pressure sensors. This iteration of the project uses two multiplexers to control 16 pressure sensors.

Figure 3.2 shows all the components mentioned above on the PMM's circuit board. Additionally, a green LED has been included so if the munition is unburied during the deployment, it will be very easy to locate. The LED is also an easy way to ensure the device is being powered properly. With all the electronics together, the entire electronic circuit requires 0.32 A of 3.3 V. This iteration of the project uses four 6000 mAh batteries, so the instrument can continuously collect

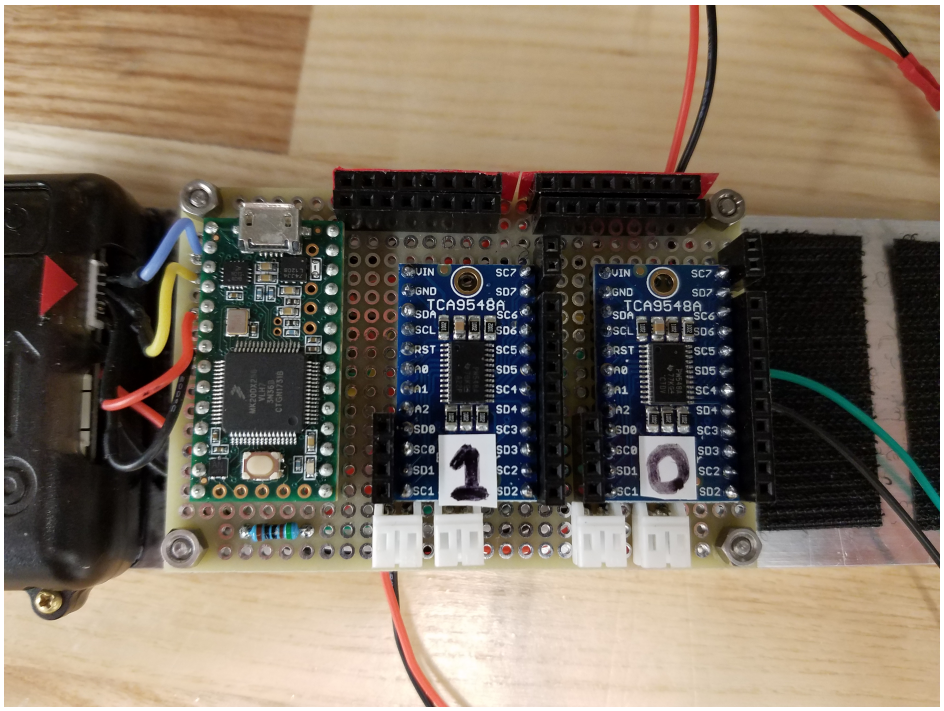

Figure 3.2: Final circuit board used in PMM. The black box on the left is the IMU, containing the RTC and SD card writer. The green component is the Teensy 3.2 microcontroller. The blue components are the multiplexers. The four white components are connectors for the batteries. The black components are ports for the wires from the 16 pressure sensors. The resistor seen below the microcontroller is in series with the green LED.

data for more than three days before the batteries need to be replaced. The data is being stored on a 200 GB microSD card, so the batteries die long before the microSD card runs out of storage.

After configuring all the electronics, it was discovered that the sampling frequency was 1.2 Hz, which is too slow to accurately measure wave motions, never mind dynamic pressure gradients. Each sensor needs to be initialized at least once so the calibration constants can be used to create accurate pressure readings, then each time a new reading is wanted, the microcontroller must ask for information and wait 20 ms for a response twice before using the requested data and the calibration constants to calculate the pressure. The original code would initialize a sensor, request and wait for the two sets of information, calculate the pressure reading, then move to the next sensor. This is why measuring the pressure from all 16 pressure sensors took a long time and lowered the sampling frequency. After making some changes to the sensor's library in C++ and switching the

pressure sensors to shielded cable to minimize interference, the code was able to initialize each sensor only once when it began running. The code now has the microcontroller request a set of data from all 16 sensors before returning to the first sensor to receive the information. With these code changes, the sampling frequency was 12 Hz, which was considered an acceptable sampling frequency. As mentioned in the Introduction, this sampling frequency can resolve vortices forming on a cylinder under steady current with a velocity up to 4 m/s.

3.3 PMM Base Construction

The PMM base constructed is a cylinder with a 144 mm diameter and 254 mm length. It is modeled after the 155 mm munitions used in research at the University of Delaware. In the future, additional fins and cones can be added to the base to recreate the size, shape, and moment of inertia of an actual 155 mm munition.

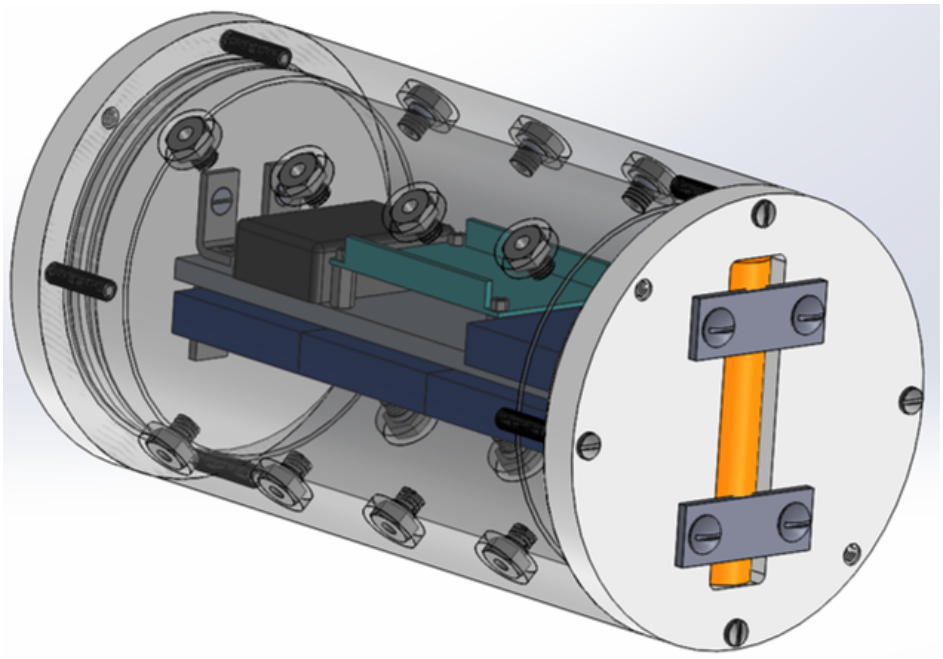

Figure 3.3: Solidworks assembly of PMM base and all its components. Visible are models of the batteries (blue), the IMU (black), the circuit board (teal), and the acoustic tracker (orange).

The majority of the PMM is made of 304 Stainless Steel so the specific gravity of the cylinder, 2.8, is comparable to that of a real munition. The cylinder has 16 pressure sensor screws on its

surface, organized in four rows of four sensors. The sensor holes needed room for the socket wrench to surround the hex screw, which is why there are large circles around each hole. These holes can be filled in with a re-workable epoxy during experiments to diminish effects to the flow field, and can be removed when the screw needs to be replaced. The PMM base has two PVC end caps, one containing the orange acoustic tracker and the other an acrylic window through which a green LED is visible. The acrylic window also uses an o-ring to create a waterproof connection. These are the two modes of recovering the PMM base after deployment.

The end caps have o-rings that make piston seals with the base, which has been machined smooth to ensure a waterproof seal. They also connect to the base using 1/4"-20 Thread, 1-1/4" Long 316 Stainless Steel screws, but these are more precautionary. The end caps support a $1/4$" thick 6061 Aluminum shelf; one end cap connects to the shelf using L-brackets and screws, while the other supports two studs extruding from the shelf. This shelf gives a sturdy surface to which the Inertial Measurement Unit (IMU), the circuit board, and the batteries can connect. The circuit board is connected to the shelf by standoff screws, the IMU is epoxied in position on the shelf, and the batteries use Velcro strips to attach to the shelf. The technical drawings of the entire PMM base can be seen in Appendix C.

Before machining the entire PMM base, the o-ring connections were validated using a test cylinder. The test cylinder is 76.2 mm long and includes the final end caps and one pressure sensor screw. The end caps also have the acrylic window to test that additional o-ring seal. The assembly and deployment of the test cylinder can be seen in Figure 3.4. The test cylinder was lowered to the bottom of the UNH Engineering Tank, which is just over 6m deep, and left submerged overnight. The design was considered waterproof when no water leakage was discovered in this experiment.

Finally, the entire base was machined and put together. All 16 sensors have four wires, so it is important to number the sensors and keep track of the wires so the instrument can properly collect data and the data can then be correctly analyzed. The sensor numbering technique can be seen in Appendix A.

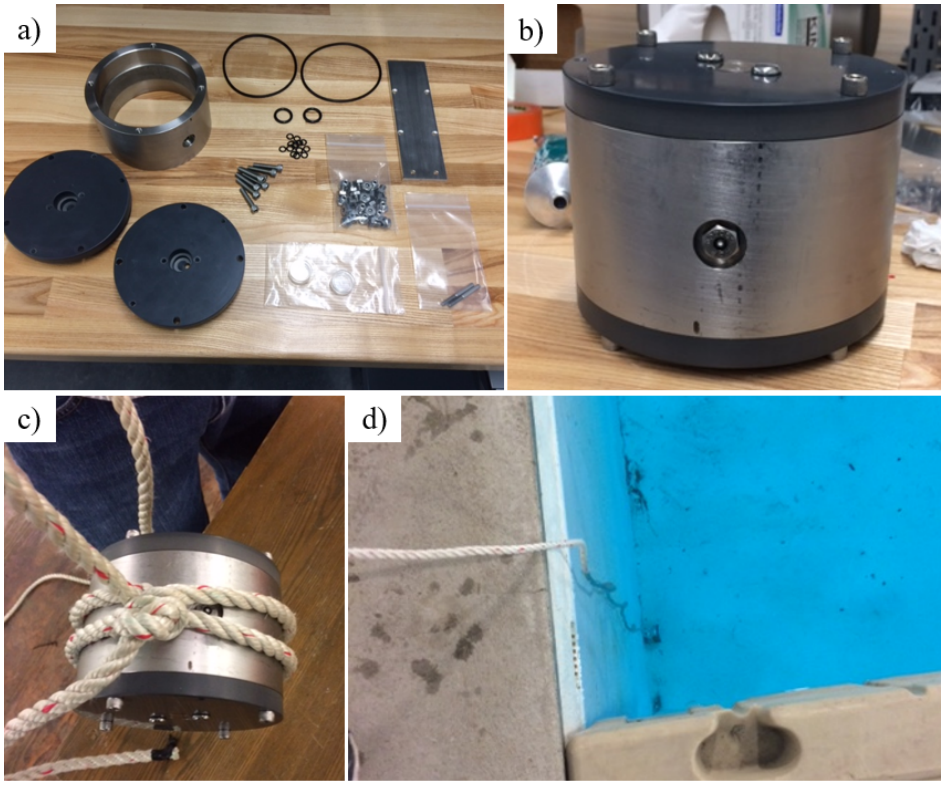

Figure 3.4: Test cylinder used to verify o-ring seals: a) disassembled test cylinder, b) assembled test cylinder, c) test cylinder tied to deployment rope, and d) test cylinder at the bottom of the UNH Engineering Tank.

As seen in Figure 3.5a, cable wraps were needed to organize the wires from the 16 pressure sensors inside the cylinder. The shelf attaches to the right end cap first, then is carefully slid into the cylinder. The entire cylinder is grounded by the ground of the circuit to ensure isolated signals. Finally, the second end cap is attached and supports the shelf by its studs. After conducting another waterproof test, the fully assembled PMM base was ready to begin validational laboratory experiments.

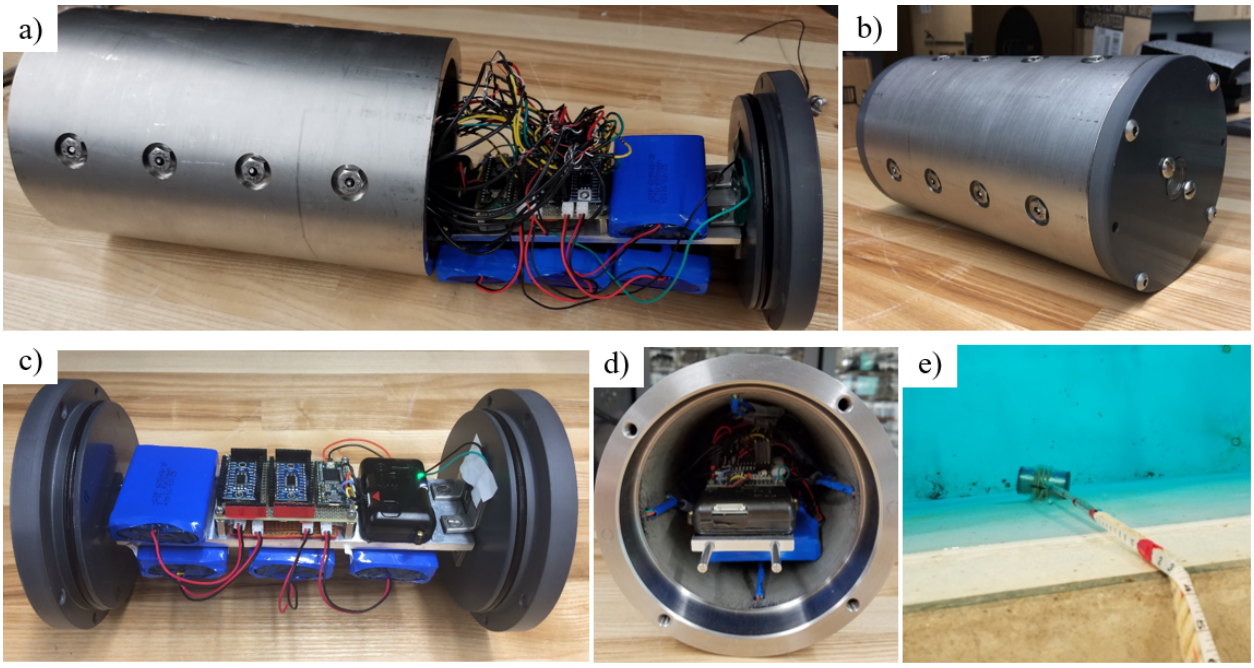

Figure 3.5: Final PMM base: a) sensors are installed, shelf supporting the circuit board, IMU and four batteries is exposed, b) fully assembled cylinder, c) internal componenets of PMM, d) internal view of shelf inside PMM base, and e) PMM being deployed to collect data at the bottom of the UNH Engineering Tank.

CHAPTER 4

EXPERIMENTS AND RESULTS

Laboratory experiments were conducted to investigate the instrument's capabilities. All experiments were conducting in UNH's Jere A. Chase Ocean Engineering Laboratory. A hydrostatic deployment test and an overnight drift test were conducted in the Engineering tank, which is 6 m deep, 12 m wide, and 18 m long. An instrument rolling test and a passing wave, sand bed and fixed floor tests were conducted in the wave and tow tank, which is 2.4 m deep, 3.6 m wide, and 30.5 m long and is equipped with a large wave-making paddle. Throughout this section, sensors will be grouped into columns, where a column is made of four sensors running horizontally along the length of the cylinder. All 16 sensors are numbered according to their column number and row number, or where they are positioned around the circumference of the cylinder. A diagram further explaining the numbering system can be seen in Appendix A.

4.1 Drift Test

The drift of the PMM pressure sensors was evaluated with an overnight submerge test in the Engineering tank. The instrument was deployed in 6 m of water and recorded data overnight.It was deployed alongside the Nortek 300 m Vector velocimeter and pressure sensor. The embedded piezoresistive pressure sensor is accurate to 0.5% of the full scale pressure and precise to 0.005% of the full scale. The Vector was a reference signal, recording any pressure changes in the tank. Figure 4.1 shows the 16 PMM pressure sensors with hydrostatic differences around the cylinder removed, meaning all 16 sensors should be reading the same pressure. These 16 sensors are plotted with their mean trend, and the Vector's pressure sensor reading. The individual sensors show a significant gain and offset relative to the Vector pressure sensor of up to 40 mbar, which is the equivalent of 40 cm of hydrostatic pressure. The manufacturer specifies that offsets from true pressure values

can be as large as 50 mbar. This suggests that a real-time calibration is required in still water environments.

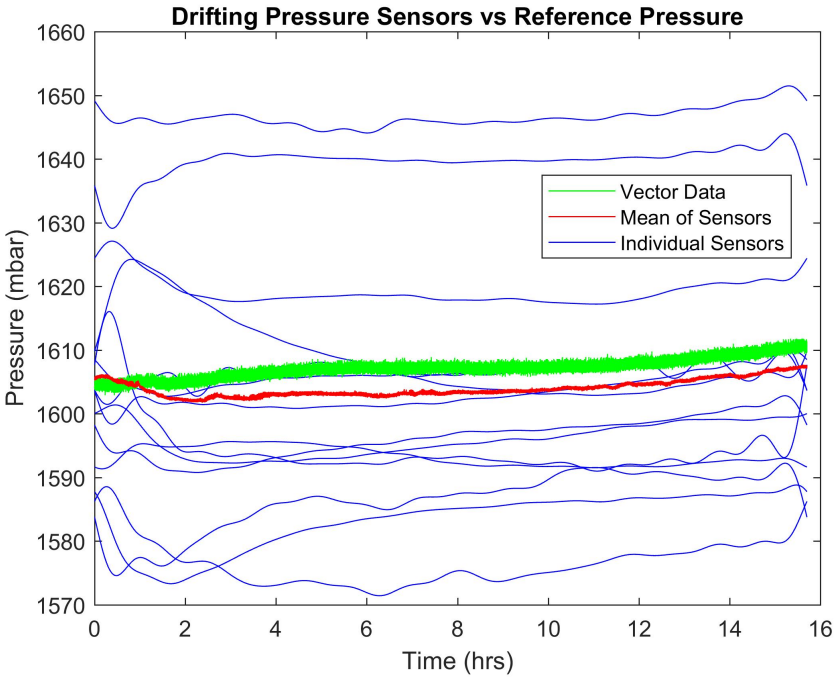

Figure 4.1: PMM with reference pressure sensor data; the PMM was deployed 6 m underwater overnight with a reference pressure sensor. The 16 individual sensors with hydrostatic offsets from the center of the PMM removed (blue) were offset and drifted, but their trend (red) and the reference pressure reading (green) agreed well.

Table 4.1: Linear Trend of Drift For Each Sensor (mbar/hr). Note that sensors 6 and 8 were unplugged during this portion of the experiment. Data analyzed for final 14 hours of drift deployment test.

Sensor	#1	#2	#3	#4	#5	#6	#7	#8	#9
mbar/hr	0.11	0.75	0.63	-0.30	0.35	n/a	0.57	n/a	0.46
Sensor	#10	#11	#12	#13	#14	#15	#16	mean	Vec
mbar/hr	0.65	0.85	0.22	0.01	0.70	0.13	-0.91	0.31	0.28

The individual sensors seem to drift the most in the first two hours. This could be due to the sensors acclimating to the temperature of the tank. However, to truly understand the effects

of temperature changes, a reliable temperature sensor will need to be added to the instrument's surface. Table 4.1 shows the slope for individual sensors after two hours of data have been recorded compared to that of the Vector pressure sensor. The drift between sensors in this experiment was unpredictable, though the mean trend is within 0.03 mbar/hr of the Vector pressure trend. These results support the data found in the initial graduated cylinder experiment; individual sensors can drift in unpredictable ways and should not be used for accurate hydrostatic measurements. However, the graduated cylinder test also included dynamic pressure changes to which the sensor responded well.

4.2 Hydrostatic Deployment Test

Another experiment was needed to test the instrument's ability to measure changes in pressure. To do so, a rope attached to a tape measure was tied around the instrument and it was lowered into the engineering tank in increments of 0.3 m until it reached the bottom at 6 m. At each depth, the PMM was suspended for at least 30 seconds. The results can be seen in Figure 4.2. The step-like response seen in the figure is the expected result and the changes in pressure are measured by each sensor, although there is less agreement on steady-state pressures between sensors as the instrument descends. To take a closer look, the mean of all 16 sensors was taken and the measured mean hydrostatic pressure was compared to the actual hydrostatic pressure based on the estimated depth of the cylinder at that time. Although the individual hydrostatic response of each sensor shows an increasing offset, every sensor measures the step-wise gradients in pressure accurately. This suggests that these sensors could be used to measure pressure gradients, but would need a reference sensor to remove its offset and drift.

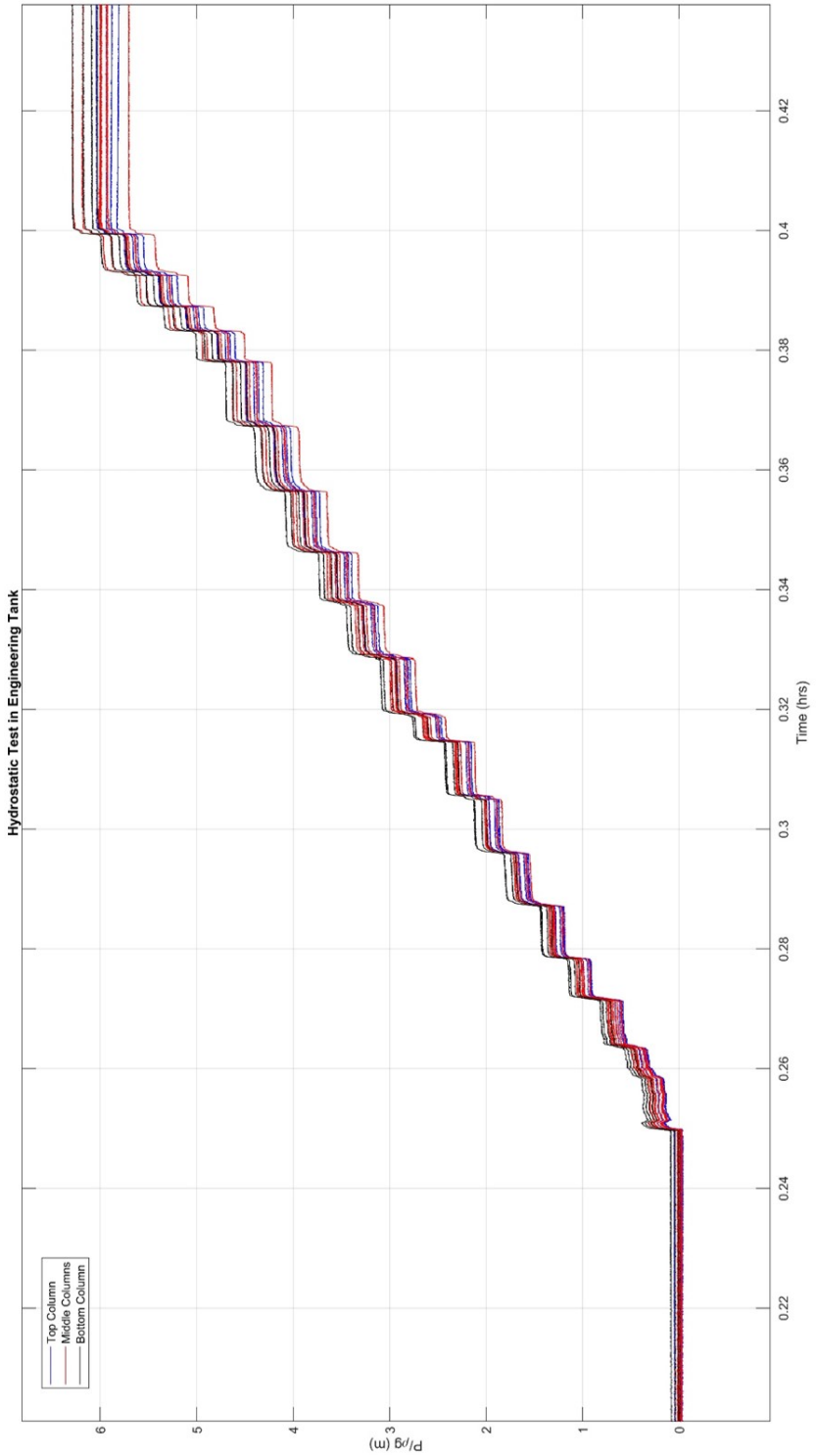

Figure 4.2: Hydrostatic deployment test: column 2 was on top as the instrument was deployed, meaning its sensors (blue) should observe the lowest pressure. Conversely, column 4 (black) was on bottom and should observe the highest pressure. Columns 1 and 3 (red) should be directly in between these two extremes. Instrument was deployed in increments of approximately 0.3 m until it reached the bottom of the tank at 6 m.

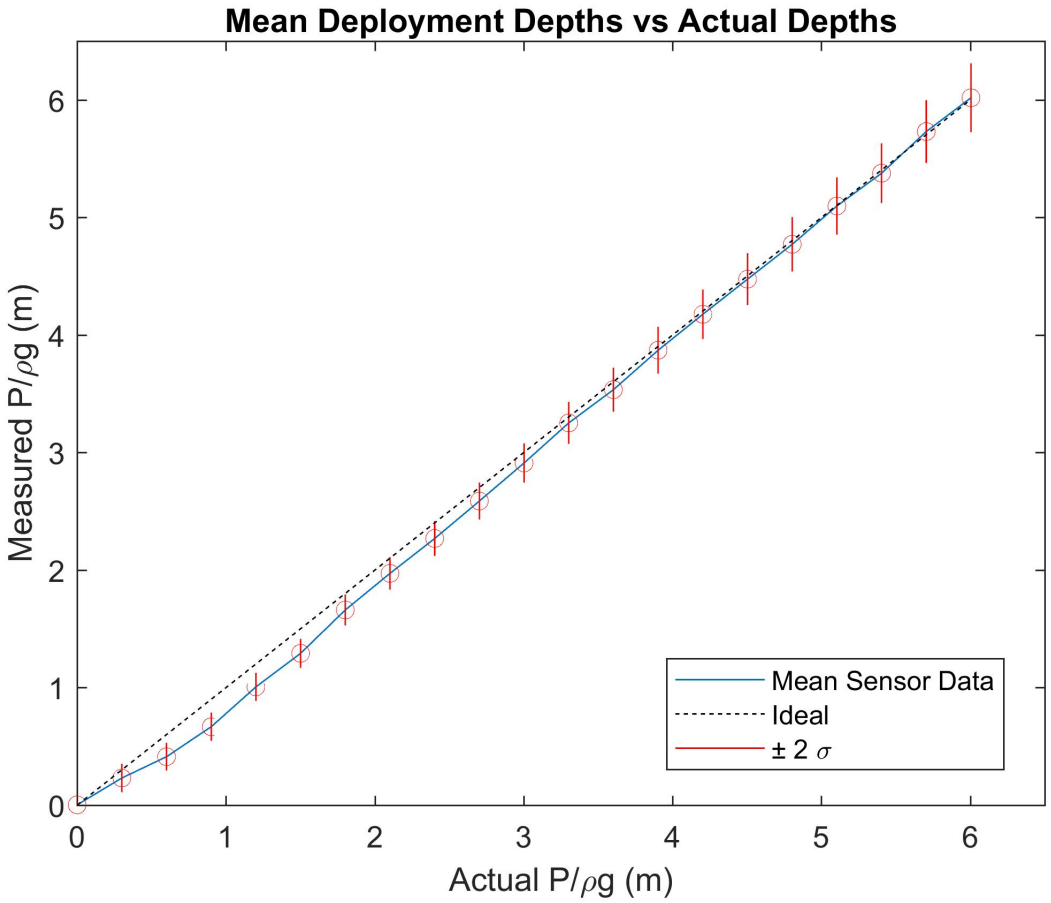

Figure 4.3: Hydrostatic deployment test results: Actual depth from measuring tape during deployment, measured depth from mean of 16 pressure sensors when instrument was at each depth. Black dashed line indicates the ideal relationship between measurements and the actual depth. Solid red lines indicate ± 2 standard deviations from the mean value.

4.3 Rolling Test

Next, a rolling test was performed to explore how the IMU and pressure sensors could be used together in a field experiment. Two thin, square PVC sheets were attached to the instrument's end caps using the pre-existing 316 stainless steel screws. These sheets were used to ensure accurate 90 degree rotations during the rolling test. Also, they have attachments for zip tie loops that can be used to raise and lower the instrument in the water with telescoping 3.7 m boat hooks. As seen in Figure 4.4a, the plates were installed such that, regardless of rotation, two columns of sensors were

at the same elevation on the top side of the cylinder and the other two were at the same elevation on the bottom side. A sketch of this can be seen in Figure 4.5.

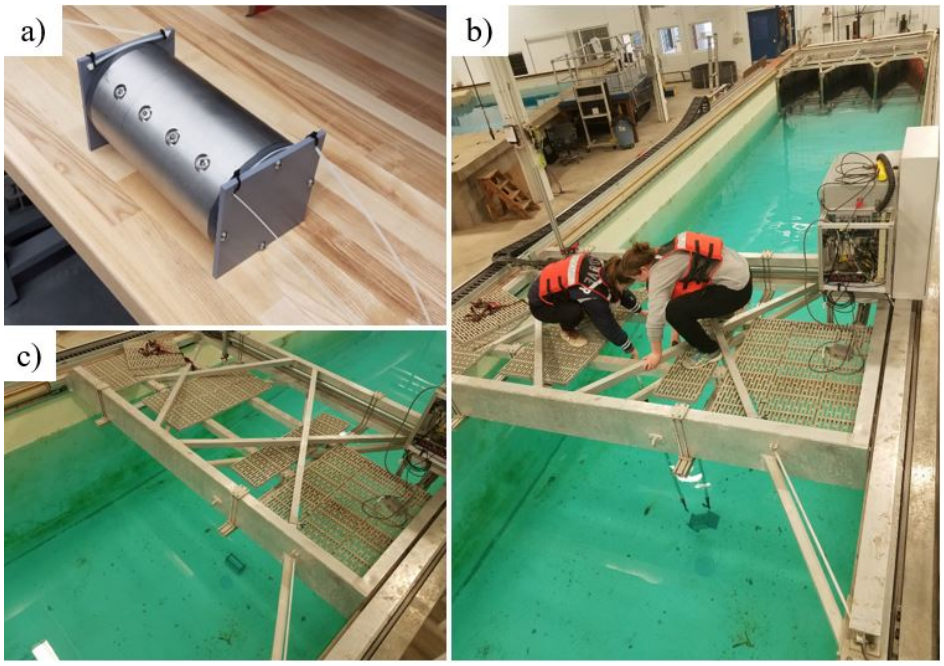

Figure 4.4: Rolling test deployment: a) Thin square sheets attached to end caps to allow for easy 90 degree rotations and attachable zip ties used to lower and raise the instrument, b) instrument being lowered into the wave tank using boat hooks, and c) cylinder at bottom of wave tank.

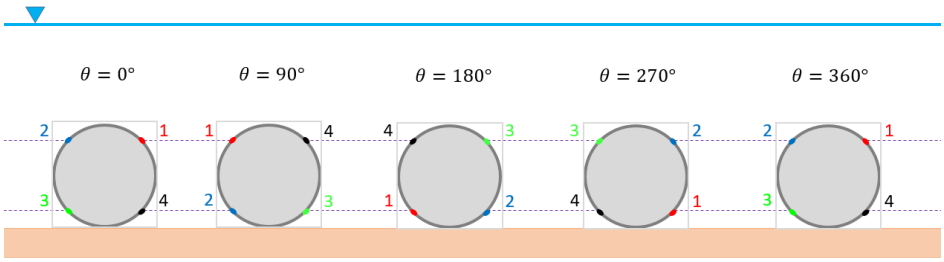

Figure 4.5: Sketch of PMM orientations during rolling test: purple dashed lines demonstrate the two vertical locations of the pressure sensors throughout the deployment. Sensor 10, shown in Figure 4.6, is in column 3, so it is expected to be under high pressure for the first two positions, then rotate to the lower pressure position.

After the instrument was assembled and lowered to the bottom of the tank, a swimmer rotated the cylinder 90 degree increments every three minutes. This was continued until the instrument

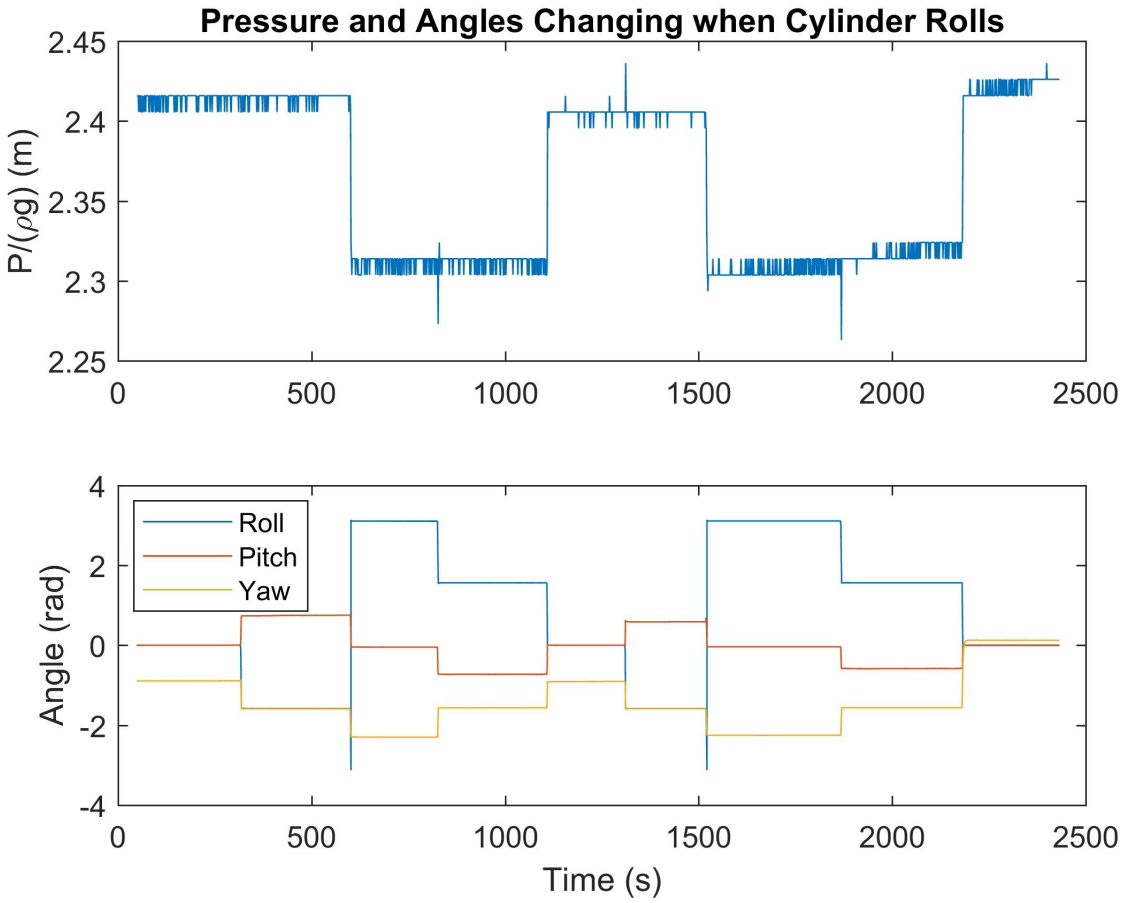

Figure 4.6: Rolling test results. Top) Pressure signal from sensor 10 on PMM. Bottom) Roll (rotation around x axis), pitch (rotation about y axis), and yaw (rotation about z axis) measured by on-board IMU.

had made two full rotations. Figure 4.6 shows the orientation and pressure data recorded by the PMM during this experiment. During this deployment, the PMM was only sampling at 1.2 Hz, which was not an issue because only hydrostatic conditions were being observed. Since there were only two hydrostatic depths regardless of rotation angle during this experiment, it is expected that the orientation would change without the hydrostatic pressure of the sensor changing every other rotation, and this can be seen in Figure 4.6. These two hydrostatic conditions are 10 cm apart, and the pressure sensor measures them as between 10 and 11 cm apart. During this experiment, the pressure signals were rounding to the nearest mbar, so the result could improve further when the

resolution of the sensors is enhanced. These results are very encouraging, as it reinforces the useful relationship between the orientation of the cylinder and the measurement of hydrostatic pressure.

4.4 Wave and Sand Test

A final laboratory experiment was conducted that simulated an environment the instrument would encounter in the field. An 80 cm long, 47 cm wide, and 30 cm tall bucket was filled with sand and placed on the bottom of the wave tank. Identical buckets were weighed down with sand and lead bricks, were covered with 3 cm tall lids, and were placed in front of and behind the sand bucket to create a raised floor, allowing for the development of a bottom boundary layer and minimizing transient boundary layers that could drastically change the flow field around the sand bed. To test flow patterns with all six buckets on the bottom of the tank, wave simulations were run in the tank before the PMM was added. Figure 4.7 shows a Solidworks representation of the experiment setup.

A tripod mount was constructed such that the Vector was parallel to the bottom of the tank and the sampling point of the instrument would be two PMM diameters above the sand bucket. The physical setup can be seen in Figure 4.8. The three prongs on the Vector instrument intersect and read velocity measurements 15 cm from the end of the instrument itself. The pressure sensor on the Vector is on its black base, so it is offset 30 cm horizontally from the velocity sampling point.

The Vector remained in this position for the experiment as well. An AWP-24-3 Wave Height Gauge from Akamina Technologies was installed on the tank's tow carriage to measure the wave characteristics at the surface of the water. Linear wave theory (LWT) predicts velocity and pressure fluctuations from a passing wave attenuate quicker with shorter wave periods. The wave simulations run in the preliminary testing and the experiment itself can be seen in the Table 4.2.

The first four wave simulations had relatively long periods, so the transitional water depth waves created fluctuations in velocity and pressure in the water column that the Vector and the PMM measured in the near bed. The last simulation had a short period, so the signals should be attenuated at those depths during these simulations. The initial Vector data were generally

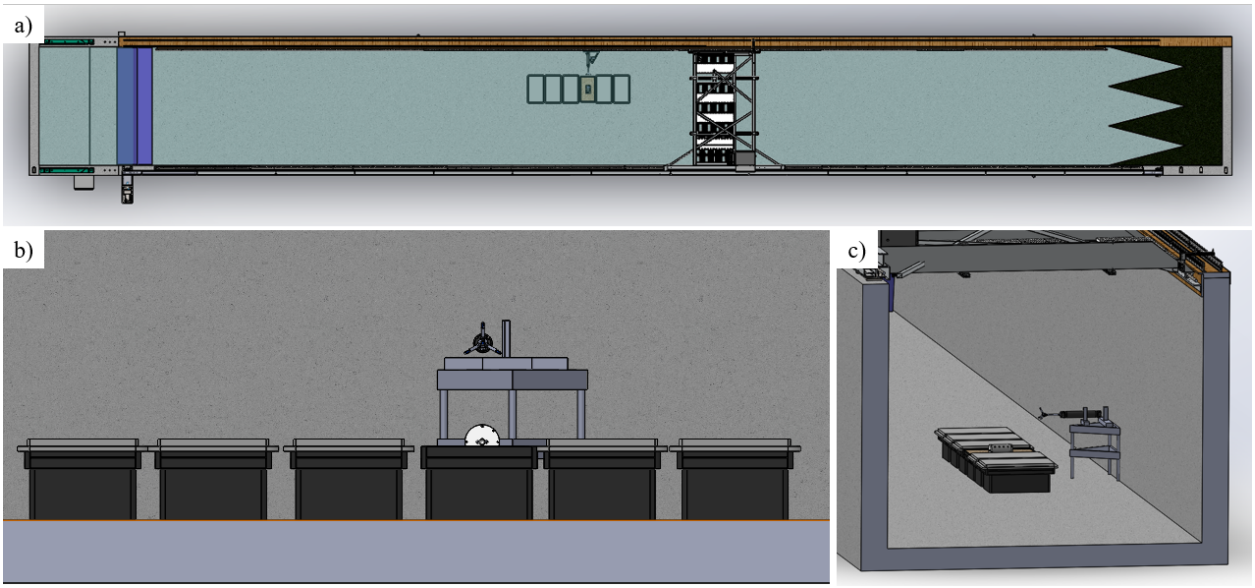

Figure 4.7: Wave and sand test experimental setup: Six buckets were placed on the bottom of the UNH wave and tow tank. The fourth bucket from the wave paddle had its lid removed and was filled with sediment. The PMM was placed in sediment bucket at different levels of exposure. The Vector is secured to a tripod mount with hose clamps and is positioned to sample velocity measurements 28 cm directly above the center of the sediment bucket (yellow lines indicate relationship between prongs and sampling point). A capacitance wave gauge (not shown) was attached to the tow carriage, measuring elevation at the water surface. The wave paddle is to the left, 24 m from the sampling point, and the beach is to the right, 16 m from the sampling point.

consistent with LWT, so the simulated waves were repeated with the PMM added to the experiment. Figure 4.9 shows the spectra for the Vector pressure observations for the different wave simulations. The energy peaks of each occur at a frequency of $1/T$, where T is the wave period.

The sampling frequency for the strain gauge was 100 Hz, the PMM was 12 Hz, and the Vector was 8 Hz. Each simulation was run for 6 minutes to ensure ther were at least 90 waves per simulation. There was a few minute break in data collection between running each simulation to allow for the water to settle. The untethered PMM collected data continuously. This time between wave simulations also allowed for an evaluation of sensor drift. During the experiment, all five simulations were run when the PMM was at five different exposure levels: completely buried in the sand, 25% exposed, 50% exposed, 75% exposed, and fully proud on the sediment bed. Based on the exposure level, some columns of sensors would be covered with sand and others would be

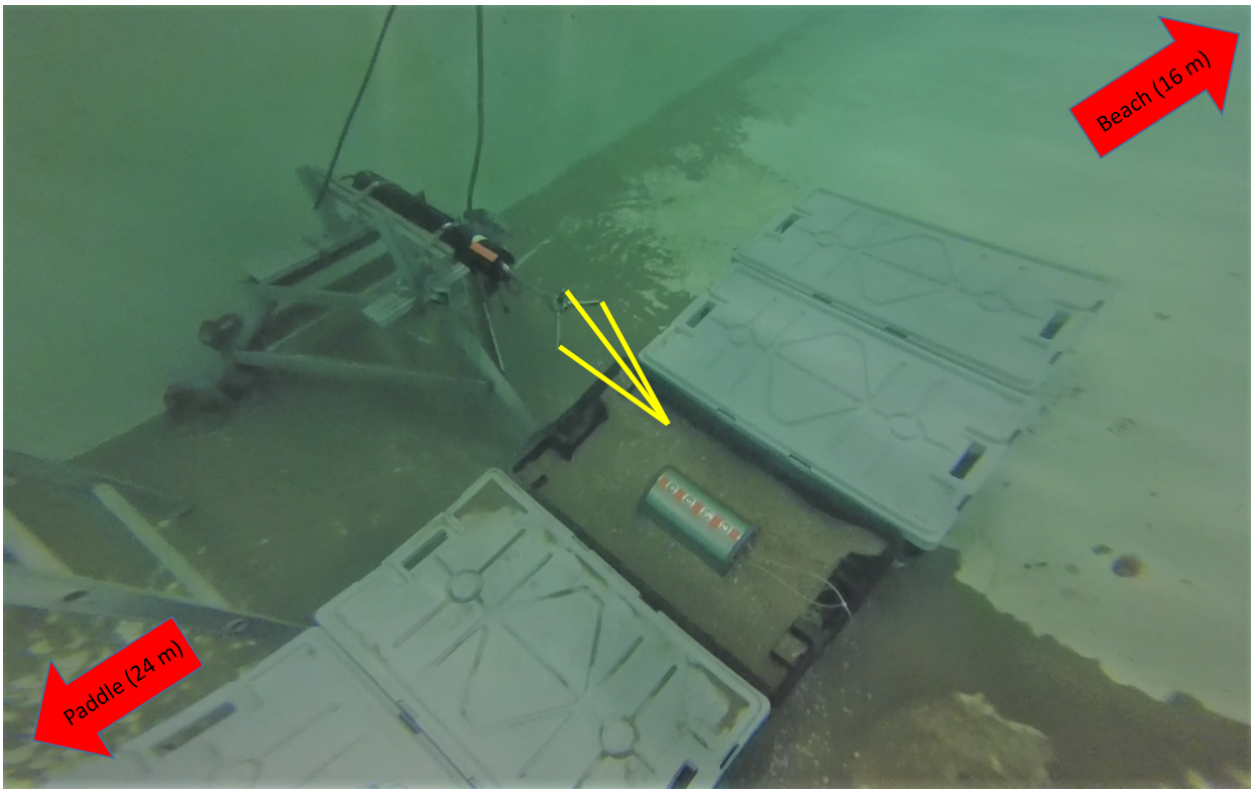

Figure 4.8: Wave and sand test experiment: Note the image distortion from the use of an underwater camera. The PMM was 50% exposed in the sand bed and was marked so column 1 of sensors was always be on top of the instrument. The ladder seen on the left of the figure was used by swimmers to get in and out of the water and the ladder was removed from the tank when the wave simulations were running.

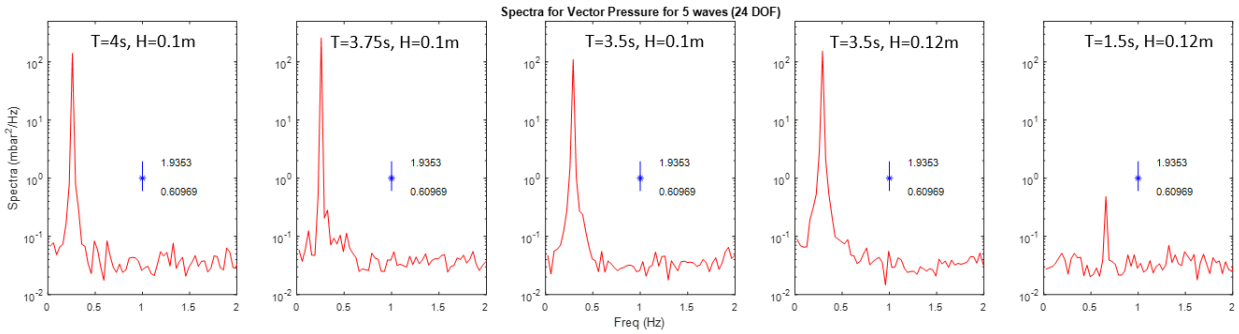

Figure 4.9: Characterizing pressure data spectra for wave simulations 1 (left) through 5 (right) with 95% Confidence Intervals

buried. Column 1 of sensors was always facing upwards throughout the experiment, as shown in the figure. Columns 2 and 4 were on either side, and column 3 was facing the bottom of the tank.

Figure 4.10 shows a sample time series from the portion of the experiment when the PMM was sitting on the sand bed (100% exposed).

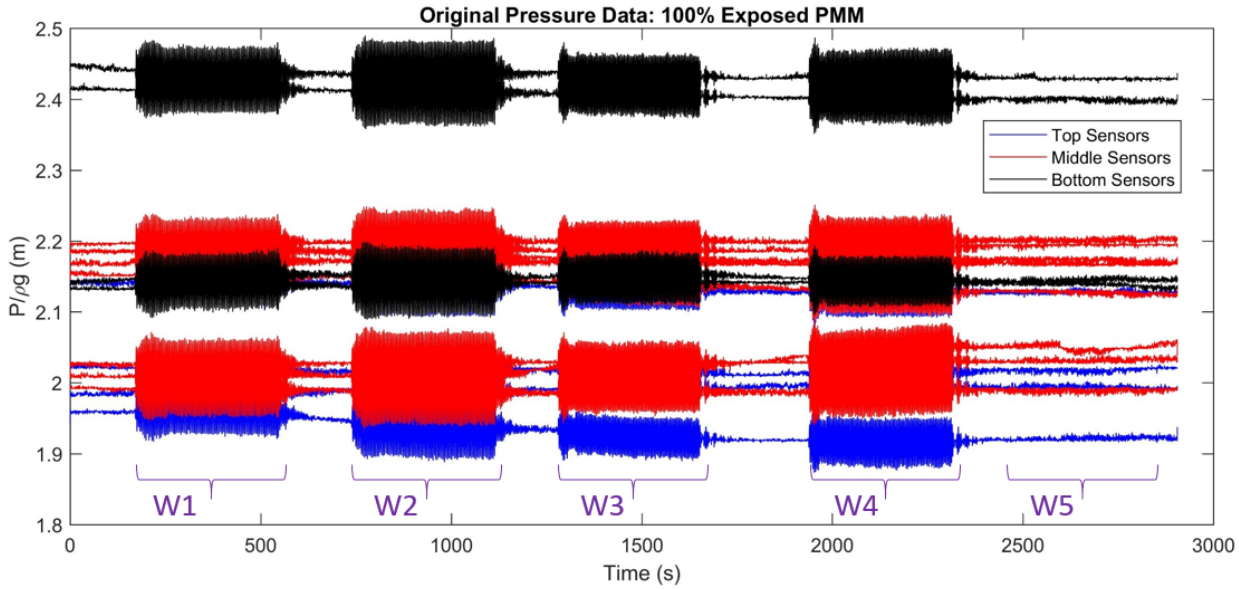

Figure 4.10: Sample of raw PMM pressure data from wave and sand test. During this portion of the experiment, the PMM is fully exposed to the flow, sitting on top of the sand. The blue sensors are in column 1 on top of the instrument, the red sensors are in the middle of the instrument in columns 2 and 4, and the black sensors are on the bottom of the cylinder in column 3. Wave simulations are numbered in purple, corresponding to their wave characteristics in Table 4.2. These results were repeatable for all exposure levels of the PMM.

Simulations were run in the order in which they appear in Table 4.2. Note that no fluctuations were measured by the Vector or the PMM during the fifth simulation towards the end of this time

Table 4.2: Wave simulation characteristics (simulation number, period (s), wave height (m), wavelength (m), normalized depth (h = 2.4 m), normalized distance from paddle (x = 24 m))

Sim	T (s)	H (m)	L (m)	h/L	x/L
1	4.00	0.10	16.55	0.145	1.450
2	3.75	0.10	15.31	0.157	1.568
3	3.50	0.10	14.05	0.171	1.708
4	3.50	0.12	14.05	0.171	1.708
5	1.50	0.12	3.51	0.683	6.838

series. As predicted by LWT, the PMM was in deep water conditions for a wave with period 1.5 s and the wave's pressure and velocity fluctuations had been attenuated before reaching these instruments Vector or the PMM. These results were repeatable for all exposure levels of the PMM.

Suring the wave and sediment simulations, the pressure sensors were recording pressure in increments of 1 mbar. This resolution can be observed in the discretization of the pressure time series seen in Figure 2.7. The resolution was improved for the next experiment and the results of the rounding errors are discussed in the next section. However, for results in this experiment, the PMM pressure sensor data is windowed in the frequency domain, resulting in a smoothed spectra that only includes frequencies between 0.1 and 1 Hz. The 0.1 to 1 Hz band pass was chosen to isolate the frequencies associated with the free surface gravity wave band.

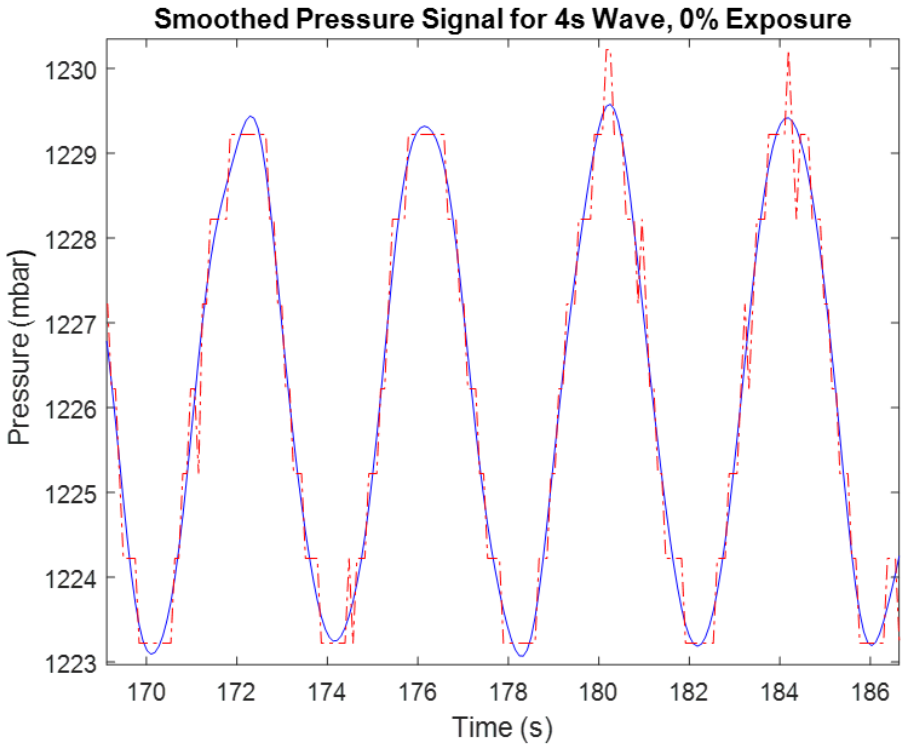

Figure 4.11: Raw (red) vs. smoothed to 1 Hz (blue) pressure signal. This representative data set was taken in the UNH wave and tow tank under a 4 s long, 0.1 m wave simulation.

Linear wave theory for a single frequency progressive wave and the standard deviation for each sensor and simulation were compared to the theoretical normalized orbital pressure magnitude[14].

According to LWT,

$$\frac{P_o}{\rho g} = \frac{\sqrt{2}\sigma_p}{\rho g} = \frac{H}{2}\frac{cosh(2\pi(d+z)/L)}{cosh(2\pi d/L)} \tag{4.1}$$

where P_o is the orbital pressure of the wave, d is the depth of the water, ρ is the density of water, and σ_p is the standard deviation of the pressure signal and z is the distance from the still water level, where locations below the surface are negative [14]. See the appendix for this derivation. Figure 4.12 shows the right-hand side of this equation as a function of distance from the still water level plotted as a solid line for each of the simulations run in this experiment. The symbols on the figure are the normalized standard deviations for each pressure sensor.

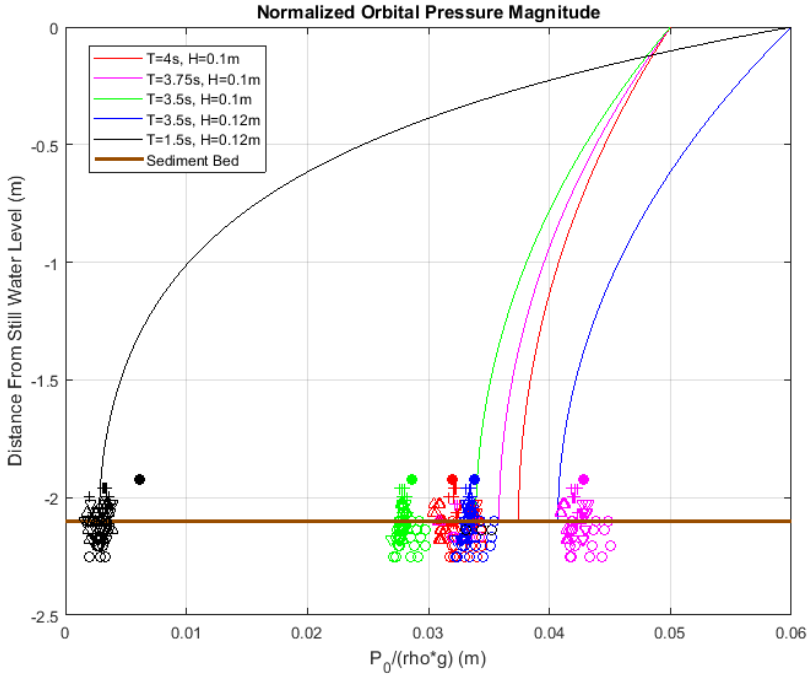

Figure 4.12: Normalized orbital pressure magnitude calculated by LWT. Symbols indicate a normalized standard deviation of the wave ($\sqrt{2}\sigma/\rho g$) for each pressure sensor (+ = top column sensors, $\triangledown$ = column facing wave paddle, $\triangle$ = column facing beach, o = bottom column sensors). Colors indicate wave parameters (red = 4 s period and 0.1 m wave height, magenta = 3.75 s period and 0.1 m wave height, green = 3.5 s period and 0.1 m wave height, blue = 3.5 s period and 0.12 m wave height, black = 1.5 s period and 0.12 m wave height). Colored circles indicate normalized standard deviation of pressure measured by the Vector.

The normalized standard deviations are plotted against their depth in the tank according to the PMM's exposure level for each simulation. Figure 4.13 shows the comparison of the progressive

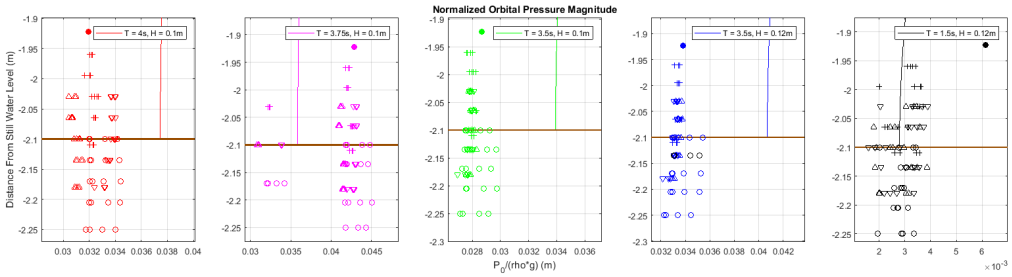

Figure 4.13: Near bed normalized orbital pressure magnitude calculated by LWT. Symbols indicate a normalized standard deviation of the wave ($\sqrt{2}\sigma/\rho g$) for each pressure sensor (+ = top column sensors, $\triangledown$ = column facing wave paddle, $\triangle$ = column facing beach, o = bottom column sensors). Colors indicate wave parameters (red = 4 s period and 0.1 m wave height, magenta = 3.75 s period and 0.1 m wave height, green = 3.5 s period and 0.1 m wave height, blue = 3.5 s period and 0.12 m wave height, black = 1.5 s period and 0.12 m wave height). Colored circles indicate normalized standard deviation of pressure measured by the Vector.

wave solution in the very near bed region. There are differences of up to 1 cm between the theoretical and calculated normalized pressure values. The Vector pressure observations are in good agreement with the top column of the PMM. However, both the Vector and PMM show variations from the LWT predictions. Possible explanations include non-linearities in the flow due to energy at harmonic frequencies, a reflection of the incident wave, or tank-generated deviations.

Additional flow parameters can be compared to further evaluate these phenomena. According to the linearized horizontal momentum equation for inviscid flow is given by:

$$\frac{du}{dt} \approx -\frac{1}{\rho}\frac{dP}{dx} \tag{4.2}$$

Above, P is the wave component of pressure[3]. Therefore, the mean was removed from the PMM smoothed sensors in the middle columns. Then each sensor facing the beach was subtracted from its sensor facing the paddle in the same row. The mean of these four rows was taken, resulting in a single mean pressure difference. This difference was then divided by the diameter of the cylinder, 0.14 m, to obtain the pressure gradient. The local horizontal acceleration was calculated with a frequency domain derivative over the free surface gravity wave band for frequencies between 0 and 1 Hz. Figure 4.14 shows the two sides of the above equation plotted against time for the 4 s

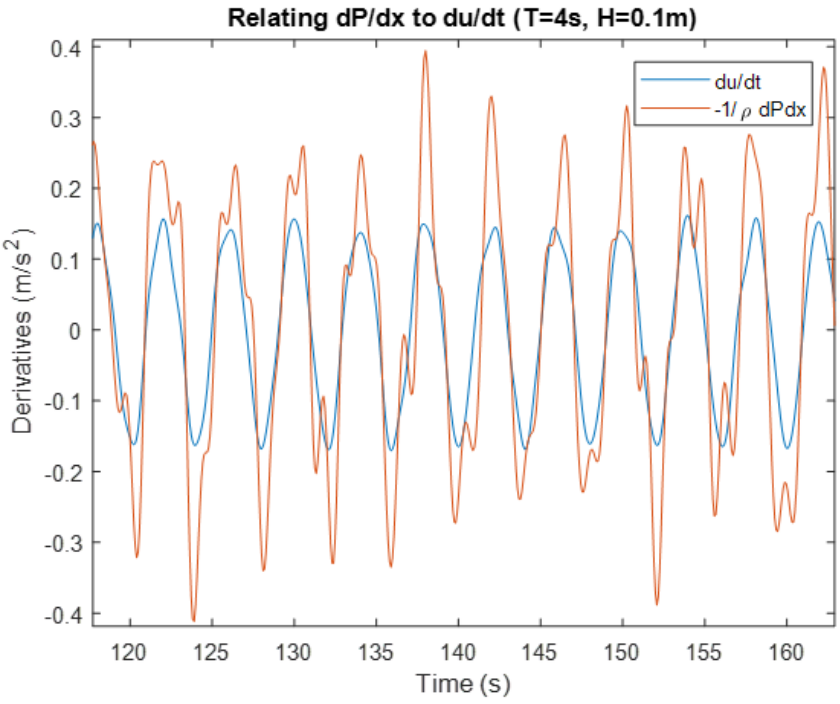

Figure 4.14: Applying horizontal momentum equation to the flow by comparing the horizontal pressure gradient (red) to the time derivative of horizontal velocity (blue). Data was taken during the 4 s, 0.1 m wave simulation.

wave simulation. The two signals are in phase, as predicted by LWT. The results are comparable for the other wave simulations, although the signals become less sinusoidal for the 3.5 s wave simulations.

When changing the PMM's exposure level, the hydrostatic pressure for each sensor changed as well. There should be no effect of burial on the hydrostatic pressure readings. Burial could dampen the energy from dynamic pressures and would affect vortex shedding, but the hydrostatic pressure experienced by the sensors is independent of burial. Figure 4.15 shows the mean hydrostatic pressure readings from the sensors at each hydrostatic level. The horizontal brown line indicated the location of the sediment bad and the diagonal cyan line indicates the theoretical hydrostatic pressure. These mean hydrostatic measurements show substantial variability when in the sand, and are more consistent when the PMM is exposed to the water. This suggests that the sensors

would benefit from a sand filter. However, even in the exposed sensors there is variation, so a reference pressure sensor should be used in the next iteration of the project.

Since the sensors were at a constant depth at each exposure level, drift comparisons can be done using the approximately still water levels in between running simulations. The mean value of all 16 pressure sensors was taken over each period of still water, as seen in Figure 4.16. The duration of the entire data set, including all 5 wave simulations, was about 45 minutes. The drift is not substantial except for the first few still water readings during the buried PMM experiment. The PMM was buried initially so this was the first data set taken, indicating that perhaps the sensors need to calibrate to their surrounding temperature. Again, the actual values for the hydrostatic measurements show consider variability, as the mean hydrostatic levels between positional changes should be spaced by 3.5 cm and this is not the case. However, as the PMM is raised as it becomes more exposed to the flow and there is an expected corresponding trend of decreasing hydrostatic pressure.

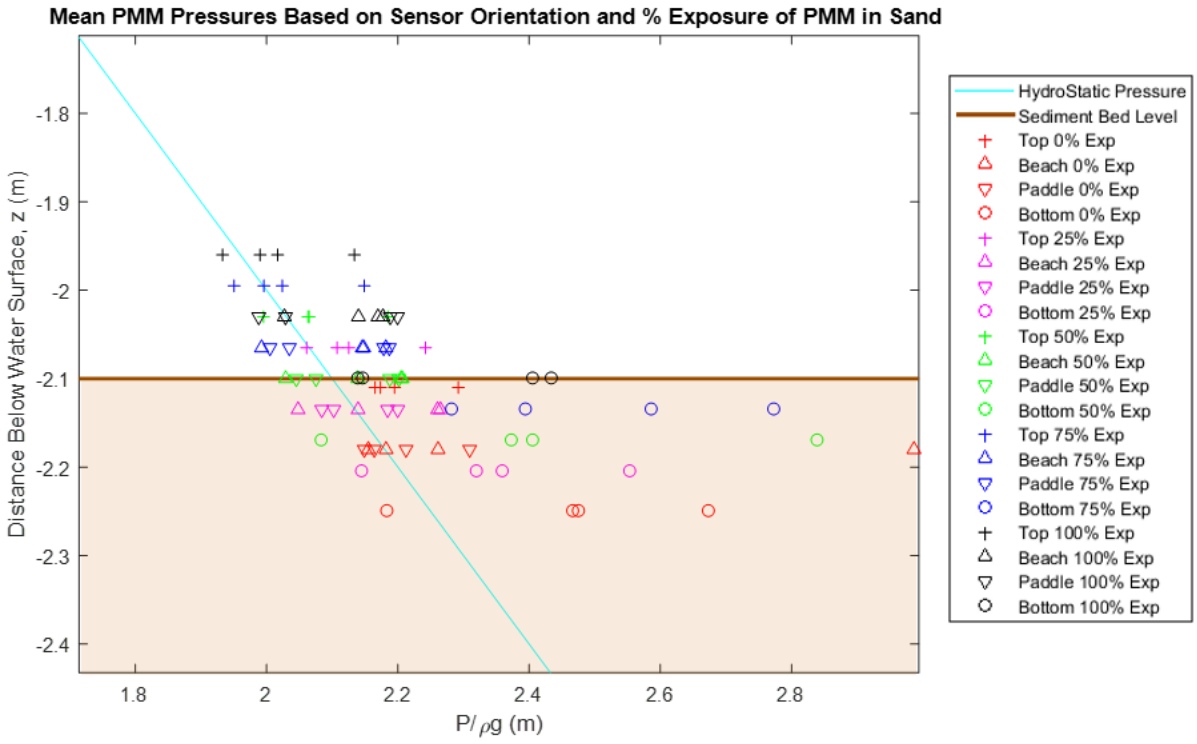

Figure 4.15: Mean hydrostatic PMM readings vs. actual depth during sand and wave test.

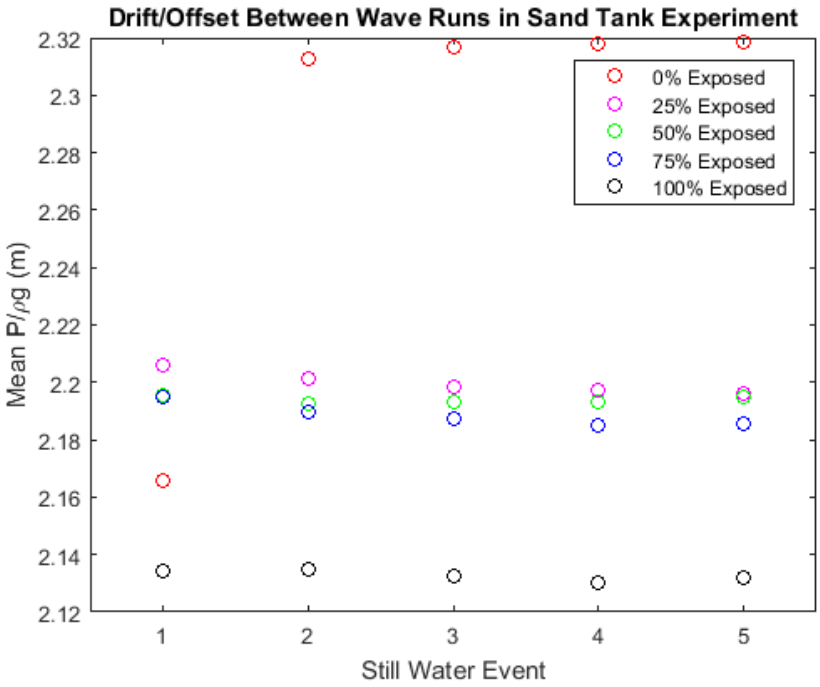

Figure 4.16: Mean hydrostatic measurements taken in still water conditions when the PMM was buried (red), 25% exposed (magenta), 50% exposed (green), 75% exposed (blue), and fully exposed (black).

Collecting data for each wave period allowed for meaningful spectral analyses of the PMM pressure sensors. Calculating the spectra, which represents the data in the frequency domain, allows for a visualization and estimation of the sensor's abilities and limitations. Figure 4.17 shows a representative spectra. The first wave conditions, with a 4 s period and 0.1 m wave height, was chosen because this simulation had the lowest frequency, so the response of the sensor is more clear. The spectra for wave simulations 2-4 were comparable, but the energy peak occurs closer to the noise floor so there is less information about the sensor. This can be seen in Figure 4.18. As mentioned previously, each pressure sensor signal was smoothed post-processing. The black spectra is for the sensor before smoothing, and the red spectra is for the sensor after smoothing. The noise floor, which is the noisy horizontal portion of the curve at high frequencies, is removed during the smoothing process, which is why the red spectra reports low energy in the signal at these frequencies.

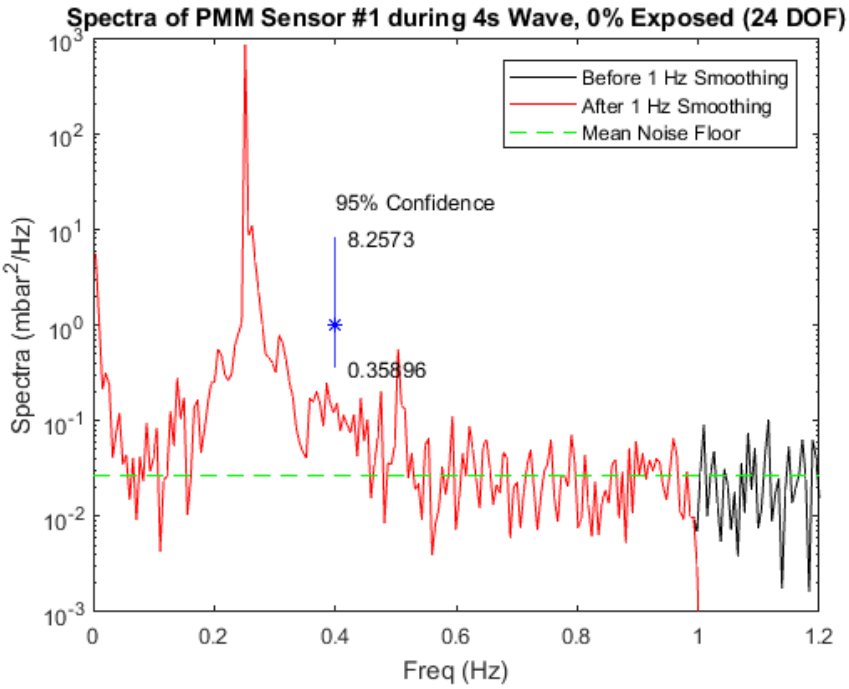

Figure 4.17: Spectra of PMM sensor: this representative data was collected during the 4 s wave simulation when the PMM was fully buried in the sand. The black spectra is for the sensor before smoothing, and the red spectra is for the sensor after smoothing.

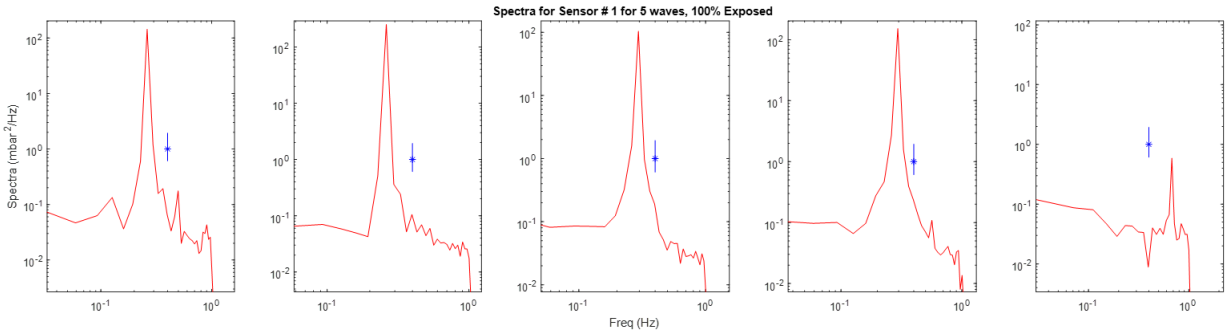

Figure 4.18: Spectra of PMM sensor #1 for wave simulations 1 (left) through 5 (right) with 95% confidence intervals and 24 DOF

In Figure 4.17, the large energy peak occurs at 0.25 Hz, correlating to the energy in the 4 s wave simulation. A harmonic is visible at 0.5 Hz, and a third may be present at 0.75 Hz but this frequency is close to the noise floor so it cannot confidently be said that this harmonic is visible. To understand more about the sensor's response, the PMM needs to be exposed to longer, higher-

energy waves, such as those in the field. Larger, longer waves would move the peak of the spectra to lower frequencies and would increase the size of the peak, revealing more about the sensor's capabilities. The wave simulations in this experiment were limited by the capabilities of the wave tank. However, the spectral value at which the noise floor occurs allows for a calculation of the root mean square of the error of the sensor by the following equation:

$$\sigma = \sqrt{S_n \frac{1}{2\Delta}} \tag{4.3}$$

where S_n is the noise floor mean value, and Δ = 0.083 s is the sampling time of the PMM. The calculated root mean square of the error for each sensor was 0.3 mbar, which is the equivalent of a 3 mm change in hydrostatic pressure. However, this value must be compared with the bit noise, resulting from the pressure sensor only reading to the nearest mbar. The standard deviation of a Gaussian noise signal of $\pm$0.5 mbar is 0.29 mbar, so this is the estimated bit noise level. This suggests that the noise floor of the sensor could be lowered if the sensor had better resolution, which can be seen in the next experiment [8].

A cross-spectra relating the PMM pressure sensors to the Vector pressure and velocity signals and the wave gauge signals can quantify how accurately the PMM pressure sensors were able to capture the wave motions. Figure 4.19 shows the spectra, squared coherency, and phase correlations for a PMM pressure sensor and the pressure signal recorded by the Vector during a 4 s wave simulation while the PMM was buried. All exposure levels had comparable results. The squared coherency demonstrates when the signals are measuring comparable energy levels at the same frequencies, and a 95% confidence critical value is included to ensure the coherency is statistically significant. As seen in the figure, the two spectra are highly correlated at 0.25 Hz and its harmonic at 0.5 Hz, and the phase between the two at these frequencies is 0 degrees, which is expected because the Vector is directly above the instrument. The velocity and wave gauge spectra also show coherency at the 0.25 Hz frequency and its first harmonic. This demonstrates that the PMM pressure signals captured the wave signals just as well as the newly-calibrated instruments used in this experiment.

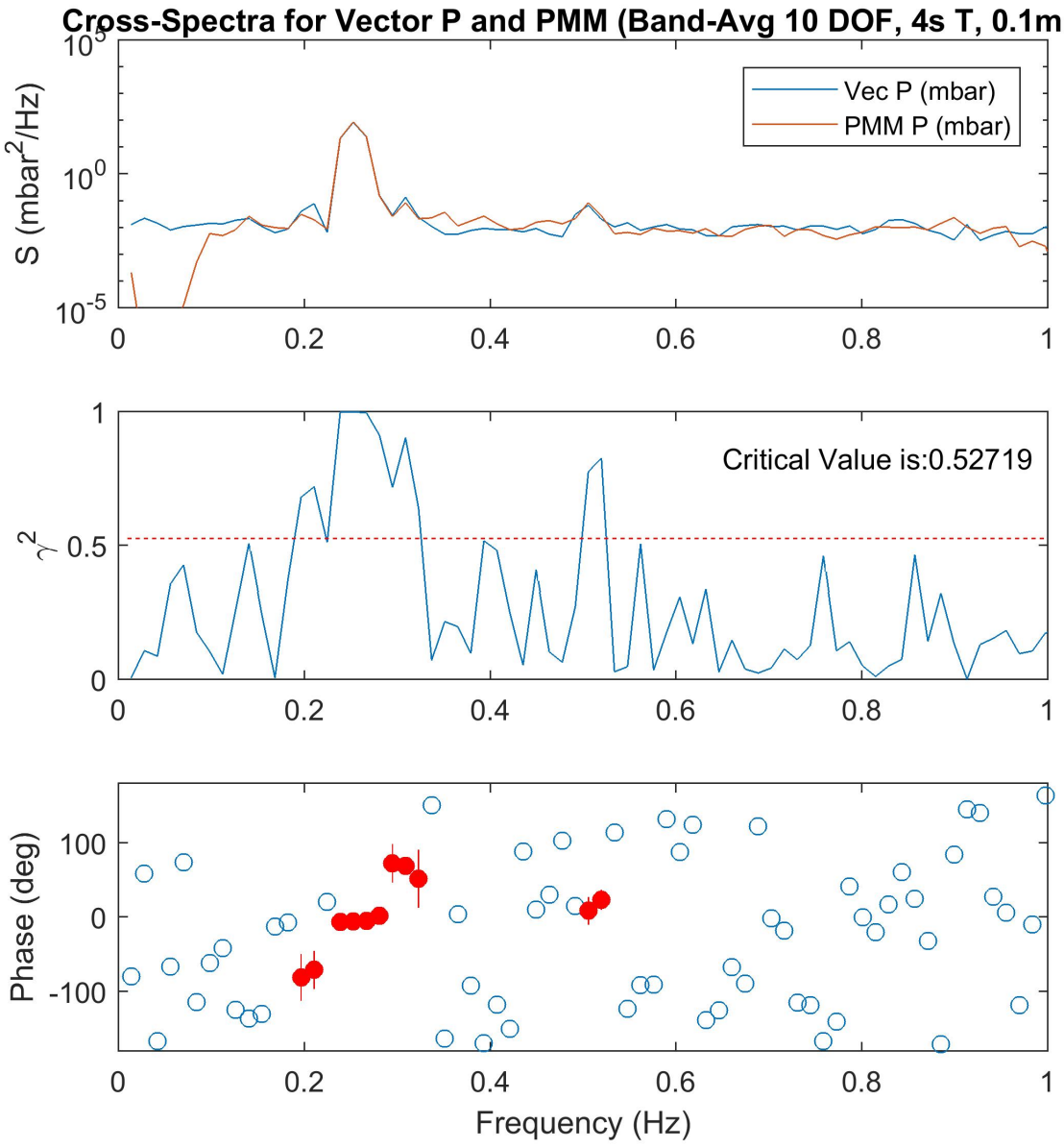

Figure 4.19: Cross-spectra between PMM pressure and vector pressure readings. Data collected during 4 s wave simulation when PMM was buried, although all exposure levels were comparable. Top plot shows the spectra for each signal. Middle plot shows the squared coherency between the two spectra and the 95% confidence critical value. Bottom plot shows the phase difference between the two spectra, with the red circles indicating phases with statistically significant squared coherency at the 95% level and red lines indicating 95% confidence intervals for the phase values.

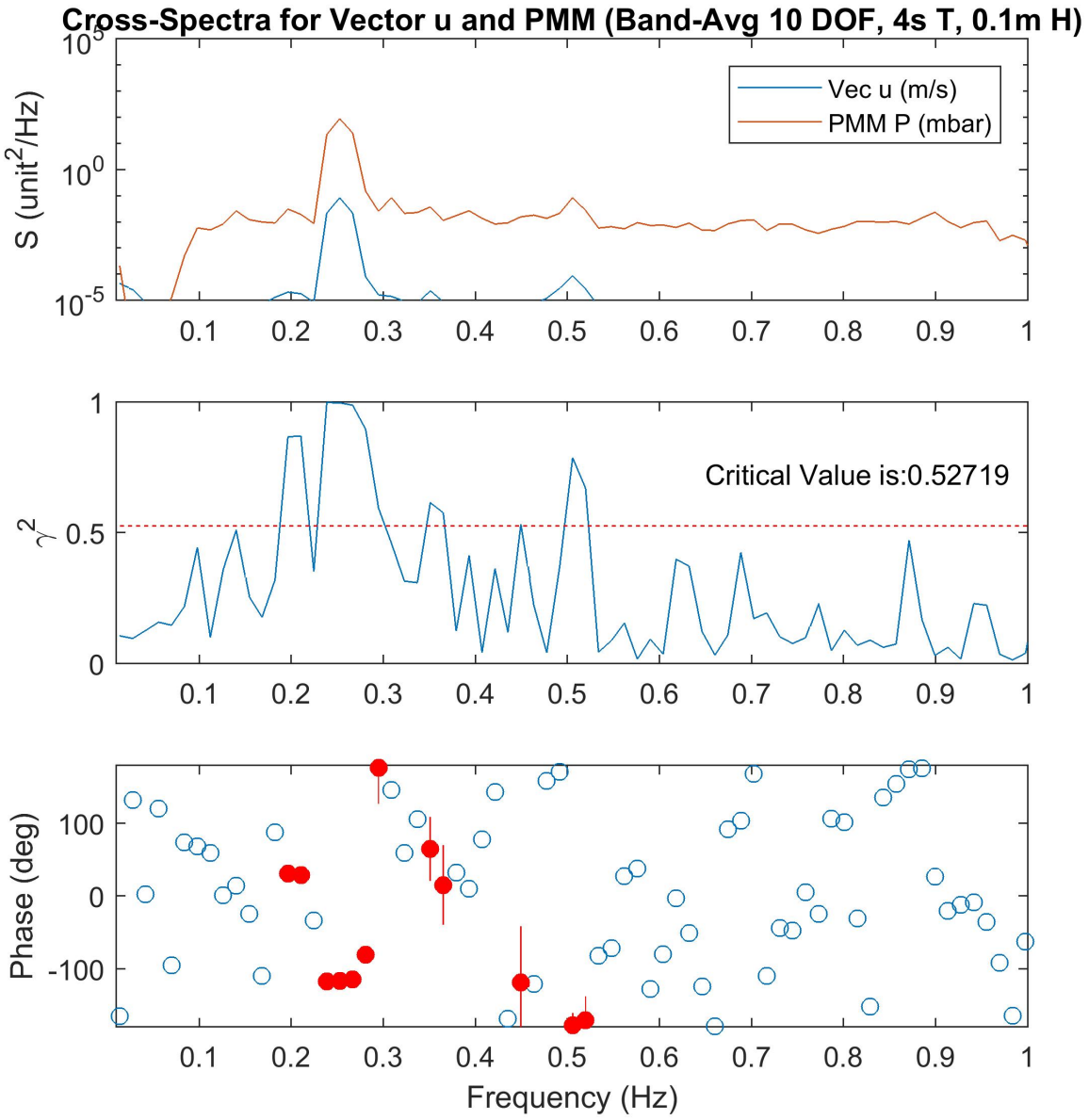

Figure 4.20: Cross-spectra between PMM pressure and vector horizontal velocity readings. Data collected during 4 s wave simulation when PMM was buried, although all exposure levels were comparable. Top plot shows the spectra for each signal. Middle plot shows the squared coherency between the two spectra and the 95% confidence critical value. Bottom plot shows the phase difference between the two spectra, with the red circles indicating phases with statistically significant squared coherency at the 95% level and red lines indicating 95% confidence intervals for the phase values.

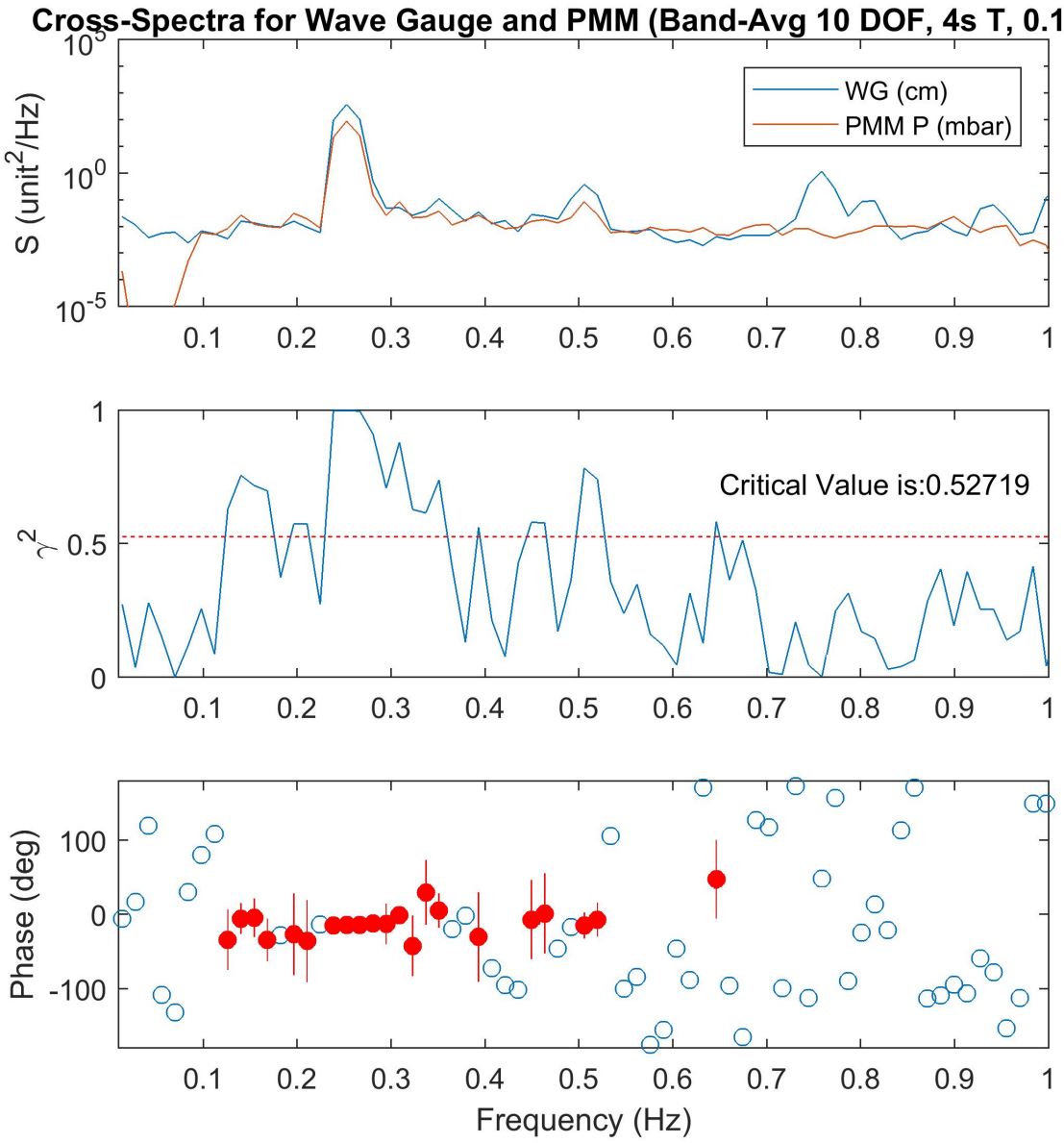

Figure 4.21: Cross-spectra between PMM Pressure and wave gauge surface elevation readings. Data collected during 4 s wave simulation when PMM was fully exposed. Top plot shows the spectra for each signal. Middle plot shows the squared coherency between the two spectra and the 95% confidence critical value. Bottom plot shows the phase difference between the two spectra, with the red circles indicating phases with statistically significant squared coherency at the 95% level and red lines indicating 95% confidence intervals for the phase values.

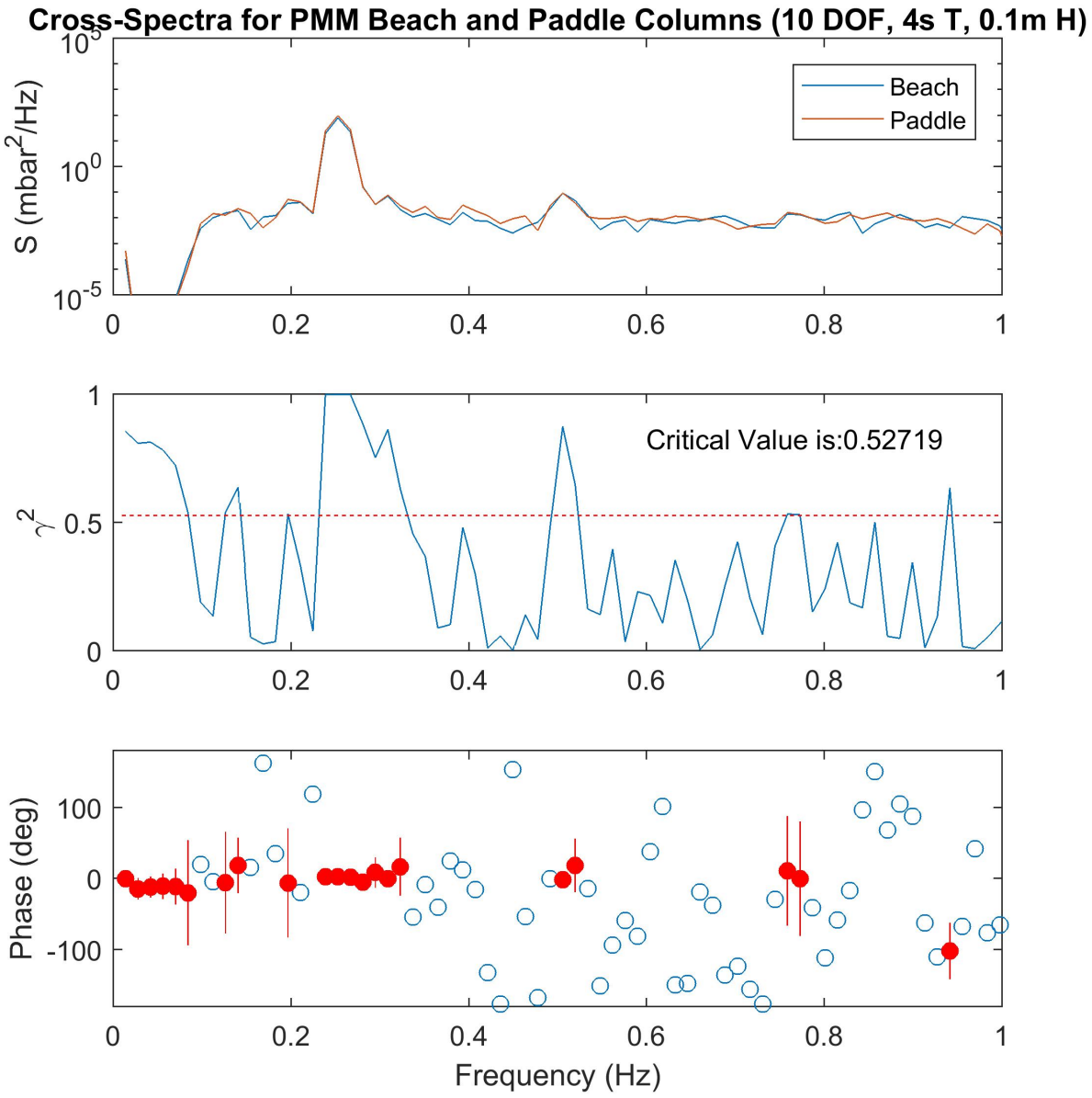

Figure 4.22: Cross-spectra between PMM Pressure sensors facing the beach and the paddle a during 4 s wave simulation when PMM was fully exposed. Top plot shows the spectra for each signal. Middle plot shows the squared coherency between the two spectra and the 95% confidence critical value. Bottom plot shows the phase difference between the two spectra, with the red circles indicating phases with statistically significant squared coherency at the 95% level and red lines indicating 95% confidence intervals for the phase values.

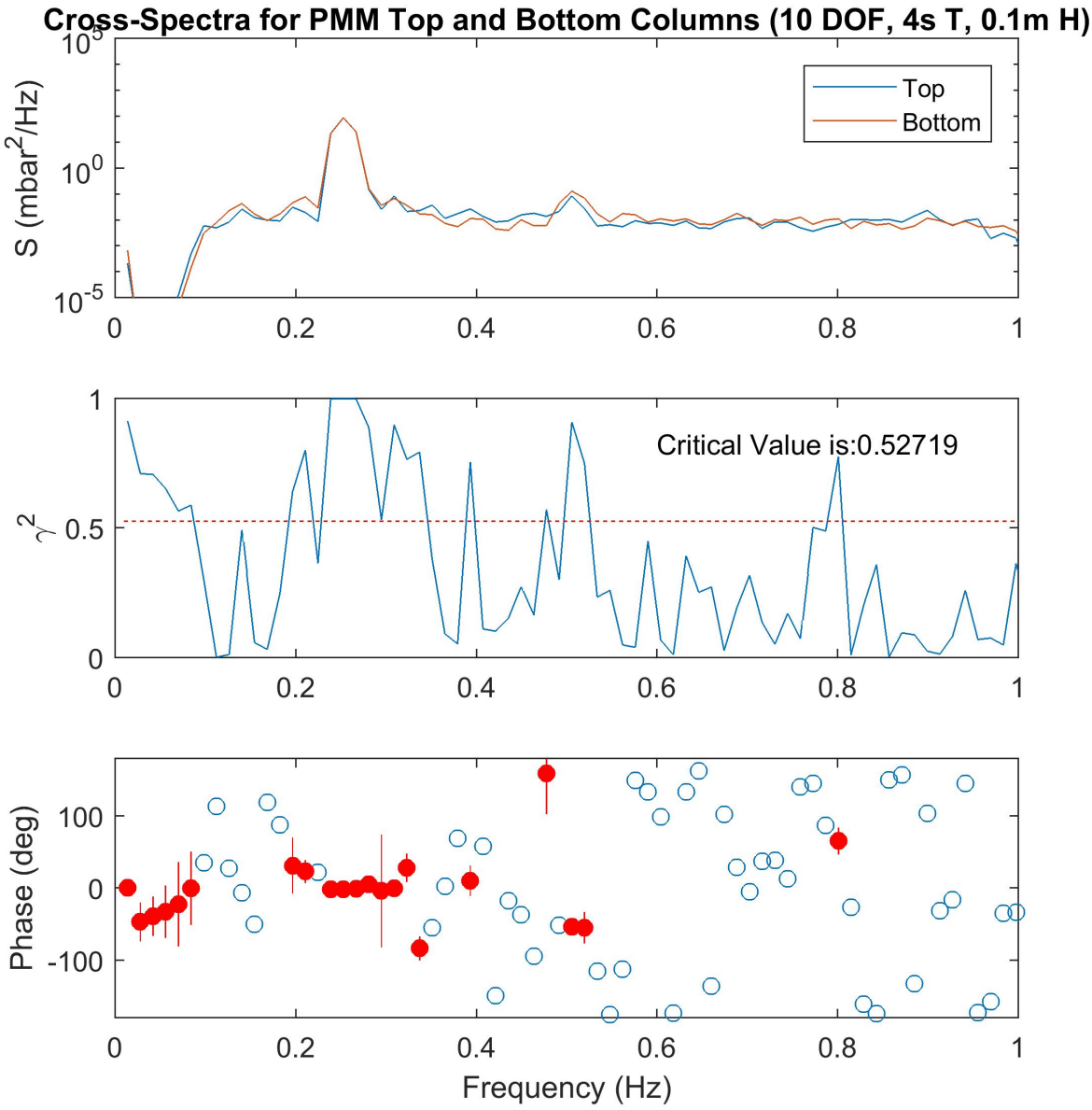

Figure 4.23: Cross-Spectra between PMM Pressure sensors on the top and bottom a during 4 s wave simulation when PMM was fully exposed. Top plot shows the spectra for each signal. Middle plot shows the squared coherency between the two spectra and the 95% confidence critical value. Bottom plot shows the phase difference between the two spectra, with the red circles indicating phases with statistically significant squared coherency at the 95% level and red lines indicating 95% confidence intervals for the phase values.

The purpose of having the pressure sensors on the surface of the PMM is to resolve the pressure in different locations on the surface and relate them to one another. Figure 4.24 demonstrates the PMM's capability of this. The top panel shows the surface elevation changing with a passing 4 s, 0.1 m simulated wave. The middle panel shows the averaged pressure of each column with the hydrostatic component removed, so only the fluctuations due to the passing wave are visible. The second panel also includes the average pressure of the four columns. The third panel shows how the column facing the beach and the column facing the wave paddle compare to the PMM instantaneous average pressure from all the columns. As the surface elevation increases, the pressure on the paddle side increases and the beach side pressure decreases. Then, as the surface elevation decreases, the paddle side pressure decreases and the beach side pressure increases. This demonstrates the PMM's ability to recreate passing waves or vortex shedding schemes that are creating dynamic pressure gradients on the surface of the cylinder. The fourth panel shows how the top and bottom columns compare to the PMM instantaneous average pressure from all the columns. The dynamics here are more complex, indicating that dP/dx and dP/dz behave differently.

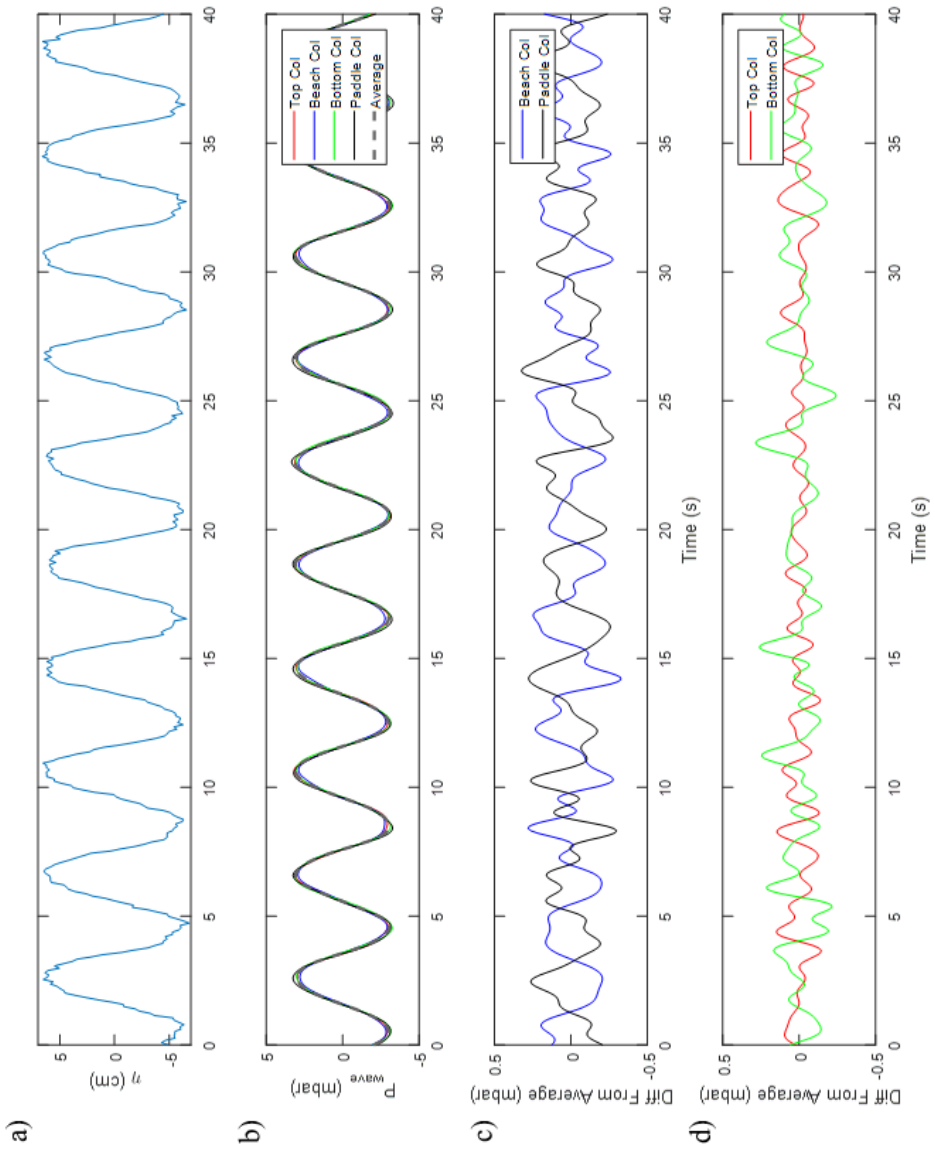

Figure 4.24: Pressure around the PMM. a) Water surface elevation vs. time for 4 s wave simulation. b) Column-average pressure fluctuations from passing wave (red, blue, green, black) and average of the four columns (gray dashed) c) Difference between single column average and average of all four columns for beach side (blue) and paddle side (black). d) Difference between single column average and average of all four columns for top side (red) and bottom side (green).

4.5 Fixed Floor Wave Test

The resolution of the sensor was improved by multiplying the pressure by a factor of 10 in the C++ library and dividing by 10 before writing the data to the SD card. As a result of this multiplication and division, the pressure sensor can now read to the nearest 0.1 mbar. Since the reported root mean square of the pressure sensor is 0.2 mbar, this is likely the most useful resolution for this sensor. To determine the impact the previous discretizing had on the sensors, a comparable experiment was run with the instrument at its higher resolution. The purpose of this experiment is to compare the root mean square of the noise with the better resolution and to rotate the PMM to ensure all sensors collect comparable data at all locations around the surface of the instrument.

The Vector's frame was deployed in the same location in the wave and tow tank, although the top portion was removed so the Vector now sampled 47.75 cm above the floor of the tank. Directly under the Vector, there was a large thin sheet of PVC with vertical and horizontal lines that allowed the diver to ensure the PMM was centered and aligned straight. The PMM went in the center of this PVC sheet, directly below the sampling point of the Vector. Before data was collected, wave simulations were run to ensure that the PVC would remain in place during the wave simulations. The PVC end cap additions used previously in the rolling test were machined to be an octagon shape, as seen in Figure 4.25.

The octagon end caps allow the PMM to be accurately rotated in 45^o increments instead of 90^o. The first column of sensors began on top of the PMM, then 45^o rotations were made towards the beach. All orientations are shown in Figure 4.26. Only two wave simulations were run in this experiment: a 4 s, 0.1 m wave and a 3.75 s, 0.1 m wave. These were the first two wave simulations used in the sand and wave experiment.

Figure 4.25: Octagon PVC end cap additions for higher resolution wave tests. Column 1 of sensors is marked with green electrical tape.

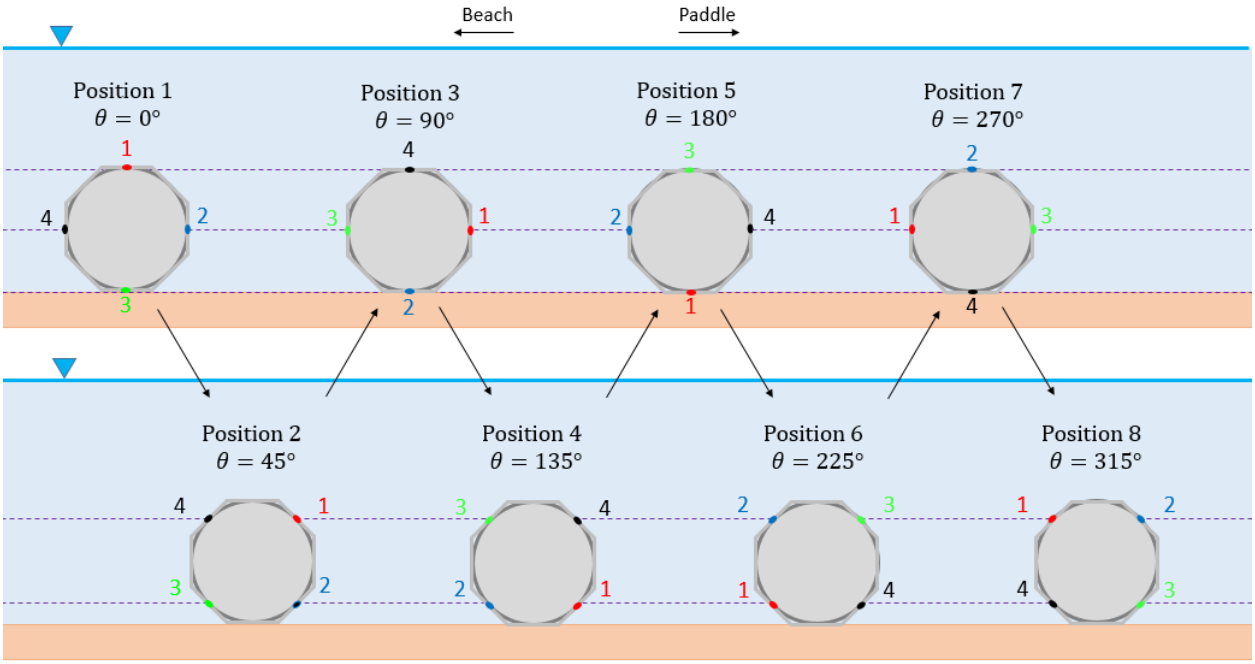

Figure 4.26: PMM orientations for higher resolution wave tests. Octagon end caps allowed for accurate 45^o rotations. PMM column numbers can be seen in red, black, green, and blue. Dashed lines indicate the various hydrostatic conditions of the sensors depending on the PMM orientation. The wave paddle is to the left and the beach is to the right.

The data analyses performed in the wave and sand experiment were repeated and the results were mostly consistent with the previous simulations. However, this second experiment allowed for a closer look at the orbital pressure magnitude and standard deviation of the pressure comparison (see Figure 4.27a). A circular pattern was present for some wave conditions in the previous experiment, but they are much more defined in this figure. Figure 4.27b is the phenomena for only the 4 s wave simulation. The colors indicate the sensor's location around the cylinder, while the symbols indicate the sensor's column number. For all sensors, the standard deviation of the pressure signal is smaller on the beach side of the PMM and larger on the paddle side. This could indicate nonlinearities in the flow introduced by nonlinearities in the forcing.

Improving the resolution of the sensor should allow for a lower noise floor in the spectra of the pressure sensors. Figure 4.28a shows a spectra from each sensor resolution during a 4 s wave simulation. The mean noise floor was lowered, and the root mean square of the noise for the 0.1 mbar resolution data is 0.25 mbar. The standard deviation of a Gaussian noise signal of ± 0.05 mbar is 0.028 mbar. This indicates that the bit noise is no longer on the same order of magnitude as the sensor noise. Figure 4.28b shows the column-averaged spectra from the two sensor resolutions.

Rotating the PMM and repeating the same wave conditions allows a comparison between columns when they are at the same location on the PMM. Figure 4.29 shows the column-averaged spectra of each column when it was at the top position of the PMM. As expected, the sensors measure the same energy at the frequency of the wave and the first harmonic. This indicates that each sensor behaves efficiently and the PMM will collect the same data regardless of which column is at a given orientation.

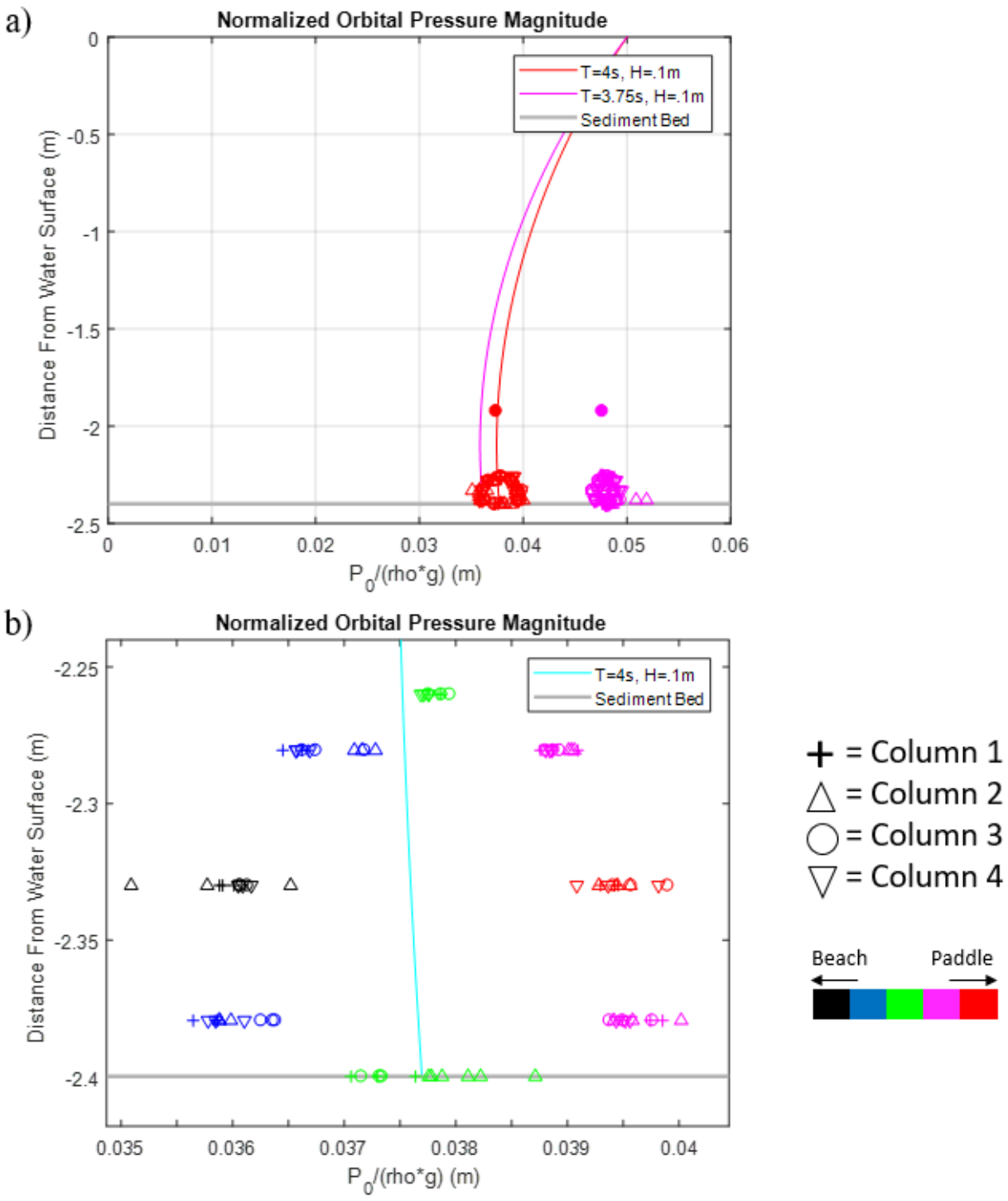

Figure 4.27: Normalized orbital pressure magnitude calculated by LWT. Symbols indicate a normalized standard deviation of the wave ($\sqrt{2}\sigma/\rho g$) for each pressure sensor (+ = column 1, △ = column 2, o = column 3, ▽ = column 4). a) Colors indicate wave parameters (red = 4 s period and 0.1 m wave height, magenta = 3.75 s period and 0.1 m wave height). Colored circles indicate normalized standard deviation of pressure measured by the Vector. b) Colors indicate location of sensor (warmer colors towards paddle, cooler colors towards beach)

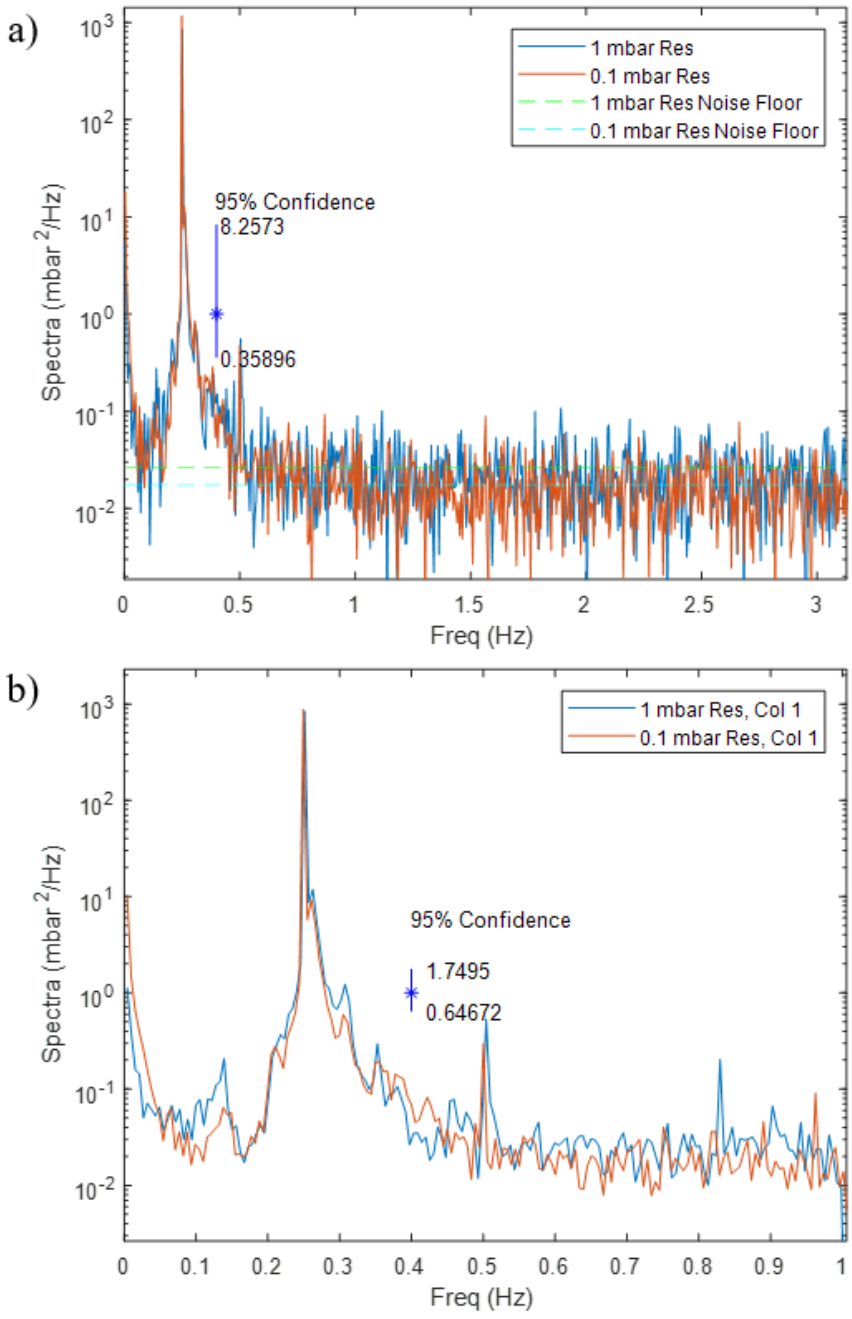

Figure 4.28: Spectra of PMM sensor: this representative data was collected during the 4 s wave. The blue spectra is from the 1 mbar resolution tests, and the red spectra is from the 0.1 mbar resolution tests. a) These spectra are from sensor 2 when it is on top of the PMM. The green dashed line is the mean noise floor for the 1 mbar spectra, and the cyan dashed line below is the mean noise floor for the 0.1 mbar spectra. b) Averaged spectra of column 1 when it is on top of the PMM.

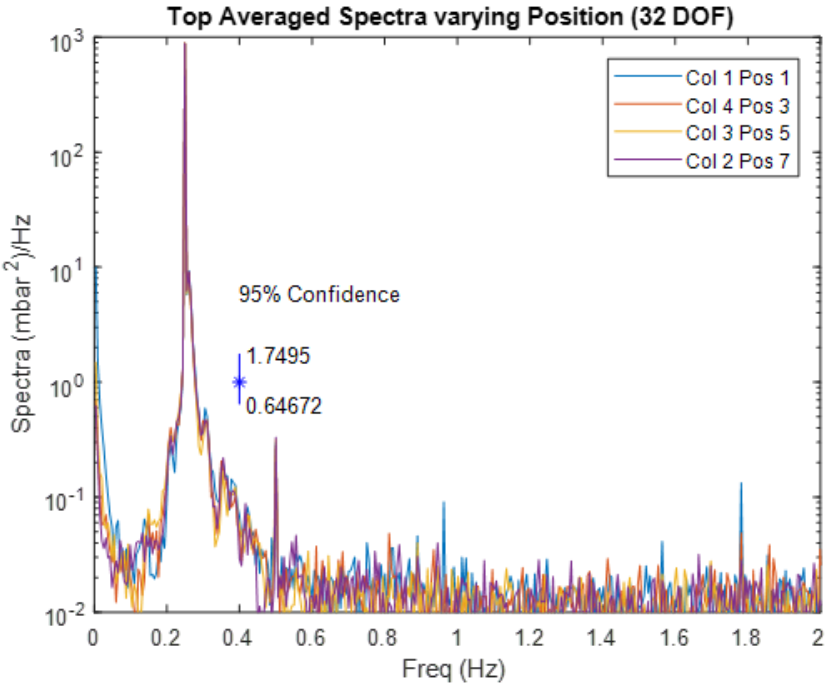

Figure 4.29: Column-averaged spectra of PMM sensor: this representative data was collected during the 4 s wave. The spectra are of each column when they were in the top position on the PMM.

CHAPTER 5

CONCLUSIONS

A pressure-mapped model munition has been designed, fabricated, and tested in a laboratory setting. The MS5837-30BA diaphragm pressure sensors used for measure surface pressure on the instrument can experience drift up to 1 mbar/hour, which is the hydrostatic equivalent of 1 cm of water per hour, and showed offsets of up to 50 mbar, or 50 cm of hydrostatic pressure. However, the pressure sensors accurately recorded changes in pressure due to hydrostatic changes and passing waves with a noise rms of only 0.25 mbar, or 2.5 mm of hydrostatic pressure.This result was promising for this research because the interest is in recording dynamic pressure gradients; however, some sort of reference pressure sensor needs to be added to the instrument so hydrostatic conditions can be calculated. The rolling experiment and the overnight drift experiment proved that a reference pressure sensor, in combination with the orientation data from the IMU on board the instrument, can be used to recreate the steady state pressures the MS5837 sensors should be recording. A reference temperature sensor installed on the surface would allow for better characterization of the instrument's response to environment changes.

The laboratory experiments have demonstrated the current PMM's capabilities to capture passing waves or vortex shedding schemes causing dynamic pressure gradients on the surface of the cylinder. The instrument also resolved wave motions as accurately as standard field instruments.The largest KC value for the flow in the laboratory experiments was 3.1, meaning that, if the cylinder were in the freestream, there would be vortices shedding twice a wave period. However, the cylinder was always sitting proud or partially buried in the bed, which limits vortex growth. While there is some literature on how vortices form, the nearshore environment is so complex that it is incredibly difficult to predict the magnitude of the pressure gradients formed by the shedding vortices in every situation it will see in the field. This instrument will allow for quantatative

measurements of vortices in controlled, laboratory experiments and in nearshore environments, improving the understanding of fluid around a cylinder. Once a reference pressure and temperature sensor is installed on its surface, the PMM is ready to be deployed in the field, where it can make a meaningful contribution to incipient motion and munition mobility research.

BIBLIOGRAPHY

[1] P. W. Bearman and M. M. Zdravkovich. Flow around a circular cylinder near a plane boundary. *Journal of Fluid Mechanics*, 1978.

[2] F. T. Boutell. I2C communication system and method enabling bi-directional communications. *US Patent Application US20050165989A1*, 1(19), 2004.

[3] P. A. Davidson. *Turbulence: An Introduction For Scientists and Engineers*. Oxford University Press, Oxford, NY, 1 edition, 2004.

[4] R. Figliola and D. Beasley. Theory and design for mechanical measurements. page 590, 2011.

[5] D. L. Foster, A. J. Bowen, R. A. Holman, and P. Natoo. Field evidence of pressure gradient induced incipient motion. *Journal of Geophysical Research: Oceans*, 2006.

[6] D. Frank, D. Foster, I. M. Sou, and J. Calantoni. Incipient motion of surf zone sediments. *Journal of Geophysical Research: Oceans*, 2015.

[7] D. L. Inman and S. A. Jenkins. Srour and Burial of Objects in Shallow Water. *Encyclopedia of Coastal Science*, pages 825–830, 2005.

[8] J. Irish and M. Levine. Digitizing error from period and frequency counting techniques. *Deep-Sea Res.*, (25):211–219, 1978.

[9] S. E. Rennie, A. Brandt, and C. T. Friedrichs. Initiation of motion and scour burial of objects underwater. *Ocean Engineering*, 131(March 2016):282–294, 2017.

[10] SERDP. Munitions Response (MR) Program Area DETECTION , CLASSIFICATION , AND REMEDIATION OF MILITARY. *SON Number: MRSON-17-01*, 2015.

[11] A. Shields. Anwendung der Aehnlichkeitsmechanik und der Turbulenzforschung auf die Geschiebebewegung. Technical report, 1936.

[12] J. F. Sleath. Conditions for plug formation in oscillatory flow. *Continental Shelf Research*, 1999.

[13] H. D. Smith, S. M. Asce, D. L. Foster, and a. M. Asce. Three-Dimensional Flow around a Bottom-Mounted Short Cylinder. 133(5):534–544, 2007.

[14] B. M. Sumer and J. Fredsoe. *The Mechanics of Scour in the Marine Environment*. World Scientific, Advanced Series on Ocean Engineering, Volume 17, 2002.

[15] B. M. Sumer and J. Fredsøe. *Hydrodynamics Around Cylindrical Structures (Revised Edition)*. World Scientific, Advanced Series on Ocean Engineering, Volume 26, 2006.

[16] TE Connectivity. MS5837-30BA Ultra Small Gel Filled Pressure Sensor. m, 2015.

[17] Tekscan. FlexiForceâĎć. pages 54–55, 2016.

APPENDIX A

SENSOR NUMBERING

There are 16 pressure sensors in this instrument, so to keep track of the sensors during the wiring and data analysis process, a numbering system had to be created. The equation below describes the relationship between each sensor number and its location on the cylinder. For example, the sensor in the first row of the first column is sensor 1, the last row in the first column is sensor 4, and the last row in the last column is sensor 16.

$$[Sensor\ \#] = [Row\ \#] + 4 * ([Column\#] - 1)$$

Columns are defined as running along the length of the cylinder, while rows describe the distance from the end cap to which the shelf brackets.

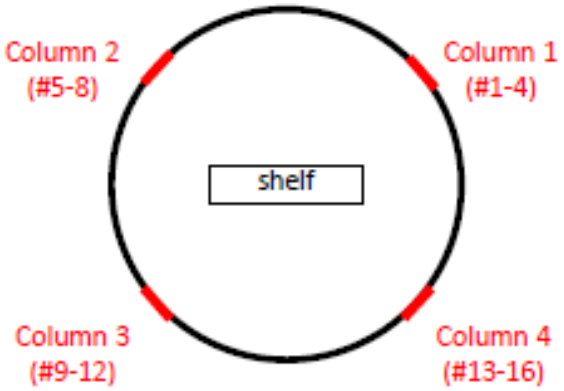

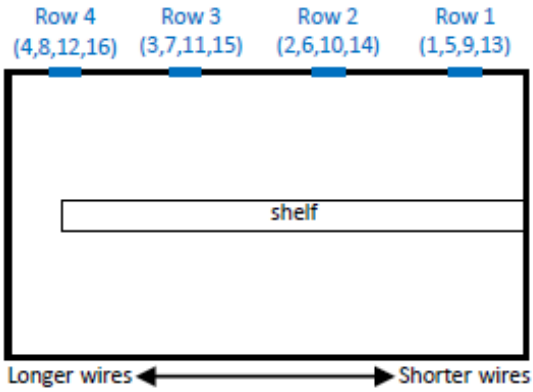

Two groups of black lines on the data and clock wires indicate the sensor number so the sensor can be plugged into the correct location on the multiplexer. This also ensures that each sensor is numbered properly during data analysis. The first group of lines closest to the pin indicates the row number, while the second indicates the column number.

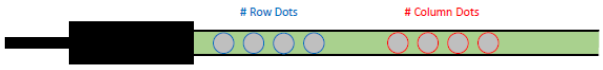

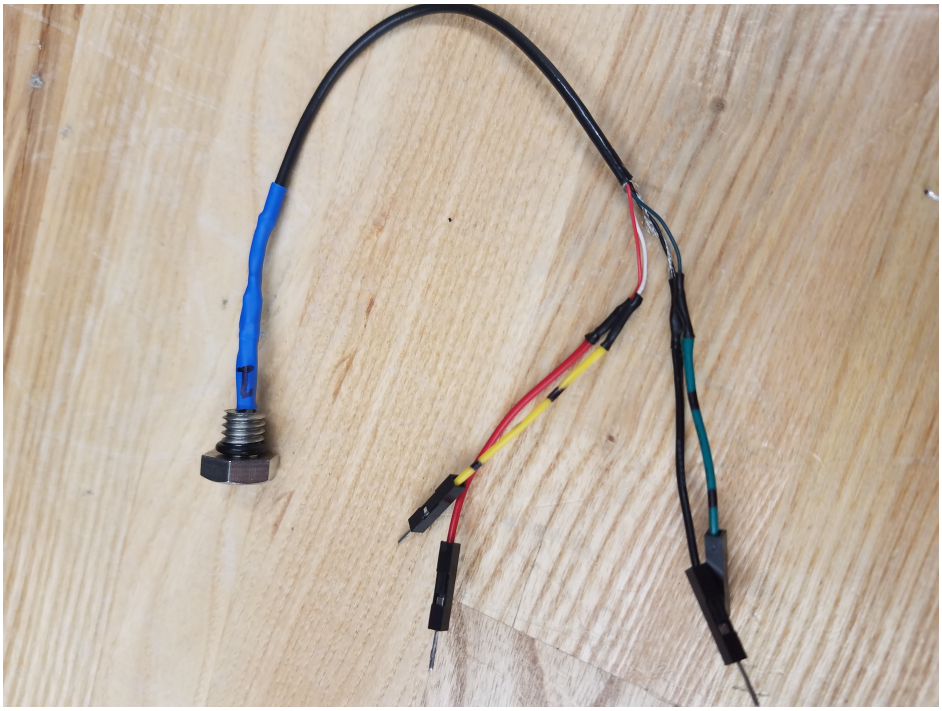

APPENDIX B

CALCULATIONS

From Linear Wave Theory [14], the sea surface elevation and pressure fluctuations are given by:

$$\eta = \frac{H}{2} cos(\frac{2\pi}{T}) \tag{B.1}$$

$$P = \rho g \eta \frac{cosh(2\pi(d+z)/L)}{cosh(2\pi d/L)} \tag{B.2}$$

Solving for the standard deviation of the sea surface elevation:

$$\sigma_\eta = \sqrt{\frac{1}{T}\int_0^T (\frac{H}{2})^2 cos^2(\frac{2\pi}{T}) dt} \tag{B.3}$$

Solving this integral gives:

$$\frac{H}{2} = \sqrt{2}\sigma_\eta \tag{B.4}$$

Solving for the standard deviation of the pressure fluctuations using the sea surface elevation standard deviation:

$$\sigma_p = \rho g \sigma_\eta \frac{cosh(2\pi(d+z)/L)}{cosh(2\pi d/L)} \tag{B.5}$$

Sow taking the pressure equation and assuming t = 0 to obtain the maximum value:

$$P_o = \rho g \frac{H}{2} \frac{cosh(2\pi(d+z)/L)}{cosh(2\pi d/L)} \tag{B.6}$$

Substituting in equations B.4 and B.5 into equation B.6 and dividing through by ρg gives:

$$\frac{P_o}{\rho g} = \frac{\sqrt{2}\sigma_p}{\rho g} = \frac{H}{2} \frac{cosh(2\pi(d+z)/L)}{cosh(2\pi d/L)} \tag{B.7}$$

APPENDIX C

TECHNICAL DRAWINGS

The following pages in this section are the technical drawings for all the machined parts of the PMM. These parts were designed and these drwaings created in Solidworks.

ITEM NO.	PART NUMBER	QTY.
1	PIPE (MCMASTER PART NO 89495K28)	1
2	ENDCAP_SCREW	1
3	ENDCAP_PEG	1
4	WINDOW	1
5	SHELF	1
6	SCREW (MCMASTER PART NO 93190A578)	16
7	STUD (MCMASTER PART NO 92314A257)	2
8	bracket	2

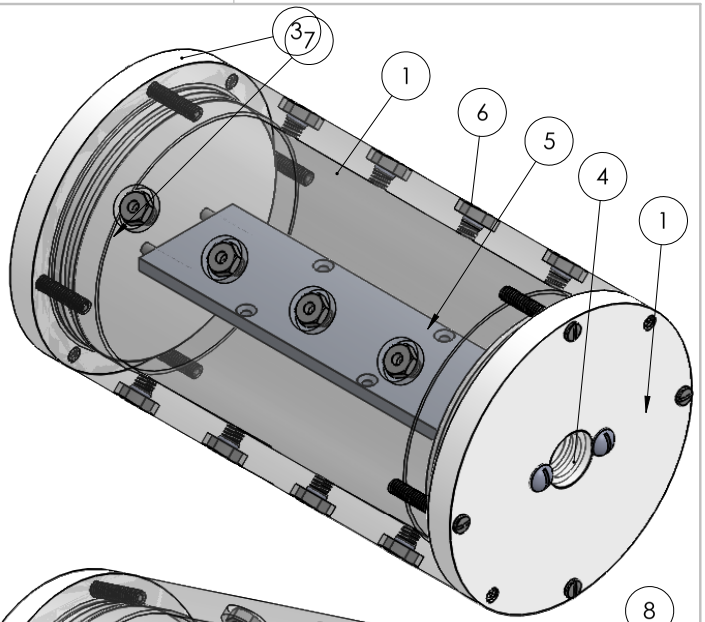

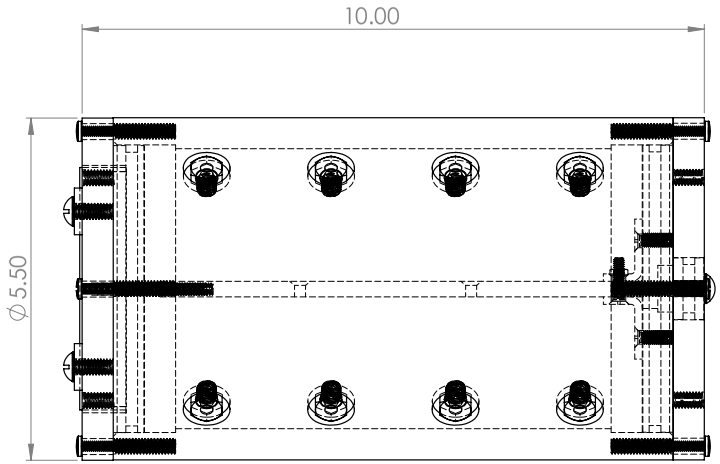

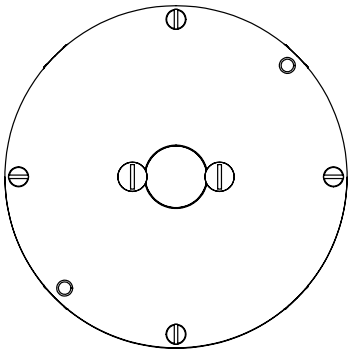

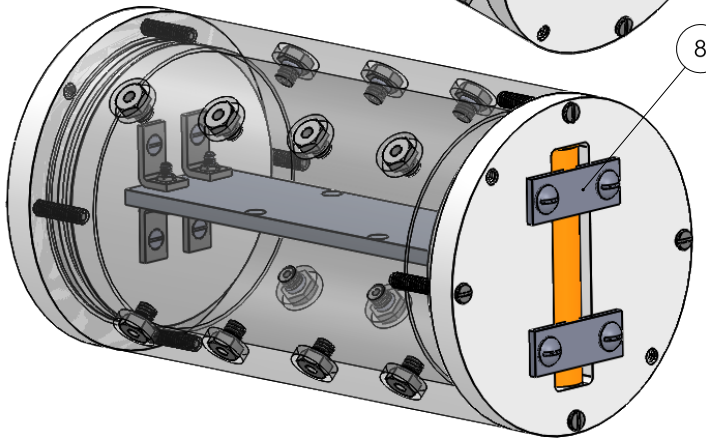

		UNLESS OTHERWISE SPECIFIED:		NAME	DATE
		DIMENSIONS ARE IN INCHES TOLERANCES: X.XXX=±0.005 X.XX=±0.01	DRAWN	SG	9/26/2017
			CHECKED		
			ENG APPR.		
			MFG APPR.		
		INTERPRET GEOMETRIC TOLERANCING PER:	Q.A.		
		MATERIAL	COMMENTS: FINAL DRAWING (10/17/2017)		
NEXT ASSY	USED ON	FINISH			
APPLICATION		DO NOT SCALE DRAWING			

TITLE: TOTAL ASSEMBLY

SIZE	DWG. NO.	REV
B	UNH_MUNITION	

SCALE: 1:2 | WEIGHT: | SHEET 1 OF 9

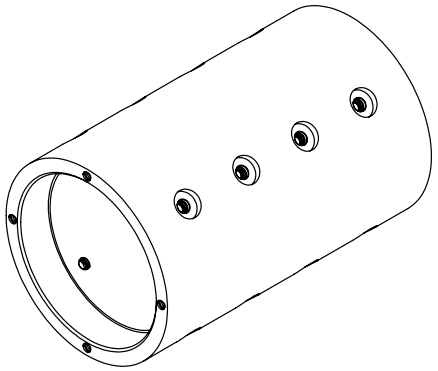

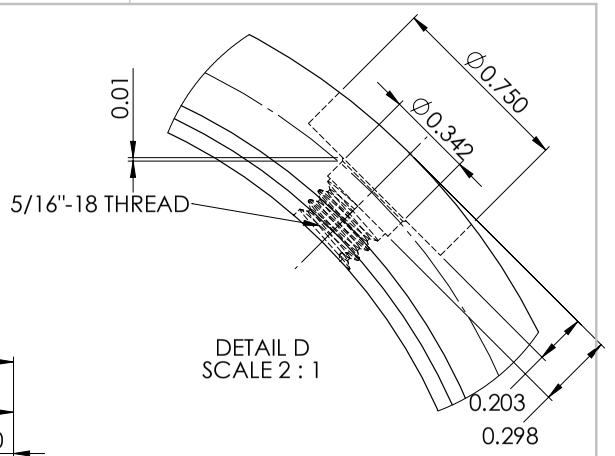

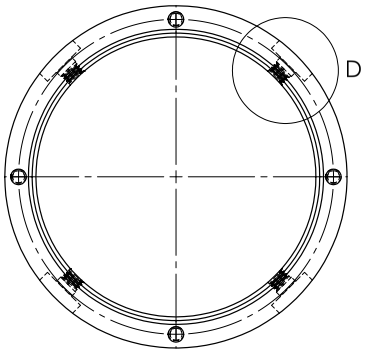

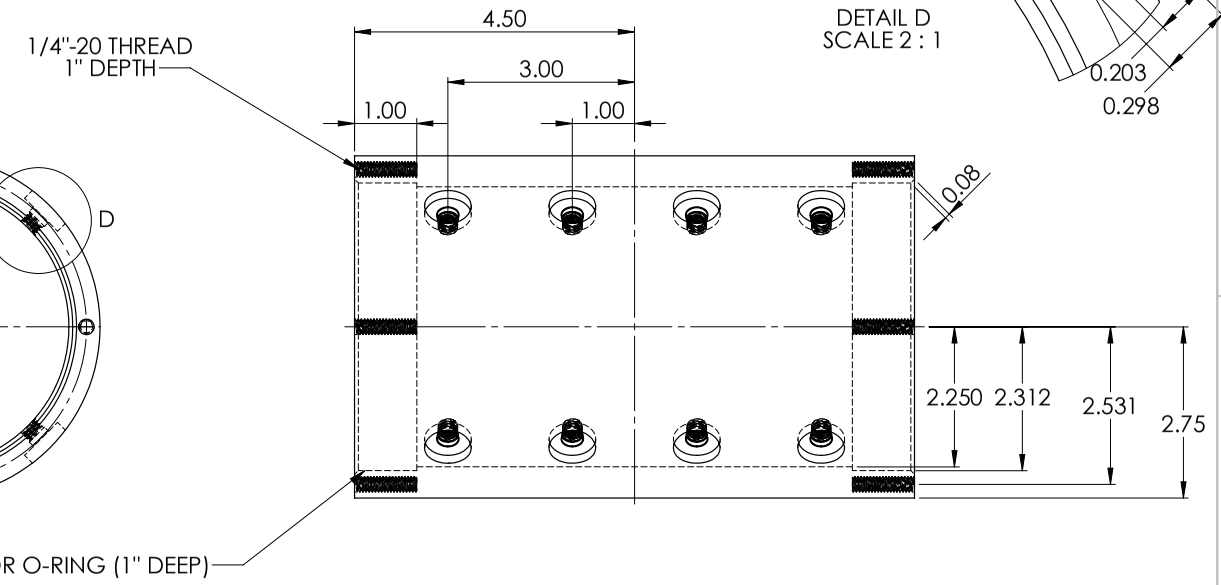

		UNLESS OTHERWISE SPECIFIED:		NAME	DATE
		DIMENSIONS ARE IN INCHES TOLERANCES: X.XXX=±0.005 X.XX=±0.01	DRAWN	SG	9/26/17
			CHECKED		
			ENG APPR.		
			MFG APPR.		
		INTERPRET GEOMETRIC TOLERANCING PER:	Q.A.		
		MATERIAL 304 STAINLESS STEEL	COMMENTS: MAKE ONE		
NEXT ASSY	USED ON	FINISH			
APPLICATION		DO NOT SCALE DRAWING			

MCMASTER PART NO 89495K28

TITLE:

PIPE (ITEM 1)

SIZE	DWG. NO.	REV
B	UNH_MUNITION	

SCALE: 1:2 | WEIGHT: | SHEET 2 OF 9

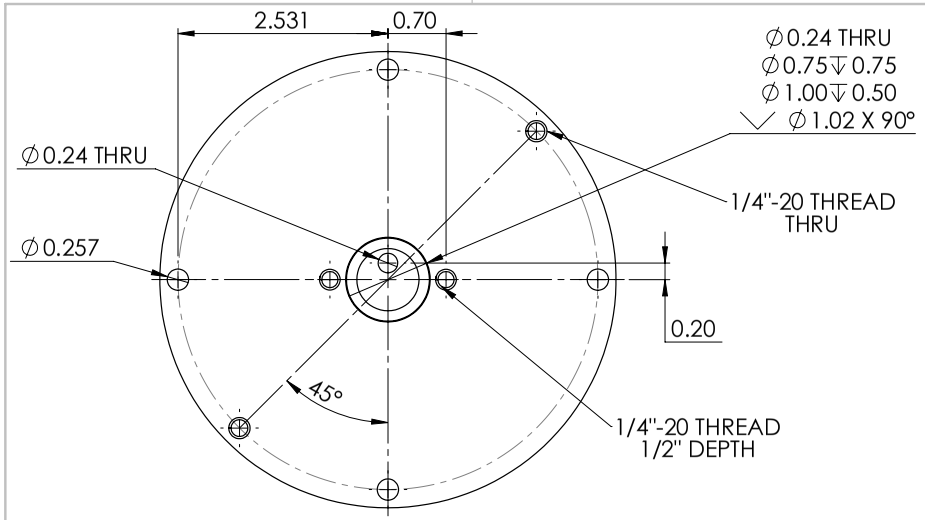

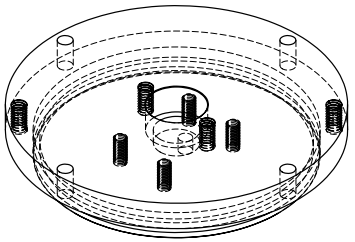

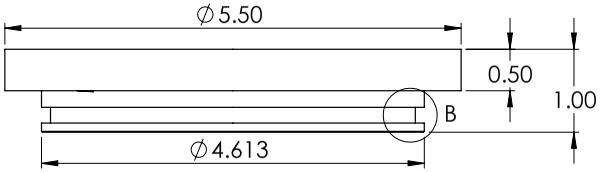

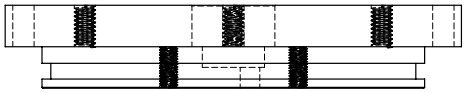

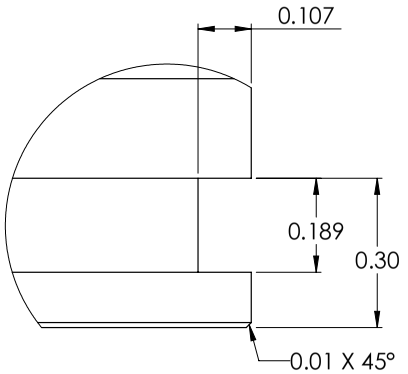

DETAIL B
SCALE 4 : 1

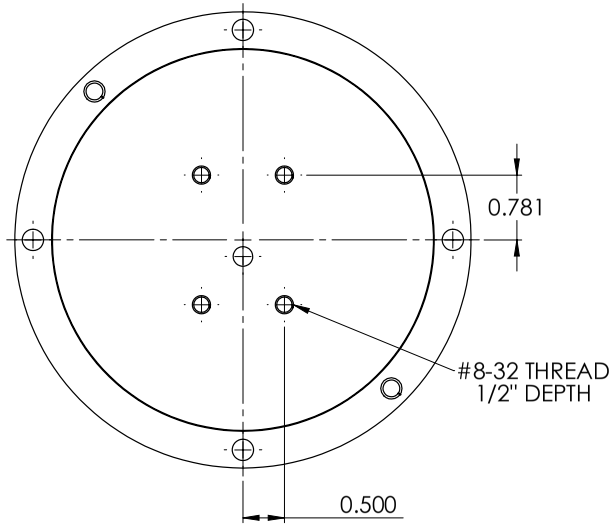

		UNLESS OTHERWISE SPECIFIED:		NAME	DATE
		DIMENSIONS ARE IN INCHES TOLERANCES: X.XXX=±0.005 X.XX=±0.01	DRAWN	SG	9/26/17
			CHECKED		
			ENG APPR.		
			MFG APPR.		
		INTERPRET GEOMETRIC TOLERANCING PER:	Q.A.		
		MATERIAL PVC	COMMENTS: MAKE ONE		
NEXT ASSY	USED ON	FINISH			
APPLICATION		DO NOT SCALE DRAWING			

TITLE:
ENDCAP_SCREW (ITEM 2)

SIZE	DWG. NO.	REV
B	UNH_MUNITION	

SCALE: 1:2 | WEIGHT: | SHEET 3 OF 9

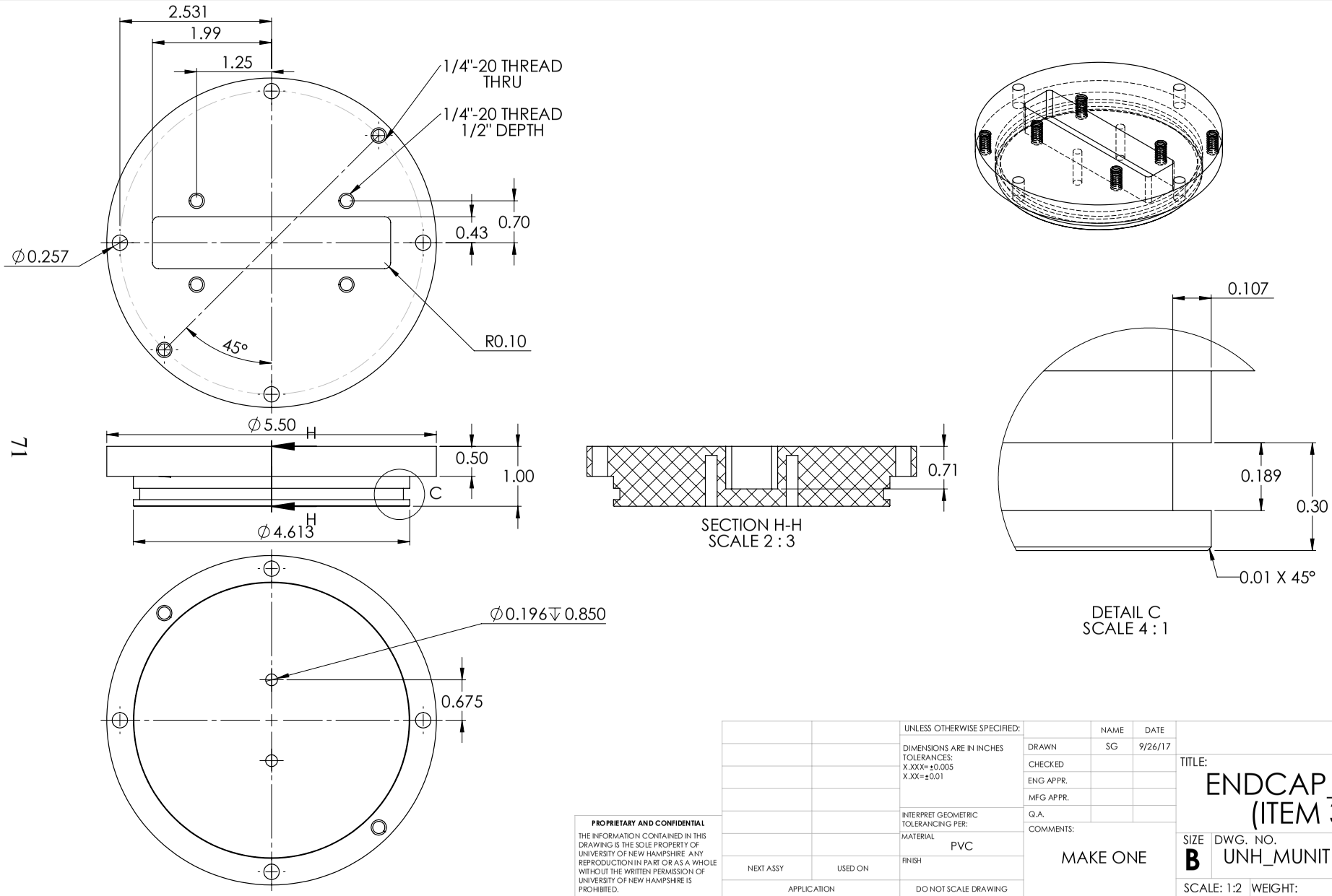

		UNLESS OTHERWISE SPECIFIED:		NAME	DATE
		DIMENSIONS ARE IN INCHES TOLERANCES: X.XXX=±0.005 X.XX=±0.01	DRAWN	SG	9/26/17
			CHECKED		
			ENG APPR.		
			MFG APPR.		
		INTERPRET GEOMETRIC TOLERANCING PER:	Q.A.		
		MATERIAL PVC	COMMENTS: MAKE ONE		
NEXT ASSY	USED ON	FINISH			
APPLICATION		DO NOT SCALE DRAWING			

TITLE:
ENDCAP_PEG (ITEM 3)

SIZE	DWG. NO.	REV
B	UNH_MUNITION	

SCALE: 1:2 | WEIGHT: | SHEET 4 OF 9

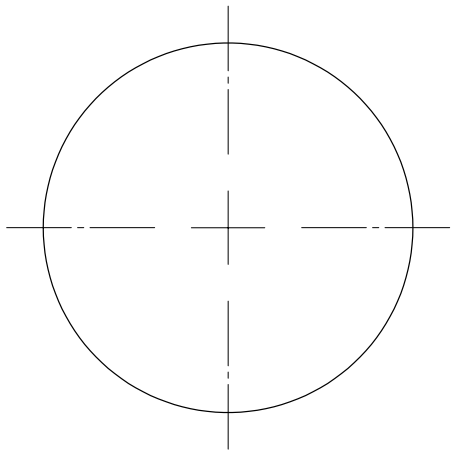

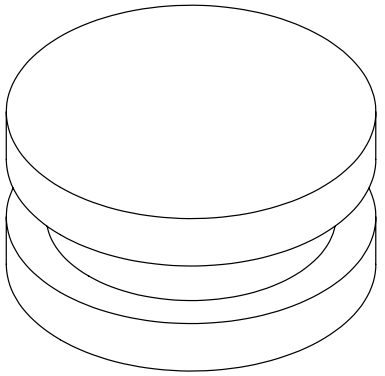

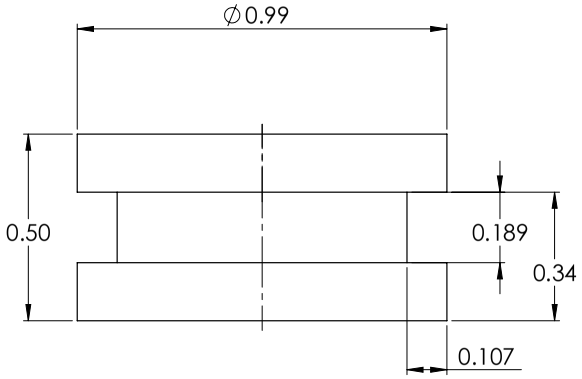

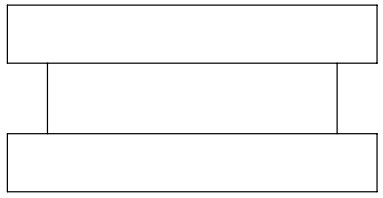

		UNLESS OTHERWISE SPECIFIED:		NAME	DATE
		DIMENSIONS ARE IN INCHES TOLERANCES: X.XXX=±0.005 X.XX=±0.01	DRAWN	SG	9/26/17
			CHECKED		
			ENG APPR.		
			MFG APPR.		
		INTERPRET GEOMETRIC TOLERANCING PER:	Q.A.		
		MATERIAL CLEAR ACRYLIC	COMMENTS: MAKE TWO		
NEXT ASSY	USED ON	FINISH			
APPLICATION		DO NOT SCALE DRAWING			

TITLE:

WINDOW (ITEM 4)

SIZE	DWG. NO.	REV
B	UNH_MUNITION	

SCALE: 3:1	WEIGHT:	SHEET 5 OF 9

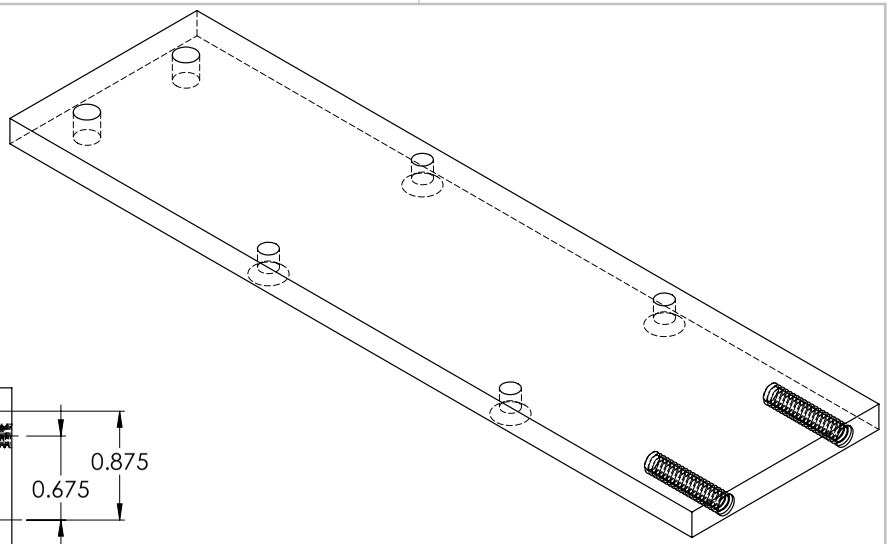

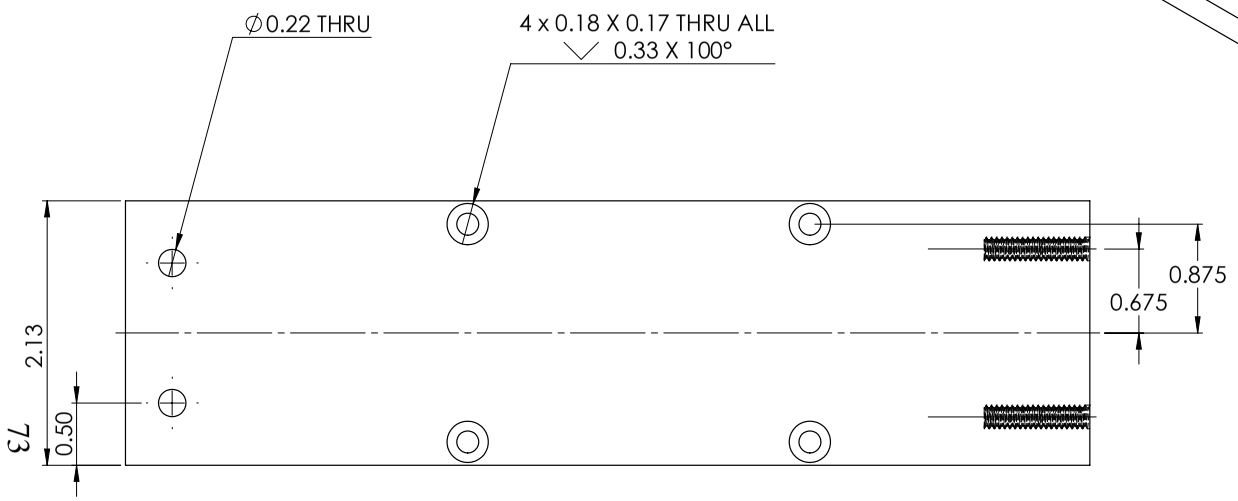

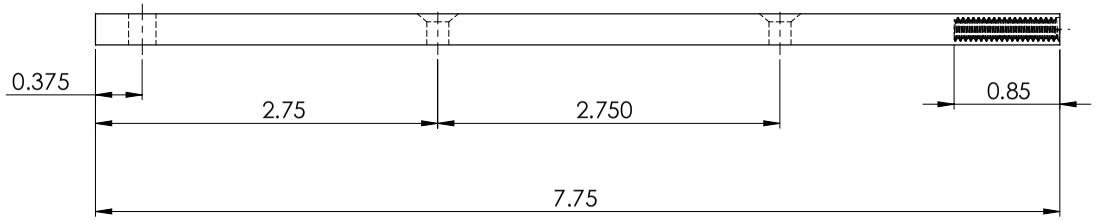

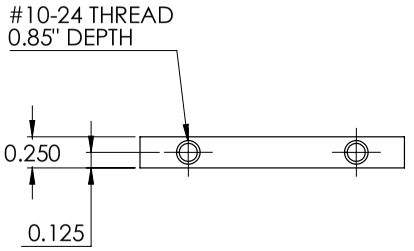

		UNLESS OTHERWISE SPECIFIED:		NAME	DATE
		DIMENSIONS ARE IN INCHES TOLERANCES: X.XXX=±0.005 X.XX=±0.01	DRAWN	SG	9/26/17
			CHECKED		
			ENG APPR.		
			MFG APPR.		
		INTERPRET GEOMETRIC TOLERANCING PER:	Q.A.		
		MATERIAL 6061 ALUMINUM	COMMENTS: MAKE ONE		
NEXT ASSY	USED ON	FINISH			
APPLICATION		DO NOT SCALE DRAWING			

TITLE:

SHELF (ITEM 5)

SIZE	DWG. NO.	REV
B	UNH_MUNITION	

SCALE: 1:2	WEIGHT:	SHEET 6 OF 9

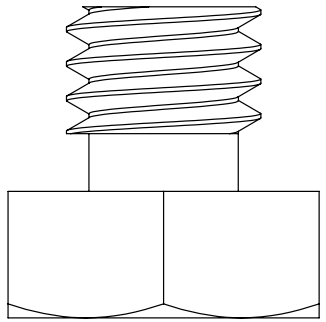

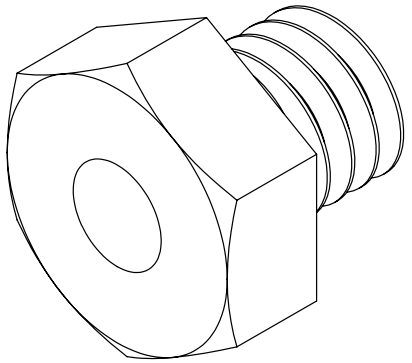

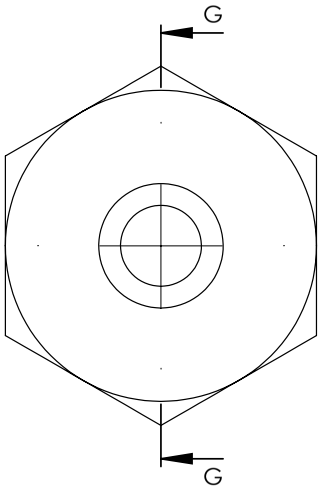

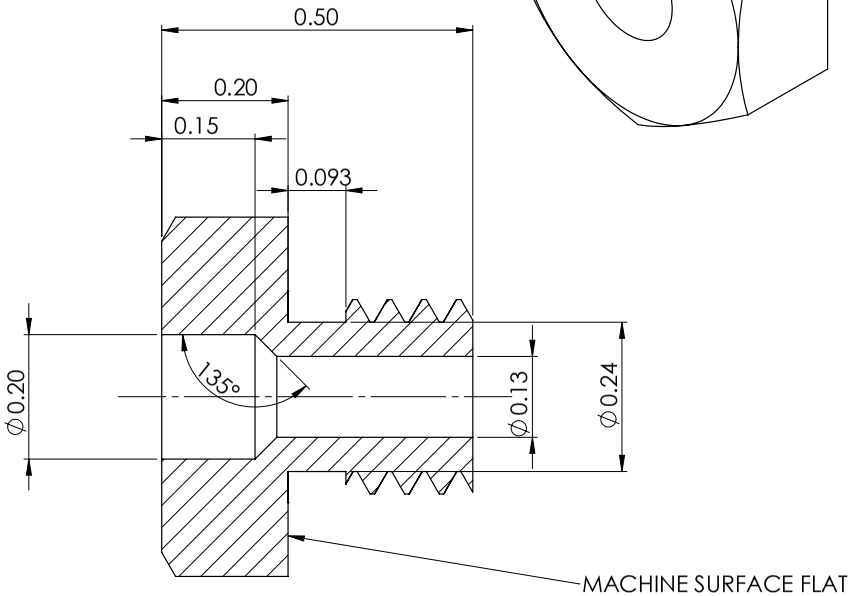

SECTION G-G
SCALE 5 : 1

		UNLESS OTHERWISE SPECIFIED:		NAME	DATE
		DIMENSIONS ARE IN INCHES TOLERANCES: X.XXX=±0.005 X.XX=±0.01	DRAWN	SG	10/9/17
			CHECKED		
			ENG APPR.		
			MFG APPR.		
		INTERPRET GEOMETRIC TOLERANCING PER:	Q.A.		
		MATERIAL ZINC-PLATED STEEL	COMMENTS: MAKE 16		
NEXT ASSY	USED ON	FINISH			
APPLICATION		DO NOT SCALE DRAWING			

MCMASTER PART NO 93190A578

TITLE:

SCREW (ITEM 6)

SIZE	DWG. NO.	REV
B	UNH_MUNITION	

SCALE: 1:2	WEIGHT:	SHEET 7 OF 9

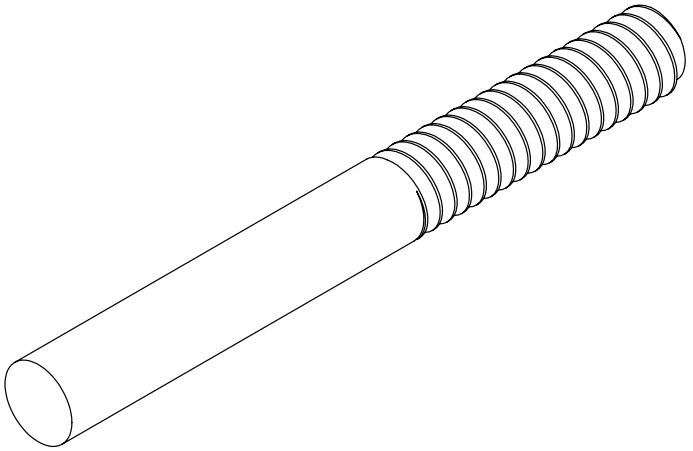

.75

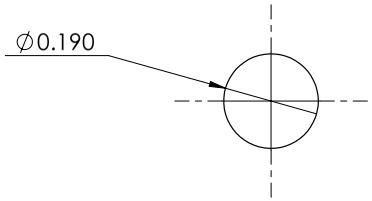

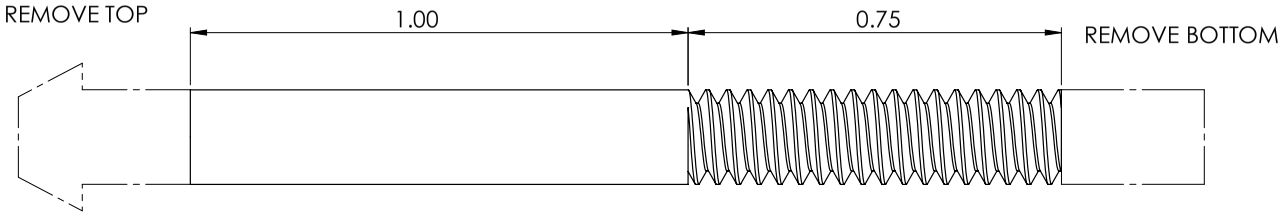

		UNLESS OTHERWISE SPECIFIED:		NAME	DATE
		DIMENSIONS ARE IN INCHES TOLERANCES: X.XXX=±0.005 X.XX=±0.01	DRAWN	SG	10/9/17
			CHECKED		
			ENG APPR.		
			MFG APPR.		
		INTERPRET GEOMETRIC TOLERANCING PER:	Q.A.		
		MATERIAL	COMMENTS: MAKE TWO		
NEXT ASSY	USED ON	FINISH			
APPLICATION		DO NOT SCALE DRAWING			

MCMASTER PART NO 92314A257

TITLE:

STUD (ITEM 7)

SIZE	DWG. NO.	REV
B	UNH_MUNITION	

SCALE: 1:2 | WEIGHT: | SHEET 8 OF 9

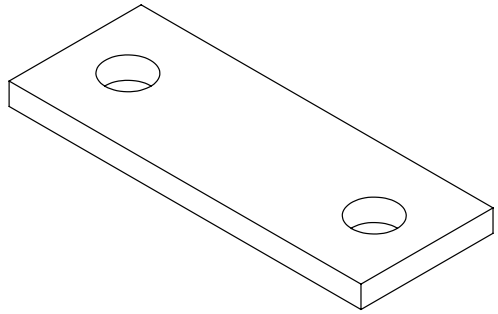

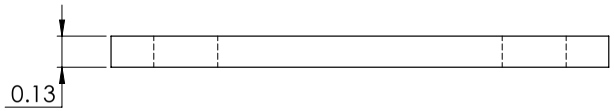

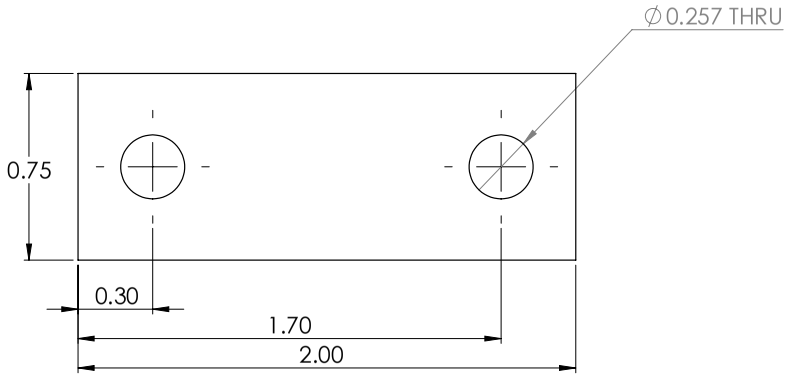

		UNLESS OTHERWISE SPECIFIED:		NAME	DATE
		DIMENSIONS ARE IN INCHES TOLERANCES: X.XXX= ±0.005 X.XX= ±0.01	DRAWN	SG	10/31/17
			CHECKED		
			ENG APPR.		
			MFG APPR.		
		INTERPRET GEOMETRIC TOLERANCING PER:	Q.A.		
		MATERIAL 304 STAINLESS STEEL	COMMENTS: MAKE TWO		
NEXT ASSY	USED ON	FINISH			
APPLICATION		DO NOT SCALE DRAWING			

TITLE: BRACKET (ITEM 8)

SIZE	DWG. NO.	REV
B	UNH_MUNITION	

SCALE: 1:2	WEIGHT:	SHEET 9 OF 9

APPENDIX D

DATASHEETS

RoHS

MS5837-30BA

Ultra Small Gel Filled Pressure Sensor

SPECIFICATIONS

- **Ceramic - metal package, 3.3 x 3.3 x 2.75mm**
- **High-resolution module 0.2 mbar**
- **Fast conversion down to 0.5 ms**
- **Low power, 0.6 µA (standby < 0.1 µA at 25°C)**
- **Integrated digital pressure sensor (24 bit ΔΣ ADC)**
- **Supply voltage 1.5 to 3.6 V**
- **Operating range: 0 to 30 bar, -20 to +85 °C**
- **I^2C interface**
- **No external components (Internal oscillator)**
- **Excellent long term stability**
- **Hermetically sealable for outdoor devices**
- **Sealing designed for 1.8 x 0.8mm O-ring**

The MS5837-30BA is a new generation of high resolution pressure sensors with I^2C bus interface for depth measurement systems with a water depth resolution of 2 mm. The sensor module includes a high linearity pressure sensor and an ultra-low power 24 bit ΔΣ ADC with internal factory calibrated coefficients. It provides a precise digital 24 Bit pressure and temperature value and different operation modes that allow the user to optimize for conversion speed and current consumption. A high resolution temperature output allows the implementation in depth measurement systems and thermometer function without any additional sensor. The MS5837-30BA can be interfaced to virtually any microcontroller. The communication protocol is simple, without the need of programming internal registers in the device. The gel protection and antimagnetic stainless steel cap make the module water resistant. This new sensor module generation is based on leading MEMS technology and latest benefits from MEAS Switzerland proven experience and know-how in high volume manufacturing, which has been widely used for over a decade.

PERFORMANCE SPECIFICATIONS

ABSOLUTE MAXIMUM RATINGS

Parameter	Symbol	Conditions	Min.	Typ.	Max	Unit
Supply voltage	V_{DD}		-0.3		+4	V
Storage temperature	T_S		-40		+85	°C
Overpressure	P_{max}	ISO 22810			50	Bar
Maximum Soldering Temperature	T_{max}	40 sec max			250	°C
ESD rating		Human Body Model	-2		+2	kV
Latch up		JEDEC standard No 78	-100		+100	mA

ELECTRICAL CHARACTERISTICS

Parameter	Symbol	Conditions		Min.	Typ.	Max	Unit
Operating Supply voltage	V_{DD}			1.5	3.0	3.6	V
Operating Temperature	T			-20	+25	+85	°C
Supply current (1 sample per sec.)	I_{DD}	OSR	8192 4096 2048 1024 512 256		20.09 10.05 5.02 2.51 1.26 0.63		µA
Peak supply current		during conversion			1.25		mA
Standby supply current		at 25°C			0.01	0.1	µA
VDD Capacitor		From VDD to GND		100	470		nF

ANALOG DIGITAL CONVERTER (ADC)

Parameter	Symbol	Conditions		Min.	Typ.	Max	Unit
Output Word					24		Bit
Conversion time (1)	t_c	OSR	8192 4096 2048 1024 512 256	14.8 7.40 3.72 1.88 0.95 0.48	16.44 8.22 4.13 2.08 1.06 0.54	18.08 9.04 4.54 2.28 1.17 0.60	ms

(1): Maximum values must be applied to determine waiting times in I2C communication

PERFORMANCE SPECIFICATIONS (CONTINUED)

PRESSURE OUTPUT CHARACTERISTICS (V_{DD} = 3 V, T = 25°C UNLESS OTHERWISE NOTED)

Parameter	Conditions		Min.	Typ.	Max	Unit
Operating Pressure Range	P_{range}	Full Accuracy	0		30	Bar
Absolute Accuracy (1), Temperature range: 0 … 40°C	0 … 6 bar 0 … 20 bar 0 … 30 bar		-50 -100 -200		+50 +100 +200	mbar
Absolute Accuracy (1), Temperature range: -20 … 85°C	0 … 6 bar 0 … 20 bar 0 … 30 bar		-100 -200 -400		+100 +200 +400	mbar
Maximum error with supply voltage (2)	V_{DD} = 1.5 V … 3.6 V			±30		mbar
Long-term stability				±30		mbar/year
Resolution RMS	OSR	8192 4096 2048 1024 512 256		0.20 0.28 0.38 0.54 0.84 1.57		mbar
Reflow soldering impact	IPC/JEDEC J-STD-020D.1 (See application note AN808 on http://meas-spec.com)			-8		mbar
Recovering time after reflow (3)				7		Days

(1) With autozero at one pressure point

(2) With autozero at 3V point

(3) Time to recover at least 66% of the reflow impact.

TEMPERATURE OUTPUT CHARACTERISTICS (V_{DD} = 3 V, T = 25°C UNLESS OTHERWISE NOTED)

Parameter	Conditions		Min.	Typ.	Max	Unit
Absolute Accuracy	0 …10 bar, 25°C 0 …10 bar, 0..60°C -20..85°C		-1.5 -2.0 -4.0		+1.5 +2.0 +4.0	°C
Maximum error with supply voltage	V_{DD} = 1.5 V … 3.6 V			± 0.3		°C
Resolution RMS	OSR	8192 4096 2048 1024 512 256		0.0022 0.0026 0.0033 0.0041 0.0055 0.0086		°C

PERFORMANCE SPECIFICATIONS (CONTINUED)

DIGITAL INPUTS (SCL, SDA)

Parameter	Symbol	Conditions	Min.	Typ.	Max	Unit
Serial data clock	SCL				400	kHz
Input high voltage	V_{IH}		80% V_{DD}		100% V_{DD}	V
Input low voltage	V_{IL}		0% V_{DD}		20% V_{DD}	V
Input leakage current	$I_{leak25°C}$	at 25°c			0.1	µA

DIGITAL OUTPUTS (SDA)

Parameter	Symbol	Conditions	Min.	Typ.	Max	Unit
Output high voltage	V_{OH}	I_{source} = 0.6 mA	80% V_{DD}		100% V_{DD}	V
Output low voltage	V_{OL}	I_{sink} = 0.6 mA	0% V_{DD}		20% V_{DD}	V

PERFORMANCE CHARACTERISTICS

PRESSURE ERROR VS PRESSURE AND TEMPERATURE

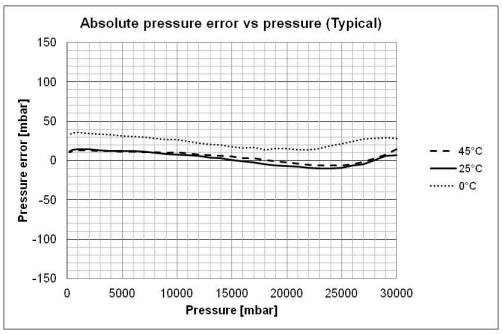

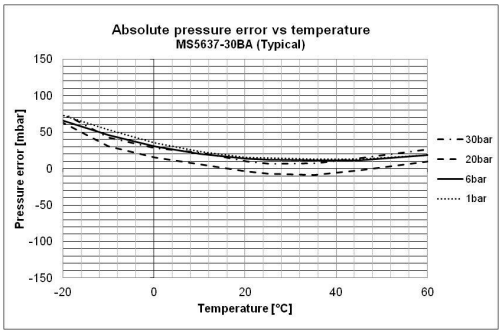

TEMPERATURE ERROR VS PRESSURE AND TEMPERATURE

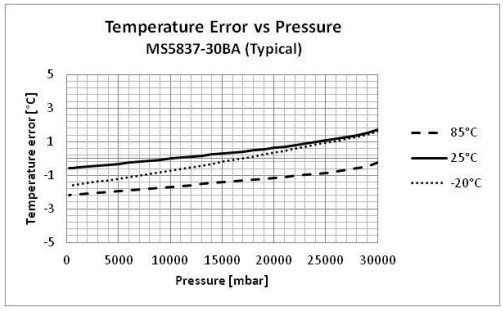

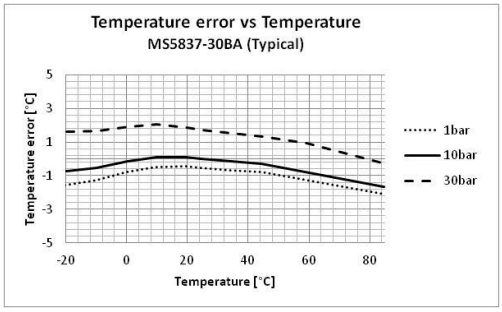

PRESSURE AND TEMPERATURE ERROR VS POWER SUPPLY

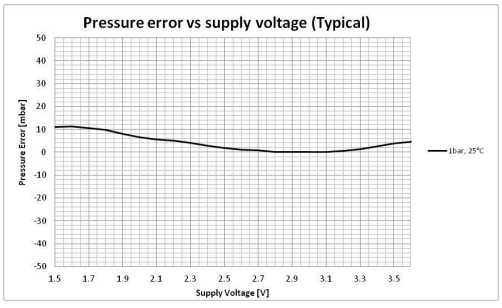

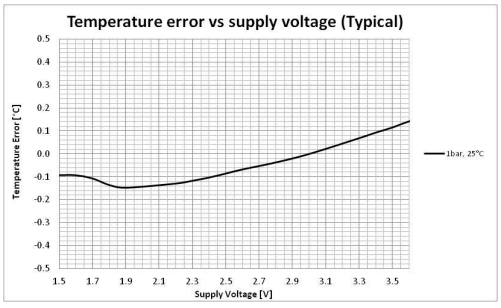

FUNCTIONAL DESCRIPTION

GENERAL

The MS5837-30BA consists of a piezo-resistive sensor and a sensor interface IC. The main function of the MS5837-30BA is to convert the uncompensated analogue output voltage from the piezo-resistive pressure sensor to a 24-bit digital value, as well as providing a 24-bit digital value for the temperature of the sensor.

FACTORY CALIBRATION

Every module is individually factory calibrated at two temperatures and two pressures. As a result, 6 coefficients necessary to compensate for process variations and temperature variations are calculated and stored in the 112-bit PROM of each module. These bits (partitioned into 6 coefficients W1 to W6) must be read by the microcontroller software and used in the program converting D1 and D2 into compensated pressure and temperature values.
The coefficients W0 is for factory configuration and CRC.

SERIAL I2C INTERFACE

The external microcontroller clocks in the data through the input SCL (Serial CLock) and SDA (Serial DAta). The sensor responds on the same pin SDA which is bidirectional for the I^2C bus interface. So this interface type uses only 2 signal lines and does not require a chip select.

Module ref	Mode	Pins used
MS5837-30BA	I^2C	SDA, SCL

PRESSURE AND TEMPERATURE CALCULATION

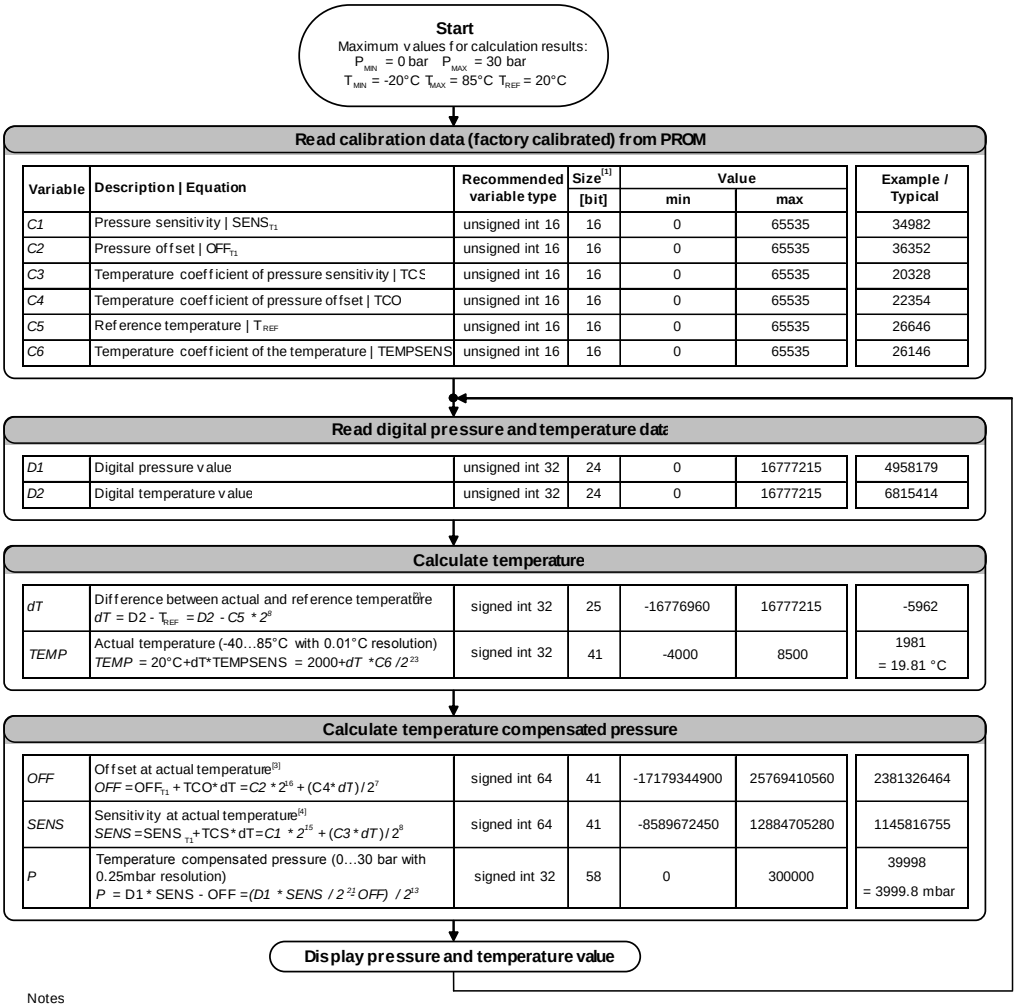

Variable	Description | Equation	Recommended variable type	Size[1] [bit]	Value min	Value max	Example / Typical
C1	Pressure sensitivity | $SENS_{T1}$	unsigned int 16	16	0	65535	34982
C2	Pressure offset | OFF_{T1}	unsigned int 16	16	0	65535	36352
C3	Temperature coefficient of pressure sensitivity | TCS	unsigned int 16	16	0	65535	20328
C4	Temperature coefficient of pressure offset | TCO	unsigned int 16	16	0	65535	22354
C5	Reference temperature | T_{REF}	unsigned int 16	16	0	65535	26646
C6	Temperature coefficient of the temperature | TEMPSENS	unsigned int 16	16	0	65535	26146
D1	Digital pressure value	unsigned int 32	24	0	16777215	4958179
D2	Digital temperature value	unsigned int 32	24	0	16777215	6815414
dT	Difference between actual and reference temperature[2] $dT = D2 - T_{REF} = D2 - C5 * 2^8$	signed int 32	25	-16776960	16777215	-5962
TEMP	Actual temperature (-40…85°C with 0.01°C resolution) $TEMP = 20°C + dT * TEMPSENS = 2000 + dT * C6 / 2^{23}$	signed int 32	41	-4000	8500	1981 = 19.81 °C
OFF	Offset at actual temperature[3] $OFF = OFF_{T1} + TCO * dT = C2 * 2^{16} + (C4 * dT) / 2^7$	signed int 64	41	-17179344900	25769410560	2381326464
SENS	Sensitivity at actual temperature[4] $SENS = SENS_{T1} + TCS * dT = C1 * 2^{15} + (C3 * dT) / 2^8$	signed int 64	41	-8589672450	12884705280	1145816755
P	Temperature compensated pressure (0…30 bar with 0.25mbar resolution) $P = D1 * SENS - OFF = (D1 * SENS / 2^{21} - OFF) / 2^{13}$	signed int 32	58	0	300000	39998 = 3999.8 mbar

Notes
[1] Maximal size of intermediate result during evaluation of variable
[2] min and max have to be defined
[3] min and max have to be defined
[4] min and max have to be defined

Flow chart for pressure and temperature reading and software compensation.

SECOND ORDER TEMPERATURE COMPENSATION

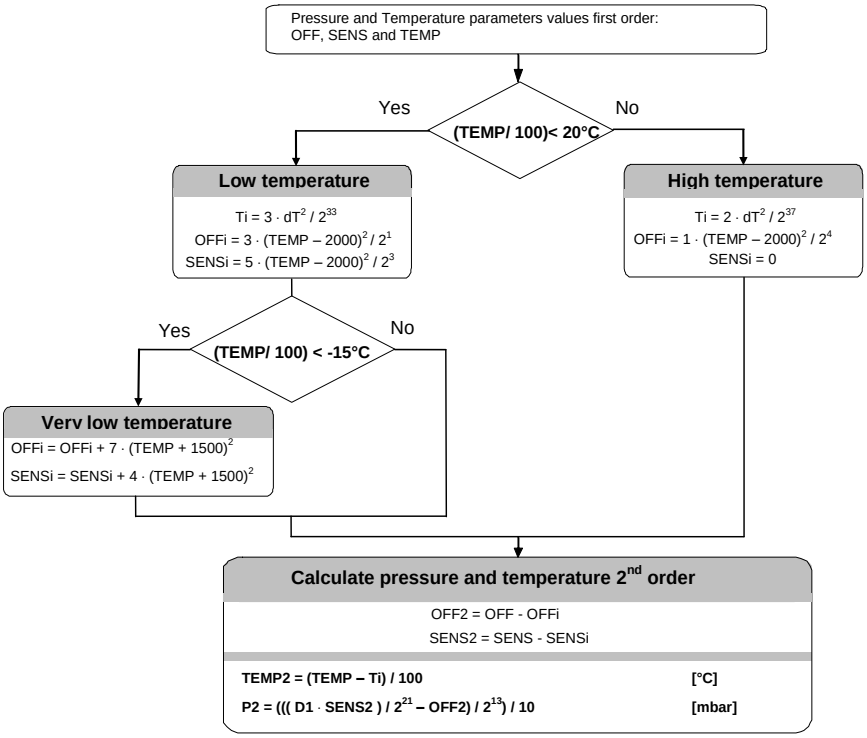

Flow chart for pressure and temperature to the optimum accuracy.

I²C INTERFACE

COMMANDS

The MS5837-30BA has only five basic commands:

1. Reset
2. Read PROM (112 bit of calibration words)
3. D1 conversion
4. D2 conversion
5. Read ADC result (24 bit pressure / temperature)

Each I²C communication message starts with the start condition and it is ended with the stop condition. The MS5837-30BA address is 1110110x (write: x=0, read: x=1).

Size of each command is 1 byte (8 bits) as described in the table below. After ADC read commands, the device will return 24 bit result and after the PROM read 16 bit results. The address of the PROM is embedded inside of the PROM read command using the a2, a1 and a0 bits.

	Command byte								**hex value**
Bit number	0	1	2	3	4	5	6	7	
Bit name	PROM	CONV	-	Typ	Ad2/ Os2	Ad1/ Os1	Ad0/ Os0	Stop	
Command									
Reset	0	0	0	1	1	1	1	0	0x1E
Convert D1 (OSR=256)	0	1	0	0	0	0	0	0	0x40
Convert D1 (OSR=512)	0	1	0	0	0	0	1	0	0x42
Convert D1 (OSR=1024)	0	1	0	0	0	1	0	0	0x44
Convert D1 (OSR=2048)	0	1	0	0	0	1	1	0	0x46
Convert D1 (OSR=4096)	0	1	0	0	1	0	0	0	0x48
Convert D1 (OSR=8192)	0	1	0	0	1	0	1	0	0x4A
Convert D2 (OSR=256)	0	1	0	1	0	0	0	0	0x50
Convert D2 (OSR=512)	0	1	0	1	0	0	1	0	0x52
Convert D2 (OSR=1024)	0	1	0	1	0	1	0	0	0x54
Convert D2 (OSR=2048)	0	1	0	1	0	1	1	0	0x56
Convert D2 (OSR=4096)	0	1	0	1	1	0	0	0	0x58
Convert D2 (OSR=8192)	0	1	0	1	1	0	1	0	0x5A
ADC Read	0	0	0	0	0	0	0	0	0x00
PROM Read	1	0	1	0	Ad2	Ad1	Ad0	0	0xA0 to 0xAE

Command structure

RESET SEQUENCE

The Reset sequence shall be sent once after power-on to make sure that the calibration PROM gets loaded into the internal register. It can be also used to reset the device PROM from an unknown condition.
The reset can be sent at any time. In the event that there is not a successful power on reset this may be caused by the SDA being blocked by the module in the acknowledge state. The only way to get the MS5837-30BA to function is to send several SCLs followed by a reset sequence or to repeat power on reset.

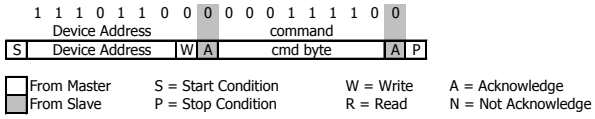

I^2C Reset Command

PROM READ SEQUENCE

The read command for PROM shall be executed once after reset by the user to read the content of the calibration PROM and to calculate the calibration coefficients. There are in total 7 addresses resulting in a total memory of 112 bit. Addresses contain factory data and the setup, calibration coefficients, the serial code and CRC. The command sequence is 8 bits long with a 16 bit result which is clocked with the MSB first. The PROM Read command consists of two parts. First command sets up the system into PROM read mode. The second part gets the data from the system.

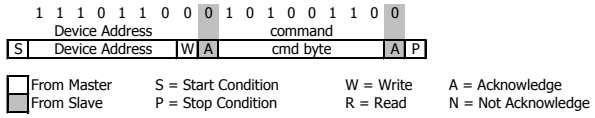

I^2C Command to read memory address= 011

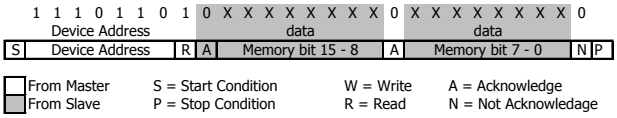

I^2C answer from MS5837-30BA

CONVERSION SEQUENCE

The conversion command is used to initiate uncompensated pressure (D1) or uncompensated temperature (D2) conversion. After the conversion, using ADC read command the result is clocked out with the MSB first. If the conversion is not executed before the ADC read command, or the ADC read command is repeated, it will give 0 as the output result. If the ADC read command is sent during conversion the result will be 0, the conversion will not stop and the final result will be wrong. Conversion sequence sent during the already started conversion process will yield incorrect result as well. A conversion can be started by sending the command to MS5837-30BA. When command is sent to the system it stays busy until conversion is done. When conversion is finished the data can be accessed by sending a Read command, when acknowledge is sent from the MS5837-30BA, 24 SCL cycles may be sent to receive all result bits. Every 8 bits the system waits for an acknowledge signal.

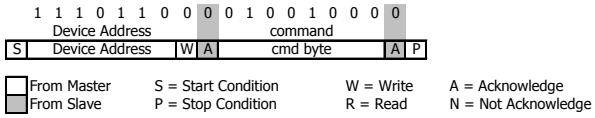

I²C command to initiate a pressure conversion (OSR=4096, typ=D1)

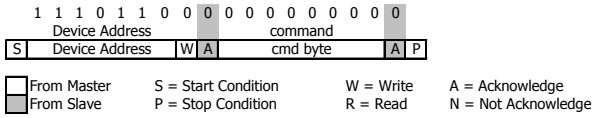

I²C ADC read sequence

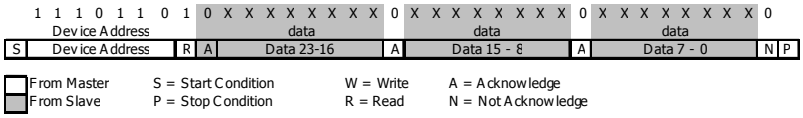

I²C answer from MS5837-30BA

CYCLIC REDUNDANCY CHECK (CRC)

MS5837-30BA contains a PROM memory with 112-Bit. A 4-bit CRC has been implemented to check the data validity in memory. The besides C code describes in detail CRC-4 calculation.

C6	DB15	DB14	DB13	DB12	DB11	DB10	DB9	DB8	DB7	DB6	DB5	DB4	DB3	DB2	DB1	DB0
0	CRC				Factory defined											
1	C1															
2	C2															
3	C3															
4	C4															
5	C5															
6																

Memory PROM mapping

C Code example for CRC-4 calculation:

```
unsigned char crc4(unsigned int n_prom[])                    // n_prom defined as 8x unsigned int (n_prom[8])
{
int cnt;                                                     // simple counter
unsigned int n_rem=0;                                        // crc remainder
unsigned char n_bit;

        n_prom[0]=((n_prom[0]) & 0x0FFF);                    // CRC byte is replaced by 0
        n_prom[7]=0;                                         // Subsidiary value, set to 0
        for (cnt = 0; cnt < 16; cnt++)                       // operation is performed on bytes
                {                                            // choose LSB or MSB

                if (cnt%2==1)       n_rem ^= (unsigned short) ((n_prom[cnt>>1]) & 0x00FF);
                else                n_rem ^= (unsigned short) (n_prom[cnt>>1]>>8);
                for (n_bit = 8; n_bit > 0; n_bit--)
                        {
                        if (n_rem & (0x8000))       n_rem = (n_rem << 1) ^ 0x3000;
                        else                        n_rem = (n_rem << 1);
                        }

                }
        n_rem= ((n_rem >> 12) & 0x000F);                     // final 4-bit remainder is CRC code
        return (n_rem ^ 0x00);
}
```

APPLICATION CIRCUIT

The MS5837 is a circuit that can be used in conjunction with a microcontroller in mobile altimeter applications.

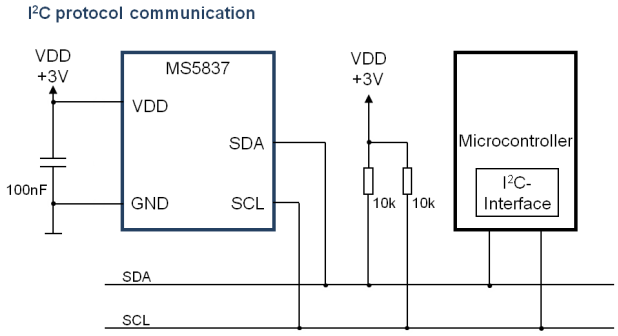

Typical application circuit

PIN CONFIGURATION AND DEVICE PACKAGE OUTLINE

UNLESS OTHERWISE SPECIFIED DIMENSIONS ARE IN MILLIMETERS. GENERAL TOLERANCE ± 0.1

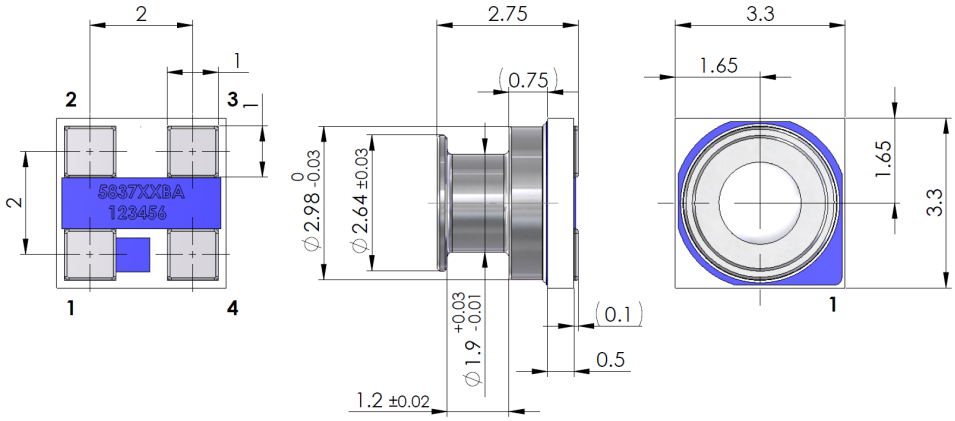

1	GND	GROUND
2	VDD	POSITIVE SUPPLY
3	SCL	I2C CLOCK
4	SDA	I2C DATA

Package outlines and Pin configuration

RECOMMENDED PAD LAYOUT

Pad layout for bottom side of the MS5837-30BA soldered onto printed circuit board.

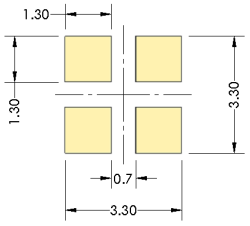

Recommended PCB footprint

SHIPPING PACKAGE

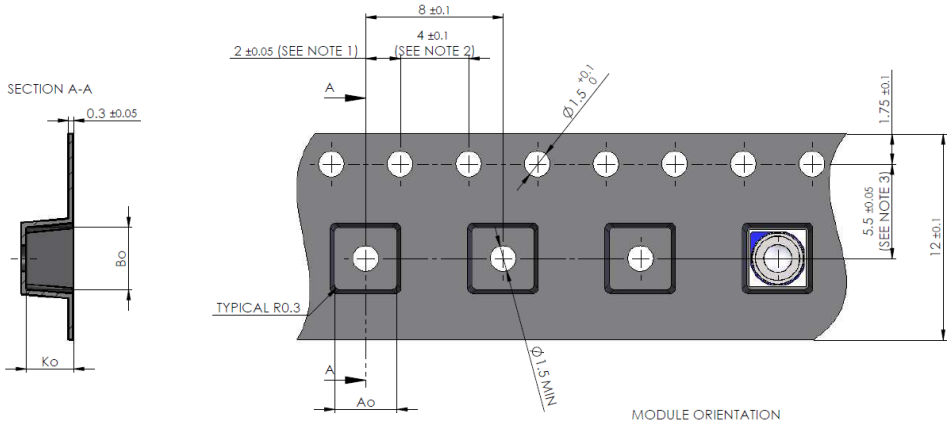

Ao	3.6±0.1
Bo	3.6±0.1
Ko	2.75±0.1

NOTE:

1: Measured from centerline of sprocket hole to centerline of pocket
2: Cumulative tolerance of 10 sprocket holes is ±0.2mm
3: Measured from centerline of sprocket hole to centerline of pocket

MOUNTING AND ASSEMBLY CONSIDERATIONS

SOLDERING

Please refer to the application note AN808 available on our website for all soldering recommendations.

MOUNTING

The MS5837-30BA can be placed with automatic Pick & Place equipment using vacuum nozzles. It will not be damaged by the vacuum. Due to the low stress assembly the sensor does not show pressure hysteresis effects. It is important to solder all contact pads.

CONNECTION TO PCB

The package outline of the module allows the use of a flexible PCB for interconnection. This can be important for applications in watches and other special devices.

SEALING WITH O-RINGS

In applications such as outdoor watches the electronics must be protected against direct water or humidity. For such applications the MS5837-30BA provides the possibility to seal with an O-ring. The O-ring shall be placed at the groove location, i.e. the small outer diameter of the metal lid. The following O-ring / housing dimensions are recommended:

O-ring inner diameter	1.8 ± 0.05 mm
O-ring cross-section diameter	0.8 ± 0.03 mm
Housing bore diameter	3.07 ± 0.03 mm

Please refer to the application note AN523 available on our website for O-ring mounting recommendations.

CLEANING

The MS5837-30BA has been manufactured under clean-room conditions. It is therefore recommended to assemble the sensor under class 10'000 or better conditions. Should this not be possible, it is recommended to protect the sensor opening during assembly from entering particles and dust. To avoid cleaning of the PCB, solder paste of type "no-clean" shall be used. Warning: cleaning might damage the sensor.

ESD PRECAUTIONS

The electrical contact pads are protected against ESD up to 2 kV HBM (human body model). It is therefore essential to ground machines and personnel properly during assembly and handling of the device. The MS5837-30BA is shipped in antistatic transport boxes. Any test adapters or production transport boxes used during the assembly of the sensor shall be of an equivalent antistatic material.

DECOUPLING CAPACITOR

Particular care must be taken when connecting the device to the power supply. A minimum of 100nF ceramic capacitor must be placed as close as possible to the MS5837-30BA VDD pin. This capacitor will stabilize the power supply during data conversion and thus, provide the highest possible accuracy.

ORDERING INFORMATION

Part Number / Art. Number	Product	Delivery Form
MS583730BA01-50	MS5837-30BA Ultra Small Gel Filled Pressure Sensor	Tape & Reel

NORTH AMERICA
Measurement Specialties, Inc.,
a TE Connectivity company
45738 Northport Loop West
Fremont, CA 94538
Tel: +1 800 767 1888
Fax: +1 510 498 1578
e-mail: pfg.cs.amer@meas-spec.com
Website: www.meas-spec.com

EUROPE
MEAS Switzerland Sàrl,
a TE Connectivity company
Ch. Chapons-des-Prés 11
CH-2022 Bevaix, Switzerland
Tel: +41 32 847 9550
Fax: +41 32 847 9569
e-mail: sales.ch@meas-spec.com
Website: www.meas-spec.com

ASIA
Measurement Specialties (China), Ltd.,
a TE Connectivity company
No. 26 Langshan Road
Shenzhen High-Tech Park (North) Nanshan
District, Shenzhen, 518057
China
Tel: +86 755 3330 5088
Fax: +86 755 3330 5099
e-mail: pfg.cs.asia@ameas-spec.com
Website: www.meas-spec.com

TE.com/sensorsolutions

CDOC-DA-0093 7

NGIMU User Manual

Version 1.3

Public Release

www.x-io.co.uk

Document updates

This document is continuously being updated to incorporate additional information requested by users and new features made available in software and firmware updates. Please check the x-io Technologies website for the latest version of this document and device firmware.

Document version history

Date	Document version	Description
07 Nov 2017	1.3	• Update the button information • Add analogue inputs section • Replace mechanical drawings with links to website • Update description of the LED indicating SD card status
10 Jan 2017	1.2	• Add send rates, sample rates, and timestamps section • Describe OSC time tag in more detail • Add auxiliary serial interface section • Add appendix for integration of a GPS module
19 Oct 2016	1.1	• Add description of the LED indicating SD card activity • Fix footnote error in overview section
23 Sep 2016	1.0	• Indicate that button must be held for half a second to switch on • Update description of OSC argument overloading • Include percentage in RSSI message • Update plastic housing photo and mechanical drawing • Add AHRS initialise and zero commands • Add altitude message
19 May 2016	0.6	• Add echo command • Add RSSI message • Add magnitudes message
29 Mar 2016	0.5	• Add communication protocol section • Correct analogue input voltage range to 3.1 V • Update LED section • Update annotated photo of board • Update plastic housing photo • Update mechanical drawing of board
19 Nov 2015	0.4	• Update photo and mechanical drawing of latest prototype plastic housing • Include mechanical drawing of board
30 Jun 2015	0.3	• Correct serial pinout tables • Mark pin 1 on annotated photo of board
9 Jun 2015	0.2	• Include photo and mechanical drawing of latest prototype plastic housing

		• Small tables are not split across pages
12 May 2015	0.1	• Update photo of prototype plastic housing
10 May 2015	0.0	• Initial release

Table of Contents

1. Overview

The Next Generation IMU (NGIMU) is a compact IMU and data acquisition platform that combines on-board sensors and data processing algorithms with a broad range of communication interfaces to create a versatile platform well suited to both real-time and data-logging applications.

The device communicates using OSC and so is immediately compatible with many software applications and straight forward to integrate with custom applications with libraries available for most programming languages.

1.1. On-board sensors & data acquisition

- Triple-axis gyroscope (±2000°/s, 400 Hz sample rate)
- Triple-axis accelerometer (±16g, 400 Hz sample rate)
- Triple-axis magnetometer (±1300 µT)
- Barometric pressure (300-1100 hPa)
- Humidity
- Temperature[1]
- Battery voltage, current, percentage, and time remaining
- Analogue inputs (8 channels, 0-3.1 V, 10-bit, 1 kHz sample rate)
- Auxiliary serial (RS-232 compatible) for GPS or custom electronics/sensors
- Real-time clock and

1.2. On-board data processing

- All sensors are calibrated
- AHRS fusion algorithm provides a measurement of orientation relative to the Earth as a quaternion, rotation matrix, or Euler angles
- AHRS fusion algorithm provides a measurement of linear acceleration
- Altimeter fusion algorithm provides a measurement of altitude[2]
- All measurements are timestamped
- Synchronisation of timestamps for all devices on a Wi-Fi network[2,3]

1.3. Communication interfaces

- USB
- Serial (RS-232 compatible)
- Wi-Fi (802.11n, 5 GHz, built-in or external antennae, AP or client mode)
- SD card (accessible as an external drive via USB)

[1] On-board thermometers are used for calibration and are not intended to provide an accurate measurement of ambient temperature.

[2] This feature is under development and will be available soon. Please contact us if this is an urgent requirement.

[3] Synchronisation requires additional hardware (Wi-Fi router and synchronisation master).

1.4. Power management

- Power from USB, external supply or battery
- Battery charging via USB or external supply
- Sleep timer
- Motion trigger wake up
- Wake up timer
- 3.3 V supply for user electronics (500 mA)

1.5. Software features

- Open-source GUI and API (C#) for Windows
- Configure device settings
- Plot real-time data
- Log real-time data to file (CSV file format for use with Excel, MATLAB, etc.)
- Maintenance and calibration tools[2]

2. Hardware

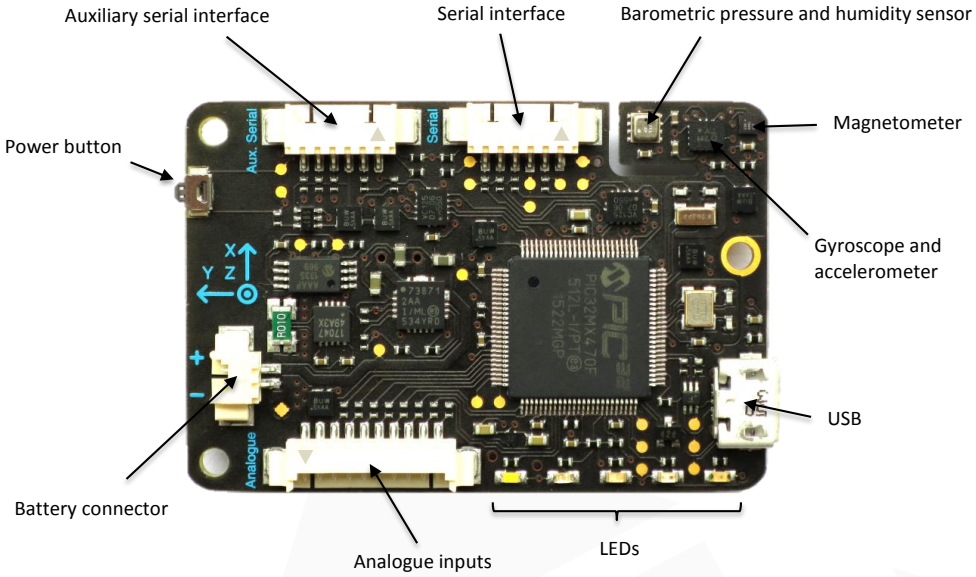

Figure 1: Top view of board

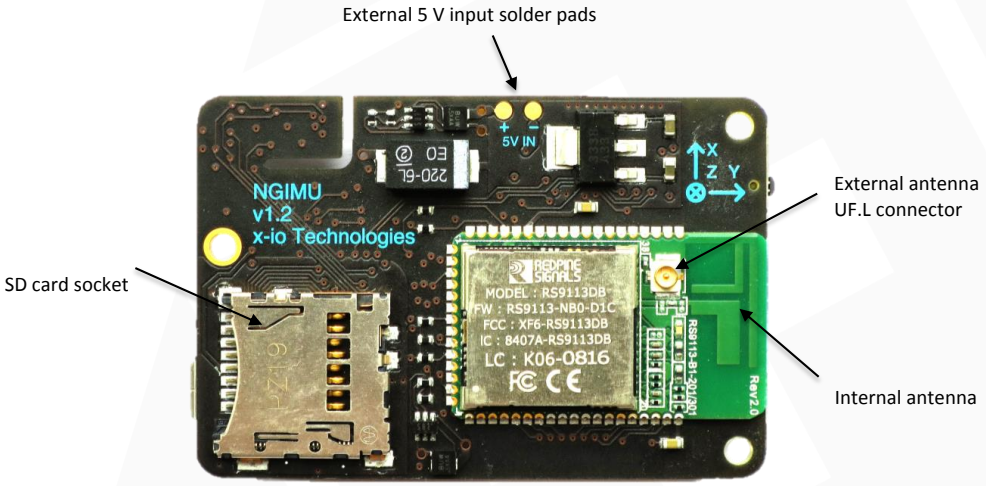

Figure 2: Bottom view of board

2.1. Power button

The power button is primarily used to turn the device on and off (sleep mode). Pressing the button while the device is off will turn it on. Pressing and holding the button for 2 seconds while it is on will turn it off.

The button can also be used as a data source by the user. The device will send a timestamped button message each time the button is pressed. This may provide a convenient user input for real-time applications or a useful means of marking events when logging data. See Section 7.1.1 for more information.

2.2. LEDs

The board features 5 LED indicators. Each LED is a different colour and has a dedicated role. Table 1 list the role and associated behaviour of each LED.

Colour	Indicates	Behaviour
White	Wi-Fi status	**Off** - Wi-Fi disabled **Slow flashing (1 Hz)** - Not connected **Fast flashing (5 Hz)** - Connected and waiting for IP address **Solid** - Connected and IP address obtained
Blue	-	-
Green	Device status	Indicates that the device is switched on. Will also blink each time the button is pressed or a message is received.
Yellow	SD card status	**Off –** No SD card present **Slow flashing (1 Hz) –** SD card present but not in use **Solid** - SD card present and logging in progress
Red	Battery charging	**Off** - Charger not connected **Solid** - Charger connected and charging in progress **Flashing (0.3 Hz)** - Charger connected and charging complete

Table 1: LED behaviour

Sending an identify command to the device will cause all the LEDs to rapidly flash for 5 seconds. This may be of use when trying to identify a specific device within a group of multiple devices. See Section 7.3.6 for more information.

The LEDs may be disabled in the device settings. This may be of use in applications where light from the LEDs is undesirable. The identify command may still be used when the LEDs are disabled and the green LED will still blink each time the button is pressed. This allows the user to check if the device is switched on while the LEDs are disabled.

2.3. Auxiliary serial pinout

Table 2 lists the auxiliary serial connector pinout. Pin 1 is physically marked on the connector by a small arrow, see Figure 1.

Pin	Direction	Name
1	N/A	Ground
2	Output	RTS
3	Output	3.3 V output
4	Input	RX
5	Output	TX
6	Input	CTS

Table 2: Auxiliary serial connector pinout

2.4. Serial pinout

Table 3 lists the serial connector pinout. Pin 1 is physically marked on the connector by a small arrow, see Figure 1.

Pin	Direction	Name
1	N/A	Ground
2	Output	RTS
3	Input	5 V input
4	Input	RX
5	Output	TX
6	Input	CTS

Table 3: Serial connector pinout

2.5. Analogue inputs pinout

Table 4 lists the analogue inputs connector pinout. Pin 1 is physically marked on the connector by a small arrow, see Figure 1.

Pin	Direction	Name
1	N/A	Ground
2	Output	3.3 V output
3	Input	Analogue channel 1
4	Input	Analogue channel 2
5	Input	Analogue channel 3
6	Input	Analogue channel 4
7	Input	Analogue channel 5
8	Input	Analogue channel 6
9	Input	Analogue channel 7
10	Input	Analogue channel 8

Table 4: Analogue input connector pinout

2.6. Connector part numbers

All board connectors are 1.25 mm pitch Molex PicoBlade™ Headers. Table 5 lists each part number used on the board and the recommended part numbers of the corresponding mating connectors. Each mating connector is created from a plastic housing part and two or more crimped wires.

Board connector	Part number	Mating part number
Battery	Molex PicoBlade™ Header, Surface Mount, Right-Angle, 2-way, P/N: 53261-0271	Molex PicoBlade™ Housing, Female, 2-way, P/N: 51021-0200 Molex Pre-Crimped Lead Single-Ended PicoBlade™ Female, 304mm, 28 AWG, P/N: 06-66-0015 (×2)
Auxiliary serial / Serial	Molex PicoBlade™ Header, Surface Mount, Right-Angle, 6-way, P/N: 53261-0671	Molex PicoBlade™ Housing, Female, 6-way, P/N: 51021-0600 Molex Pre-Crimped Lead Single-Ended PicoBlade™ Female, 304mm, 28 AWG, P/N: 06-66-0015 (×6)
Analogue inputs	Molex PicoBlade™ Header, Surface Mount, Right-Angle, 10-way, P/N: 53261-1071	Molex PicoBlade™ Housing, Female, 10-way, P/N: 51021-1000 Molex Pre-Crimped Lead Single-Ended PicoBlade™ Female, 304mm, 28 AWG, P/N: 06-66-0015 (×10)

Table 5: Board connector part numbers

2.7. Board dimensions

A 3D STEP file and mechanical drawing detailing all board dimensions are available on the x-io Technologies website.

3. Plastic housing

The plastic housing encloses the board with a 1000 mAh battery. The housing provides access to all board interfaces and is translucent so that the LED indicators may be seen. Figure 3 shows the board assembled with 1000 mAh battery in plastic housing.

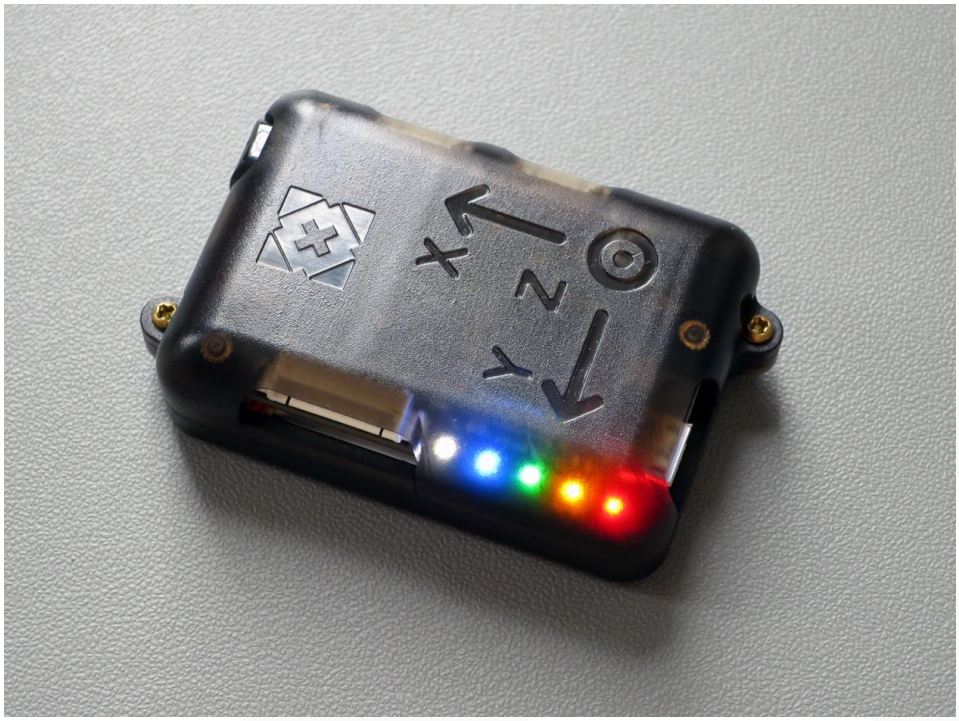

Figure 3: Board assembled with 1000 mAh battery in plastic housing

A 3D STEP file and mechanical drawing detailing all housing dimensions are available on the x-io Technologies website.

4. Analogue inputs

The analogue inputs interface is used to measure voltages and obtain data from external sensors that provide measurements as an analogue voltage. For example, a resistive force sensor can be arranged in a potential divider circuit to provide measurements of force as an analogue voltage. Voltage measurements are sent by the device as timestamped analogue inputs messages as described in Section 7.1.13.

The analogue inputs pinout is described in Section 2.3, and the part numbers for a mating connector are listed in Section 2.6.

4.1. Analogue inputs specification

- Number of channels: **8**
- ADC resolution: **10-bit**
- Sample rate: **1000 Hz**
- Voltage range: **0 V to 3.1 V**

4.2. 3.3 V supply output

The analogue input interface provides a 3.3 V output which may be used to power external electronics. This output is switched off when the device enters sleep mode to prevent the external electronics from draining the battery when the device is not active.

5. Auxiliary serial interface

The auxiliary serial interface is used to communicate with external electronics via a serial connection. For example, Appendix A describes how a GPS module may be connected directly to the auxiliary serial interface to log and stream GPS data alongside existing sensor data. Alternatively, a microcontroller connected to the auxiliary serial interface can be used to add general purpose input/output functionality.

The auxiliary serial interface pinout is described in Section 2.3, and the part numbers for a mating connector are listed in Section 2.6.

5.1. Auxiliary serial specification

- Baud rate: **7 bps to 12 Mbps**
- RTS/CTS hardware flow control: **enabled/disabled**
- Invert data lines (for RS-232 compatibility): **enabled/disabled**
- Data: **8-bit (no party)**
- Stop bits: 1
- Voltage: **3.3 V (inputs are tolerant of RS-232 voltages)**

5.2. Sending data

Data is sent from the auxiliary serial interface by sending an auxiliary serial data message to the device. See Section 7.1.15 for more information.

5.3. Receiving data

Data received by the auxiliary serial interface is sent by the device as an auxiliary serial data message as described in Section 7.2.1. Received bytes are buffered before being sent together in a single message when one of the following conditions is met:

- The number of bytes stored in the buffer matches the *buffer size*
- No bytes have been received for more than the *timeout* period

- Reception of a byte equal to the *framing character*

The *buffer size*, *timeout*, and *framing character* can be adjusting in the device settings. An example use of these settings is to set the *framing character* to the value of a new-line character ('\n', decimal value 10) so that each ASCII string, terminated by a new-line character, received by auxiliary serial interface is sent as a separate time-stamped message.

5.4. OSC passthrough

If OSC passthrough mode is enabled then the auxiliary serial interface will not send and receive in the way described in Sections 5.2 and 5.3. Instead, the auxiliary serial interface will send and receive OSC packets encoded as SLIP packets. OSC content received by the auxiliary serial interface is forwarded to all active communication channels as a timestamped OSC bundle. OSC messages received via any active communication channel that are not recognised will be forwarded to the auxiliary serial interface. This allows direct communication with third party and custom serial-based OSC devices through messages sent and received alongside existing OSC traffic.

The NGIMU Teensy I/O Expansion Example demonstrates how a Teensy (an Arduino compatible microcontroller) connected to the auxiliary serial interface can be used to control LEDs and provide sensor data using OSC passthrough mode.

5.5. RTS/CTS hardware flow control

If RTS/CTS hardware flow control is not enabled in the device settings then the CTS input and RTS output may be controlled manually. This provides a general purpose digital input and output which may be used to interface to external electronics. For example: to detect the pressing of a button or to control an LED. The RTS output state is set by sending an auxiliary serial RTS message to the device as described in Section 7.2.2. A timestamped auxiliary serial CTS message is sent by the device each time the CTS input states changes as described in Section 7.1.16.

5.6. 3.3 V supply output

The auxiliary serial interface provides a 3.3 V output which may be used to power external electronics. This output is switched off when the device enters sleep mode to prevent the external electronics from draining the battery when the device is not active.

6. Send rates, sample rates, and timestamps

The device settings allow the user to specify the send rate of each measurement message type, for example: sensors message (Section 7.1.2), quaternion message (Section 7.1.4), etc. The send rate has no effect on the sample rate of the corresponding measurements. All measurements are acquired internally at the fixed sample rates listed in Table 6. The timestamp for each measurement is created when the sample is acquired. The timestamp is therefore a reliable measurement, independent of the latency or buffering associated with a given commutation channel.

Measurement	Sample Rate
Gyroscope	400 Hz
Accelerometer	400 Hz
Magnetometer	20 Hz
Barometric pressure	25 Hz
Humidity	25 Hz
Processor temperature	1 kHz
Gyroscope and accelerometer temperature	100 Hz
Environmental sensor temperature	25 Hz
Battery (percentage, time to empty, voltage, current)	5 Hz
Analogue inputs	1 kHz
RSSI	5 Hz

Table 6: Fixed internal sample rates

If a specified send rate is greater than the sample rate of the associate measurement then measurements will be repeated within multiple messages. Repeated measurements can be identified as a repeated timestamp. It is possible to specify send rates that exceed the bandwidth of a communication channel. This will result in messages being lost. Timestamps should be used to ensure that the receiving system is robust to lost messages.

7. Communication protocol

All communication is encoded as OSC. Data sent over UDP uses OSC as per the OSC v1.0 specification. Data set over USB, serial or written to the SD card is OSC encoded as SLIP packets as per the OSC v1.1 specification. The OSC implementation uses the following simplifications:

- OSC messages sent to the device may use numerical argument types (int32, float32, int64, OSC time tag, 64-bit double, character, boolean, nil, or infinitum) interchangeably, and blob and string argument types interchangeably.
- OSC address patterns sent to the device may not contain any special characters: '?', '*', '[]', or '{}'.
- OSC messages sent to the device may be sent within OSC bundles. However, message scheduling will be ignored.

7.1. Data from device

All data sent from the device is sent as a timestamped OSC bundle containing a single OSC message. All data messages, with the exception of the button, auxiliary serial and serial messages, are sent continuously at the send rates specified in the device settings.

The timestamp of an OSC bundle is an OSC time tag. This is a 64-bit fixed-point number. The first 32 bits specify the number of seconds since 00:00 on January 1st, 1990, and the last 32 bits specify fractional parts of a second to a precision of about 200 picoseconds. This is the representation used by Internet NTP timestamps. An OSC time tag can be converted to a decimal value of seconds by first

interpreting the value as a 64-bit unsigned integer and then dividing this value by 2^{32}. It is important that this calculation is implemented using a double-precision floating-point type otherwise the lack of precision will result in significant errors.

7.1.1. Button message

OSC address: `/button`

The button message is sent each time the power button is pressed. The message contains no arguments.

7.1.2. Sensors

OSC address: `/sensors`

The sensors message contains measurements from the gyroscope, accelerometer, magnetometer, and barometer. The message arguments are summarised in Table 7.

Argument	Type	Description
1	float32	Gyroscope x axis in °/s
2	float32	Gyroscope y axis in °/s
3	float32	Gyroscope z axis in °/s
4	float32	Accelerometer x axis in g
5	float32	Accelerometer y axis in g
6	float32	Accelerometer z axis in g
7	float32	Magnetometer x axis in µT
8	float32	Magnetometer y axis in µT
9	float32	Magnetometer z axis in µT
10	float32	Barometer in hPa

Table 7: Sensor message arguments

7.1.3. Magnitudes

OSC address: `/magnitudes`

The magnitudes message contains measurements of the gyroscope, accelerometer, and magnetometer magnitudes. The message arguments are summarised in Table 8: Magnitudes message arguments.

Argument	Type	Description
1	float32	Gyroscope magnitude in °/s
2	float32	Accelerometer magnitude in g
3	float32	Magnetometer magnitude in µT

Table 8: Magnitudes message arguments

7.1.4. Quaternion

OSC address: `/quaternion`

The quaternion message contains the quaternion output of the on-board AHRS algorithm describing the orientation of the device relative to the Earth (NWU convention). The message arguments are summarised in Table 9.

Argument	Type	Description
1	float32	Quaternion w element
2	float32	Quaternion x element
3	float32	Quaternion y element
4	float32	Quaternion z element

Table 9: Quaternion message arguments

7.1.5. Rotation matrix

OSC address: `/matrix`

The rotation matrix message contains the rotation matrix output of the on-board AHRS algorithm describing the orientation of the device relative to the Earth (NWU convention). The message arguments describe the matrix in row-major order as summarised in Table 10.

Argument	Type	Description
1	float32	Rotation matrix xx element
2	float32	Rotation matrix xy element
3	float32	Rotation matrix xz element
4	float32	Rotation matrix yx element
5	float32	Rotation matrix yy element
6	float32	Rotation matrix yz element
7	float32	Rotation matrix zx element
8	float32	Rotation matrix zy element
9	float32	Rotation matrix zz element

Table 10: Rotation matrix message arguments

7.1.6. Euler angles

OSC address: `/euler`

The Euler angles message contains the Euler angle output of the on-board AHRS algorithm describing the orientation of the device relative to the Earth (NWU convention). The message arguments are summarised in Table 11.

Argument	Type	Description
1	float32	Roll (x) angle in degrees
2	float32	Pitch (y) angle in degrees
3	float32	Yaw/heading (z) angle in degrees

Table 11: Euler angle message arguments

7.1.7. Linear acceleration

OSC address: `/linear`

The linear acceleration message contains the linear acceleration output of the on-board sensor fusion algorithm describing gravity-free acceleration in the sensor coordinate frame. The message arguments are summarised in Table 12.

Argument	Type	Description
1	float32	Acceleration in the sensor x axis
2	float32	Acceleration in the sensor y axis
3	float32	Acceleration in the sensor z axis

Table 12: Linear acceleration message arguments

7.1.8. Earth acceleration

OSC address: `/earth`

The Earth acceleration message contains the Earth acceleration output of the on-board sensor fusion algorithm describing gravity-free acceleration in the Earth coordinate frame. The message arguments are summarised in Table 13.

Argument	Type	Description
1	float32	Acceleration in the Earth x axis
2	float32	Acceleration in the Earth y axis
3	float32	Acceleration in the Earth z axis

Table 13: Earth acceleration message arguments

7.1.9. Altitude

OSC address: `/altitude`

The altitude message contains the measurement of altitude above sea level. The message argument is summarised in Table 14.

Argument	Type	Description
1	float32	Altitude above sea level in m

Table 14: Altitude message argument

7.1.10. Temperature

OSC address: `/temperature`

The temperature message contains the measurements from each of the devices on-board temperature sensors. The message arguments are summarised in Table 15.

Argument	Type	Description
1	float32	Processor temperature in °C
2	float32	Gyroscope/accelerometer temperature in °C
3	float32	Barometer temperature in °C

Table 15: Temperature message arguments

7.1.11. Humidity

OSC address: `/humidity`

The humidity message contains the relative humidity measurement. The message argument is summarised in Table 16.

Argument	Type	Description
1	float32	Relative humidity in %

Table 16: Humidity message argument

7.1.12. Battery

OSC address: `/battery`

The battery message contains the battery voltage and current measurements as well as the states of the fuel gauge algorithm. The message arguments are summarised in Table 17.

Argument	Type	Description
1	float32	Battery level in %
2	float32	Time to empty in minutes
3	float32	Battery voltage in V
4	float32	Battery current in mA
5	string	Charger state

Table 17: Battery message arguments

7.1.13. Analogue inputs

OSC address: `/analogue`

The analogue inputs message contains measurements of the analogue inputs voltages. The message arguments are summarised in Table 18.

Argument	Type	Description
1	float32	Channel 1 voltage in V
2	float32	Channel 2 voltage in V
3	float32	Channel 3 voltage in V
4	float32	Channel 4 voltage in V
5	float32	Channel 5 voltage in V
6	float32	Channel 6 voltage in V
7	float32	Channel 7 voltage in V
8	float32	Channel 8 voltage in V

Table 18: Analogue inputs message arguments

7.1.14. RSSI

OSC address: `/rssi`

The RSSI message contains the RSSI (Receive Signal Strength Indicator) measurement for the wireless connection. This measurement is only valid if the Wi-Fi module is operating in client mode. The message arguments are summarised in Table 19.

Argument	Type	Description
1	float32	RSSI measurement in dBm
2	float32	RSSI measurement as a percentage where 0% to 100% represents the range -100 dBm to -50 dBm.

Table 19: RSSI message argument

7.1.15. Auxiliary serial data

OSC address: `/auxserial`

The auxiliary serial message contains the data received through the auxiliary serial interface. The message argument may be one of two types depending on the device settings as summarised in Table 20.

Argument	Type	Description
1	blob	Data received through the auxiliary serial interface.
1	string	Data received through the auxiliary serial interface with all null bytes replaced with the character pair "`/0`".

Table 20: Auxiliary serial data message argument

7.1.16. Auxiliary serial CTS input

OSC address: `/auxserial/cts`

The auxiliary serial CTS input message contains the CTS input state of the auxiliary serial interface when hardware flow control is disabled. This message is sent each time the state of the CTS input changes. The message argument is summarised in Table 21.

Argument	Type	Description
1	boolean	CTS input state. False = low, True = high.

Table 21: Auxiliary serial CTS input message argument

7.1.17. Serial CTS input

OSC address: `/serial/cts`

The serial CTS input message contains the CTS input state of the serial interface when hardware flow control is disabled. This message is sent each time the state of the CTS input changes. The message argument is summarised in Table 22.

Argument	Type	Description
1	boolean	CTS input state. False = low, True = high.

Table 22: Serial CTS input message argument

7.2. Data to device

Data is sent to the device as OSC messages. The device will not send an OSC message in response.

7.2.1. Auxiliary serial data

OSC address: `/auxserial`

The auxiliary serial message is used to send data (one or more bytes) from the auxiliary serial interface. This message may only be sent if 'OSC passthrough' mode is not enabled. The message argument is summarised in Table 23.

Argument	Type	Description
1	OSC-blob / OSC-string	Data to be transmitted from the auxiliary serial interface

Table 23: Auxiliary serial data message arguments

7.2.2. Auxiliary serial RTS output

OSC address: `/auxserial/rts`

The auxiliary serial RTS message is used to control the RTS output of the auxiliary serial interface. This message may only be sent if hardware flow control is disabled. The message argument is summarised in Table 24.

Argument	Type	Description
1	Int32/float32/boolean	RTS output state. 0 or false = low, non-zero or true = high.

Table 24: Auxiliary serial RTS output message arguments

7.2.3. Serial RTS output

OSC address: `/serial/rts`

The serial RTS message is used to control the RTS output of the serial interface. This message may only be sent if hardware flow control is disabled. The message argument is summarised in Table 25.

Argument	Type	Description
1	Int32/float32/boolean	RTS output state. 0 or false = low, non-zero or true = high.

Table 25: Serial RTS output message arguments

7.3. Commands

All commands are sent as OSC messages. The device will confirm reception of a command by sending an identical OSC message back to the host.

7.3.1. Set time

OSC address: `/time`

The set time command sets the date and time on the device. The message argument is an OSC-timetag.

7.3.2. Mute

OSC address: `/mute`

The mute command inhibits the sending of all data messages listed in Section 7.1. Command confirmation messages and setting read/write response messages will still be sent. The device will remain muted until an unmute command is sent.

7.3.3. Unmute

OSC address: `/unmute`

The unmute command will undo the mute state described in Section 7.3.2.

7.3.4. Reset

OSC address: `/reset`

The reset command will perform a software reset. This is equivalent to switching the device off and then on again. The software reset will be performed 3 seconds after the command is received to ensure that the host is able to confirm the command before it is executed.

7.3.5. Sleep

OSC address: `/sleep`

The sleep command will put the device into sleep mode (switched off). The device will not enter sleep mode until 3 seconds after the command is received to ensure that the host is able to confirm the command before it is executed.

7.3.6. Identify

OSC address: `/identify`

The identify command will cause all the LEDs to rapidly flash for 5 seconds. This may be of use when trying to identify a specific device within a group of multiple devices.

7.3.7. Apply

OSC address: `/apply`

The apply command will force the device to immediately apply all pending settings that have been written but not yet applied. The confirmation of this command is sent after all settings have been applied.

7.3.8. Restore default

OSC address: `/default`

The restore default command will reset all device settings to their factory default values.

7.3.9. AHRS initialise

OSC address: `/ahrs/initialise`

The AHRS initialise command will reinitialise the AHRS algorithm.

7.3.10. AHRS zero yaw

OSC address: `/ahrs/zero`

The AHRS zero yaw command will zero the yaw component of the current orientation of the AHRS algorithm. This command may only be issued if the magnetometer is ignored in the AHRS settings.

7.3.11. Echo

OSC address: `/echo`

The echo command may be sent with any arguments and the device will respond with an identical OSC message.

7.4. Settings

Device settings are read and written using OSC messages. The settings tab of the device software provides access to all device settings and includes detailed documentation for each setting.

7.4.1. Read

Settings are read by sending an OSC message with the corresponding setting OSC address and no arguments. The device will respond with an OSC message with the same OSC address and the current setting value as an argument.

7.4.2. Write

Settings are written by sending an OSC message with the corresponding setting OSC address and an argument value. The device will respond with an OSC message with the same OSC address and the new setting value as an argument.

Some setting writes are not applied immediately because this may result in loss of communication with the device if a setting affecting the communication channel is modified. These settings are applied 3 seconds after the last write of any setting.

7.5. Errors

The device will send error messages as an OSC message with the OSC address: `/error` and a single string argument.

A. Integrating a GPS module with the NGIMU

This section describes how to integrate an off-the-shelf GPS module with the NGIMU. The NGIMU is compatible with any serial GPS module, the "Adafruit Ultimate GPS Breakout - 66 channel w/10 Hz updates - Version 3" was chosen here for the purposes of demonstration. This module can be purchased from Adafruit or any other their distributors.

A.1. Hardware setup

The CR1220 coin cell battery clip and auxiliary serial interface connecter wires must be soldered to the GPS module board. The auxiliary serial interface connector part numbers are detailed in Section 2.6. The required connections between the auxiliary serial port and the GPS module are described in Table 26. Figure 5 shows the assembled GPS module with connector for auxiliary serial interface.

Auxiliary serial pin	GPS module pin
Ground	"GND"
RTS	Not connected
3.3 V output	"3.3V"
RX	"TX"
TX	"RX"
CTS	Not connected

Table 26: Auxiliary serial interface connections to the GPS module

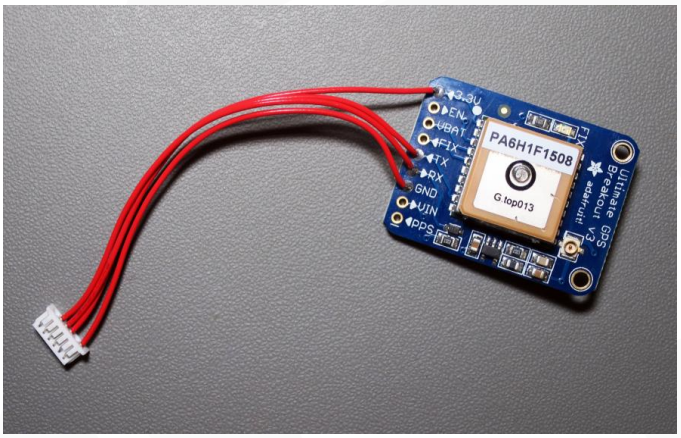

Figure 4: Assembled GPS module with connector for auxiliary serial interface

The CR1220 coin cell battery is necessary to preserve GPS module settings and to power the real-time clock while external power is not present. The GPS module will lose power each time the NGIMU is switched off. The real-time clock significantly reduces the time required to obtain a GPS lock. The battery can be expected to last approximately 240 days.

A.2. NGIMU settings

The auxiliary serial baud rate setting must be set to 9600. This is the default baud rate of the GPS module. The GPS module sends data in separate ASCII packets, each terminated by a new-line character. The auxiliary serial framing character setting must therefore be set to 10 so that each ASCII packet is timestamped and transmitted/logged by the NGIMU separately. The auxiliary serial 'send as string' setting must be enabled so that packets are interpreted as strings by the NGIMU software. All other settings should be left at default values so that the settings match those shown in Figure 5.

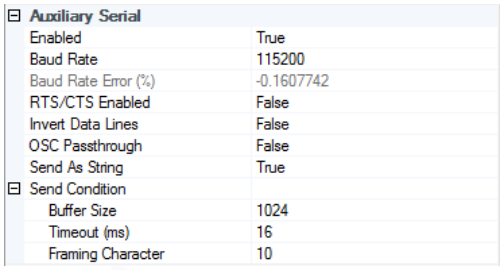

Figure 5: Auxiliary serial interface settings configured for a GPS module

A.3. Viewing and processing GPS data

Once the NGIMU settings have been configured as described in Section A.2, GPS data will be received and forwarded to all active communication channels as a timestamped auxiliary serial data message as described in Section 7.1.15. The NGIMU GUI can be used to view incoming GPS data using the Auxiliary Serial Terminal (under the Tools menu). Figure 6 shows incoming GPS data after a GPS fix has been achieved. The module may take tens of minutes to achieve a fix when powered for the first time.

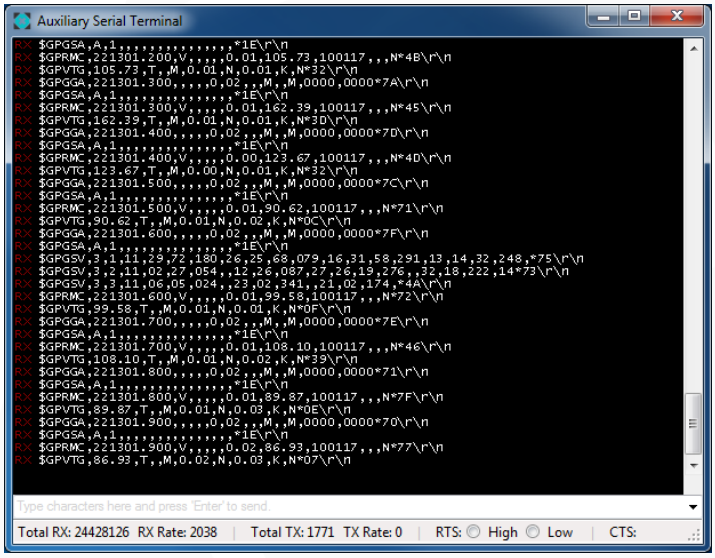

Figure 6: In coming GPS data displayed in the Auxiliary Serial Terminal

The default GPS module settings provide GPS data in four NMEA packet types: GPGGA, GPGSA, GPRMC, and GPVTG. The NMEA Reference Manual provides detailed description of the data contained in each of these packets.

The NGIMU software can be used to log real-time data as CSV files or to convert data logged to the SD card file to CSV files. GPS data is provided in the auxserial.csv file. The file contains two columns: the first column is the timestamp of a given NMEA packet generated by the NGIMU when the packet was received from the GPS module, and the second column is the NMEA packet. The user must handle the importing and interpretation this data.

A.4. Configuring for 10 Hz update rate

The GPS module default settings send data with a 1 Hz update rate. The module can be configured to send data with a 10 Hz update rate. This is achieved by sending command packets to adjust the settings as described in Sections A.4.1 and A.4.2. Each command packet may be sent using the NGIMU GUI's Auxiliary Serial Terminal (under the Tools menu). The GPS module will revert to default settings if the battery is removed.

The command packets described in this section are created as per the GlobalTop PMTK command packet documentation with checksums calculated using an on-line NMEA checksum calculator.

A.4.1. Step 1 – Change baud rate to 115200

Send the command packet "`$PMTK251,115200*1F\r\n`" to the GPS module. The incoming data will then appear as 'garbage' data because the current auxiliary serial baud rate of 9600 does not match the new GPS module baud rate of 115200. The auxiliary serial baud rate setting must then be set to 115200 in the NGIMU settings before for the data appears correctly again.

A.4.2. Step 2 – Change output rate to 10 Hz

Send the command packet "`$PMTK220,100*2F\r\n`" to the GPS module. The GPS module will now send data with a 10 Hz update rate.

A.4.3. Saving GPS module settings

The GPS module will save settings automatically. However, the GPS module will revert to default settings if the battery is removed.

TCA9548A Low-Voltage 8-Channel I²C Switch With Reset

1 Features

- 1-to-8 Bidirectional Translating Switches
- I²C Bus and SMBus Compatible
- Active-Low Reset Input
- Three Address Pins, Allowing up to Eight TCA9548A Devices on the I²C Bus
- Channel Selection Through an I²C Bus, In Any Combination
- Power Up With All Switch Channels Deselected
- Low R_{ON} Switches
- Allows Voltage-Level Translation Between 1.8-V, 2.5-V, 3.3-V, and 5-V Buses
- No Glitch on Power Up
- Supports Hot Insertion
- Low Standby Current
- Operating Power-Supply Voltage Range of 1.65-V to 5.5-V
- 5-V Tolerant Inputs
- 0- to 400-kHz Clock Frequency
- Latch-Up Performance Exceeds 100 mA Per JESD 78, Class II
- ESD Protection Exceeds JESD 22
  - ±2000-V Human-Body Model (A114-A)
  - 200-V Machine Model (A115-A)
  - ±1000-V Charged-Device Model (C101)

2 Applications

- Servers
- Routers (Telecom Switching Equipment)
- Factory Automation
- Products With I²C Slave Address Conflicts (Such as Multiple, Identical Temperature Sensors)

3 Description

The TCA9548A device has eight bidirectional translating switches that can be controlled through the I²C bus. The SCL/SDA upstream pair fans out to eight downstream pairs, or channels. Any individual SCn/SDn channel or combination of channels can be selected, determined by the contents of the programmable control register.

The system master can reset the TCA9548A in the event of a time-out or other improper operation by asserting a low in the $\overline{\text{RESET}}$ input. Similarly, the power-on reset deselects all channels and initializes the I²C/SMBus state machine. Asserting $\overline{\text{RESET}}$ causes the same reset and initialization to occur without powering down the part.

The pass gates of the switches are constructed so that the VCC pin can be used to limit the maximum high voltage, which is passed by the TCA9548A. Limiting the maximum high voltage allows the use of different bus voltages on each pair, so that 1.8-V or 2.5-V or 3.3-V parts can communicate with 5-V parts, without any additional protection. External pullup resistors pull the bus up to the desired voltage level for each channel. All I/O pins are 5-V tolerant.

Device Information[1]

PART NUMBER	PACKAGE	BODY SIZE (NOM)
TCA9548A	TSSOP (24)	7.80 mm × 4.40 mm
	VQFN (24)	4.00 mm × 4.00 mm

(1) For all available packages, see the orderable addendum at the end of the data sheet.

4 Simplified Application Diagram

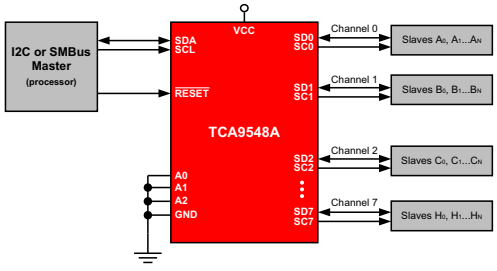

Table of Contents

5 Revision History

NOTE: Page numbers for previous revisions may differ from page numbers in the current version.

Changes from Revision C (November 2013) to Revision D — **Page**

- Added *Pin Configuration and Functions* section, *ESD Ratings* table, *Feature Description* section, *Device Functional Modes*, *Application and Implementation* section, *Power Supply Recommendations* section, *Layout* section, *Device and Documentation Support* section, and *Mechanical, Packaging, and Orderable Information* section ... 1
- Updated Typical Application schematic. ... 18

Changes from Revision B (November 2013) to Revision C — **Page**

- Updated V_{POR} and I_{CC} standby specification. ... 5

Changes from Revision A (July 2012) to Revision B — **Page**

- Updated document formatting. ... 1
- Removed ordering information. ... 1

6 Pin Configuration and Functions

PW PACKAGE
(TOP VIEW)

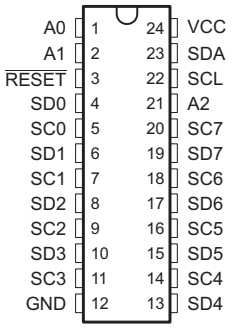

RGE PACKAGE
(TOP VIEW)

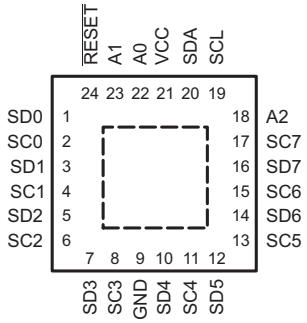

Pin Functions

PIN			TYPE	DESCRIPTION
NAME	TSSOP (PW)	QFN (RGE)		
A0	1	22	Input	Address input 0. Connect directly to V_{CC} or ground.
A1	2	23	Input	Address input 1. Connect directly to V_{CC} or ground.
$\overline{RESET}$	3	24	Input	Active-low reset input. Connect to V_{CC} or V_{DPUM}(1) through a pull-up resistor, if not used.
SD0	4	1	I/O	Serial data 0. Connect to V_{DPU0}(1) through a pull-up resistor.
SC0	5	2	I/O	Serial clock 0. Connect to V_{DPU0}(1) through a pull-up resistor.
SD1	6	3	I/O	Serial data 1. Connect to V_{DPU1}(1) through a pull-up resistor.
SC1	7	4	I/O	Serial clock 1. Connect to V_{DPU1}(1) through a pull-up resistor.
SC2	8	5	I/O	Serial data 2. Connect to V_{DPU2}(1) through a pull-up resistor.
SC2	9	6	I/O	Serial clock 2. Connect to V_{DPU2}(1) through a pull-up resistor.
SD3	10	7	I/O	Serial data 3. Connect to V_{DPU3}(1) through a pull-up resistor.
SC3	11	8	I/O	Serial clock 3. Connect to V_{DPU3}(1) through a pull-up resistor.
GND	12	9	Ground	Ground
SD4	13	10	I/O	Serial data 4. Connect to V_{DPU4}(1) through a pull-up resistor.
SC4	14	11	I/O	Serial clock 4. Connect to V_{DPU4}(1) through a pull-up resistor.
SD5	15	12	I/O	Serial data 5. Connect to V_{DPU5}(1) through a pull-up resistor.
SC5	16	13	I/O	Serial clock 5. Connect to V_{DPU5}(1) through a pull-up resistor.
SD6	17	14	I/O	Serial data 6. Connect to V_{DPU6}(1) through a pull-up resistor.
SC6	18	15	I/O	Serial clock 6. Connect to V_{DPU6}(1) through a pull-up resistor.
SD7	19	16	I/O	Serial data 7. Connect to V_{DPU7}(1) through a pull-up resistor.
SC7	20	17	I/O	Serial clock 7. Connect to V_{DPU7}(1) through a pull-up resistor.
A2	21	18	Input	Address input 2. Connect directly to V_{CC} or ground.
SCL	22	19	I/O	Serial clock bus. Connect to V_{DPUM}(1) through a pull-up resistor.
SDA	23	20	I/O	Serial data bus. Connect to V_{DPUM}(1) through a pull-up resistor.
VCC	24	21	Power	Supply voltage

(1) V_{DPUX} is the pull-up reference voltage for the associated data line. V_{DPUM} is the master I^2C reference voltage and V_{DPU0}-V_{DPU7} are the slave channel reference voltages.

7 Specifications

7.1 Absolute Maximum Ratings(1)

over operating free-air temperature range (unless otherwise noted)

		MIN	MAX	UNIT
V_{CC}	Supply voltage	–0.5	7	V
V_I	Input voltage(2)	–0.5	7	V
I_I	Input current	–20	20	mA
I_O	Output current	–25		mA
I_{CC}	Supply current	–100	100	mA
T_{stg}	Storage temperature	–65	150	°C

(1) Stresses beyond those listed under Absolute Maximum Ratings may cause permanent damage to the device. These are stress ratings only, and functional operation of the device at these or any other conditions beyond those indicated under *Recommended Operating Conditions* is not implied. Exposure to absolute-maximum-rated conditions for extended periods may affect device reliability.
(2) The input negative-voltage and output voltage ratings may be exceeded if the input and output current ratings are observed.

7.2 ESD Ratings

			VALUE	UNIT
$V_{(ESD)}$	Electrostatic discharge	Human body model (HBM), per ANSI/ESDA/JEDEC JS-001(1)	±2000	V
		Charged-device model (CDM), per JEDEC specification JESD22-C101(2)	±1000	

(1) JEDEC document JEP155 states that 500-V HBM allows safe manufacturing with a standard ESD control process.
(2) JEDEC document JEP157 states that 250-V CDM allows safe manufacturing with a standard ESD control process.

7.3 Recommended Operating Conditions

			MIN	MAX	UNIT
V_{CC}	Supply voltage		1.65	5.5	V
V_{IH}	High-level input voltage	SCL, SDA	0.7 × V_{CC}	6	V
		A2–A0, $\overline{RESET}$	0.7 × V_{CC}	V_{CC} + 0.5	
V_{IL}	Low-level input voltage	SCL, SDA	–0.5	0.3 × V_{CC}	V
		A2–A0, $\overline{RESET}$	–0.5	0.3 × V_{CC}	
T_A	Operating free-air temperature		–40	85	°C

7.4 Thermal Information

THERMAL METRIC(1)		TCA9548A		UNIT
		PW	RGE	
		24 PINS	24 PINS	
$R_{\theta JA}$	Junction-to-ambient thermal resistance	108.8	57.2	°C/W
$R_{\theta JC(top)}$	Junction-to-case (top) thermal resistance	54.1	62.5	
$R_{\theta JB}$	Junction-to-board thermal resistance	62.7	34.4	
ψ_{JT}	Junction-to-top characterization parameter	10.9	3.8	
ψ_{JB}	Junction-to-board characterization parameter	62.3	34.4	
$R_{\theta JC(bot)}$	Junction-to-case (bottom) thermal resistance	N/A	15.5	

(1) For more information about traditional and new thermal metrics, see the *IC Package Thermal Metrics* application report, SPRA953.

7.5 Electrical Characteristics(1)

V_{CC} = 2.3 V to 3.6 V, over recommended operating free-air temperature range (unless otherwise noted)

PARAMETER			TEST CONDITIONS	V_{CC}	MIN	TYP(2)	MAX	UNIT
V_{PORR}	Power-on reset voltage, V_{CC} rising		No load, $V_I = V_{CC}$ or GND(3)			1.2	1.5	V
V_{PORF}	Power-on reset voltage, V_{CC} falling(4)		No load, $V_I = V_{CC}$ or GND(3)		0.8	1		V
$V_{o(sw)}$	Switch output voltage		$V_{i(sw)} = V_{CC}$, I_{SWout} = –100 µA	5 V		3.6		V
				4.5 V to 5.5 V	2.6		4.5	
				3.3 V		1.9		
				3 V to 3.6 V	1.6		2.8	
				2.5 V		1.5		
				2.3 V to 2.7 V	1.1		2	
				1.8 V		1.1		
				1.65 V to 1.95 V	0.9		1.25	
I_{OL}	SDA		V_{OL} = 0.4 V	1.65 V to 5.5 V	3	6		mA
			V_{OL} = 0.6 V		6	9		
I_I	SCL, SDA		$V_I = V_{CC}$ or GND(3)	1.65 V to 5.5 V	–1		1	µA
	SC7–SC0, SD7–SD0				–1		1	
	A2–A0				–1		1	
	$\overline{RESET}$				–1		1	
I_{CC}	Operating mode	f_{SCL} = 400 kHz	$V_I = V_{CC}$ or GND(3), I_O = 0	5.5 V		50	80	µA
				3.6 V		20	35	
				2.7 V		11	20	
				1.65 V		6	10	
		f_{SCL} = 100 kHz	$V_I = V_{CC}$ or GND(3), I_O = 0	5.5 V		9	30	
				3.6 V		6	15	
				2.7 V		4	8	
				1.65 V		2	4	
	Standby mode	Low inputs	V_I = GND(3), I_O = 0	5.5 V		0.2	2	
				3.6 V		0.1	2	
				2.7 V		0.1	1	
				1.65 V		0.1	1	
		High inputs	$V_I = V_{CC}$, I_O = 0	5.5 V		0.2	2	
				3.6 V		0.1	2	
				2.7 V		0.1	1	
				1.65 V		0.1	1	
ΔI_{CC}	Supply-current change	SCL, SDA	SCL or SDA input at 0.6 V, Other inputs at V_{CC} or GND(3)	1.65 V to 5.5 V		3	20	µA
			SCL or SDA input at V_{CC} – 0.6 V, Other inputs at V_{CC} or GND(3)			3	20	
C_i	A2–A0		$V_I = V_{CC}$ or GND(3)	1.65 V to 5.5 V		4	5	pF
	$\overline{RESET}$					4	5	
	SCL		$V_I = V_{CC}$ or GND(3), Switch OFF			20	28	
$C_{io(off)}$ (5)	SDA		$V_I = V_{CC}$ or GND(3), Switch OFF	1.65 V to 5.5 V		20	28	pF
	SC7–SC0, SD7–SD0					5.5	7.5	

(1) For operation between specified voltage ranges, refer to the worst-case parameter in both applicable ranges.
(2) All typical values are at nominal supply voltage (1.8-V, 2.5-V, 3.3-V, or 5-V V_{CC}), T_A = 25°C.
(3) $\overline{RESET}$ = V_{CC} (held high) when all other input voltages, V_I = GND.
(4) The power-on reset circuit resets the I^2C bus logic with $V_{CC} < V_{PORF}$.
(5) $C_{io(ON)}$ depends on internal capacitance and external capacitance added to the SCn lines when channels(s) are ON.

Electrical Characteristics(1) (continued)

V_{CC} = 2.3 V to 3.6 V, over recommended operating free-air temperature range (unless otherwise noted)

PARAMETER		TEST CONDITIONS	V_{CC}	MIN	TYP(2)	MAX	UNIT
R_{ON}	Switch-on resistance	V_O = 0.4 V, I_O = 15 mA	4.5 V to 5.5 V	4	10	20	Ω
			3 V to 3.6 V	5	12	30	
		V_O = 0.4 V, I_O = 10 mA	2.3 V to 2.7 V	7	15	45	
			1.65 V to 1.95 V	10	25	70	

7.6 I²C Interface Timing Requirements

over recommended operating free-air temperature range (unless otherwise noted) (see Figure 5)

			STANDARD MODE I²C BUS		FAST MODE I²C BUS		UNIT
			MIN	MAX	MIN	MAX	
f_{scl}	I²C clock frequency		0	100	0	400	kHz
t_{sch}	I²C clock high time		4		0.6		µs
t_{scl}	I²C clock low time		4.7		1.3		µs
t_{sp}	I²C spike time			50		50	ns
t_{sds}	I²C serial-data setup time		250		100		ns
t_{sdh}	I²C serial-data hold time		0(1)		0(1)		µs
t_{icr}	I²C input rise time			1000	20 + 0.1C_b (2)	300	ns
t_{icf}	I²C input fall time			300	20 + 0.1C_b (2)	300	ns
t_{ocf}	I²C output (SDn) fall time (10-pF to 400-pF bus)			300	20 + 0.1C_b (2)	300	ns
t_{buf}	I²C bus free time between stop and start		4.7		1.3		µs
t_{sts}	I²C start or repeated start condition setup		4.7		0.6		µs
t_{sth}	I²C start or repeated start condition hold		4		0.6		µs
t_{sps}	I²C stop condition setup		4		0.6		µs
$t_{vdL(Data)}$	Valid-data time (high to low)(3)	SCL low to SDA output low valid		1		1	µs
$t_{vdH(Data)}$	Valid-data time (low to high)(3)	SCL low to SDA output high valid		0.6		0.6	µs
$t_{vd(ack)}$	Valid-data time of ACK condition	ACK signal from SCL low to SDA output low		1		1	µs
C_b	I²C bus capacitive load			400		400	pF

(1) A device internally must provide a hold time of at least 300 ns for the SDA signal (referred to the V_{IH} min of the SCL signal), to bridge the undefined region of the falling edge of SCL.
(2) C_b = total bus capacitance of one bus line in pF
(3) Data taken using a 1-kΩ pull-up resistor and 50-pF load (see Figure 6)

7.7 Switching Characteristics

over recommended operating free-air temperature range, C_L ≤ 100 pF (unless otherwise noted) (see Figure 5)

PARAMETER			FROM (INPUT)	TO (OUTPUT)	MIN	MAX	UNIT
t_{pd} (1)	Propagation delay time	R_{ON} = 20 Ω, C_L = 15 pF	SDA or SCL	SDn or SCn		0.3	ns
		R_{ON} = 20 Ω, C_L = 50 pF				1	
t_{rst} (2)	$\overline{RESET}$ time (SDA clear)		$\overline{RESET}$	SDA		500	ns

(1) The propagation delay is the calculated RC time constant of the typical ON-state resistance of the switch and the specified load capacitance, when driven by an ideal voltage source (zero output impedance).
(2) t_{rst} is the propagation delay measured from the time the $\overline{RESET}$ pin is first asserted low to the time the SDA pin is asserted high, signaling a stop condition. It must be a minimum of t_{WL}.

7.8 Reset Timing Requirements

over recommended operating free-air temperature range (unless otherwise noted)

PARAMETER		MIN	MAX	UNIT
$t_{w(L)}$	Pulse duration, $\overline{RESET}$ low	6		ns
$t_{REC(STA)}$	Recovery time from $\overline{RESET}$ to start	0		ns

7.9 Typical Characteristics

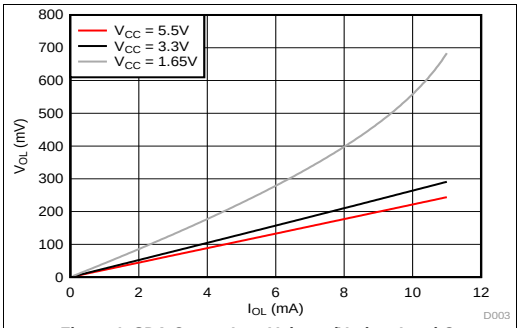

Figure 1. SDA Output Low Voltage (V_{OL}) vs Load Current (I_{OL}) at Three V_{CC} Levels

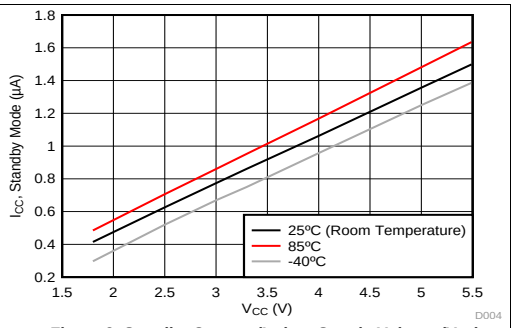

Figure 2. Standby Current (I_{CC}) vs Supply Voltage (V_{CC}) at Three Temperature Points

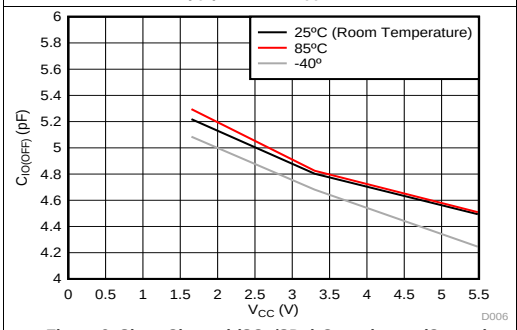

Figure 3. Slave Channel (SCn/SDn) Capacitance ($C_{io(OFF)}$) vs. Supply Voltage (V_{CC}) at Three Temperature Points

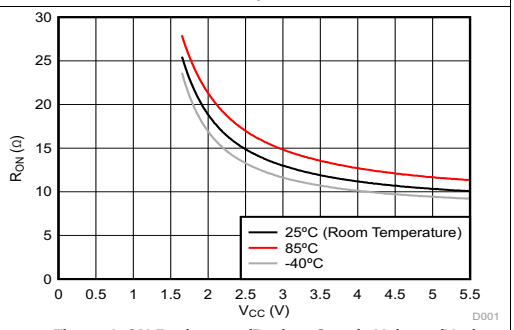

Figure 4. ON-Resistance (R_{ON}) vs Supply Voltage (V_{CC}) at Three Temperatures

8 Parameter Measurement Information

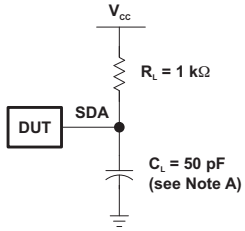

SDA LOAD CONFIGURATION

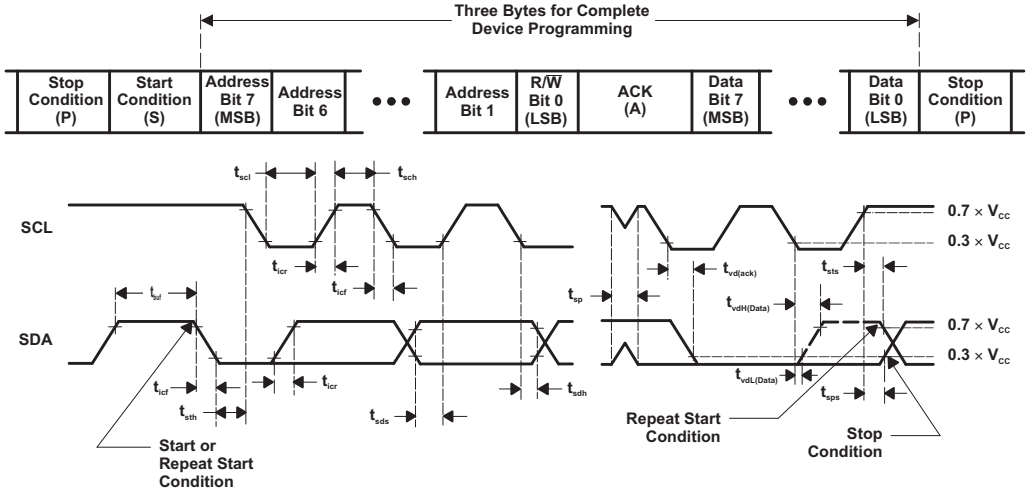

VOLTAGE WAVEFORMS

BYTE	DESCRIPTION
1	I^2C address
2, 3	P-port data

A. C_L includes probe and jig capacitance.

B. All inputs are supplied by generators having the following characteristics: PRR ≤ 10 MHz, Z_O = 50 Ω, t_r/t_f ≤ 30 ns.

C. Not all parameters and waveforms are applicable to all devices.

Figure 5. I^2C Load Circuit and Voltage Waveforms

Parameter Measurement Information (continued)

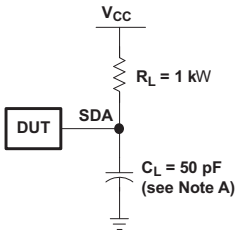

SDA LOAD CONFIGURATION

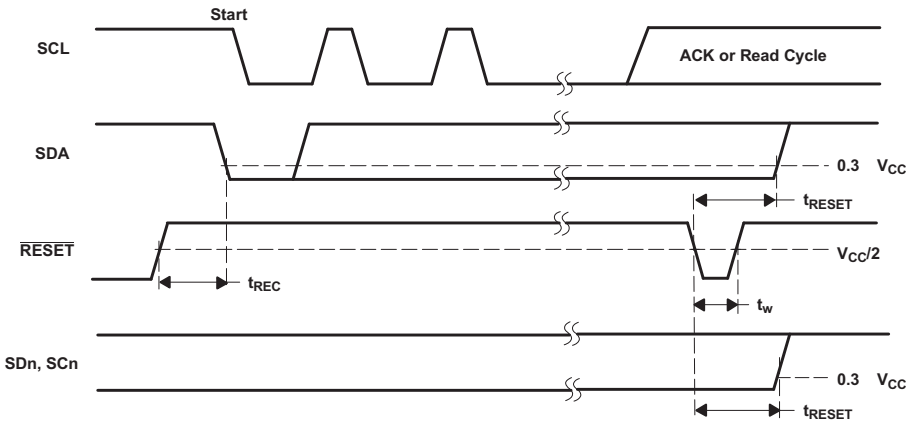

A. C_L includes probe and jig capacitance.
B. All inputs are supplied by generators having the following characteristics: PRR ≤ 10 MHz, Z_O = 50 Ω, t_r/t_f ≤ 30 ns.
C. I/Os are configured as inputs.
D. Not all parameters and waveforms are applicable to all devices.

Figure 6. Reset Load Circuit and Voltage Waveforms

9 Detailed Description

9.1 Overview

The TCA9548A is an 8-channel, bidirectional translating I^2C switch. The master SCL/SDA signal pair is directed to eight channels of slave devices, SC0/SD0-SC7/SD7. Any individual downstream channel can be selected as well as any combination of the eight channels.

The device offers an active-low $\overline{\text{RESET}}$ input which resets the state machine and allows the TCA9548A to recover should one of the downstream I^2C buses get stuck in a low state. The state machine of the device can also be reset by cycling the power supply, V_{CC}, also known as a power-on reset (POR). Both the $\overline{\text{RESET}}$ function and a POR will cause all channels to be deselected.

The connections of the I^2C data path are controlled by the same I^2C master device that is switched to communicate with multiple I^2C slaves. After the successful acknowledgment of the slave address (hardware selectable by A0, A1, and A2 pins), a single 8-bit control register is written to or read from to determine the selected channels.

The TCA9548A may also be used for voltage translation, allowing the use of different bus voltages on each SCn/SDn pair such that 1.8-V, 2.5-V, or 3.3-V parts can communicate with 5-V parts. This is achieved by using external pull-up resistors to pull the bus up to the desired voltage for the master and each slave channel.

9.2 Functional Block Diagram

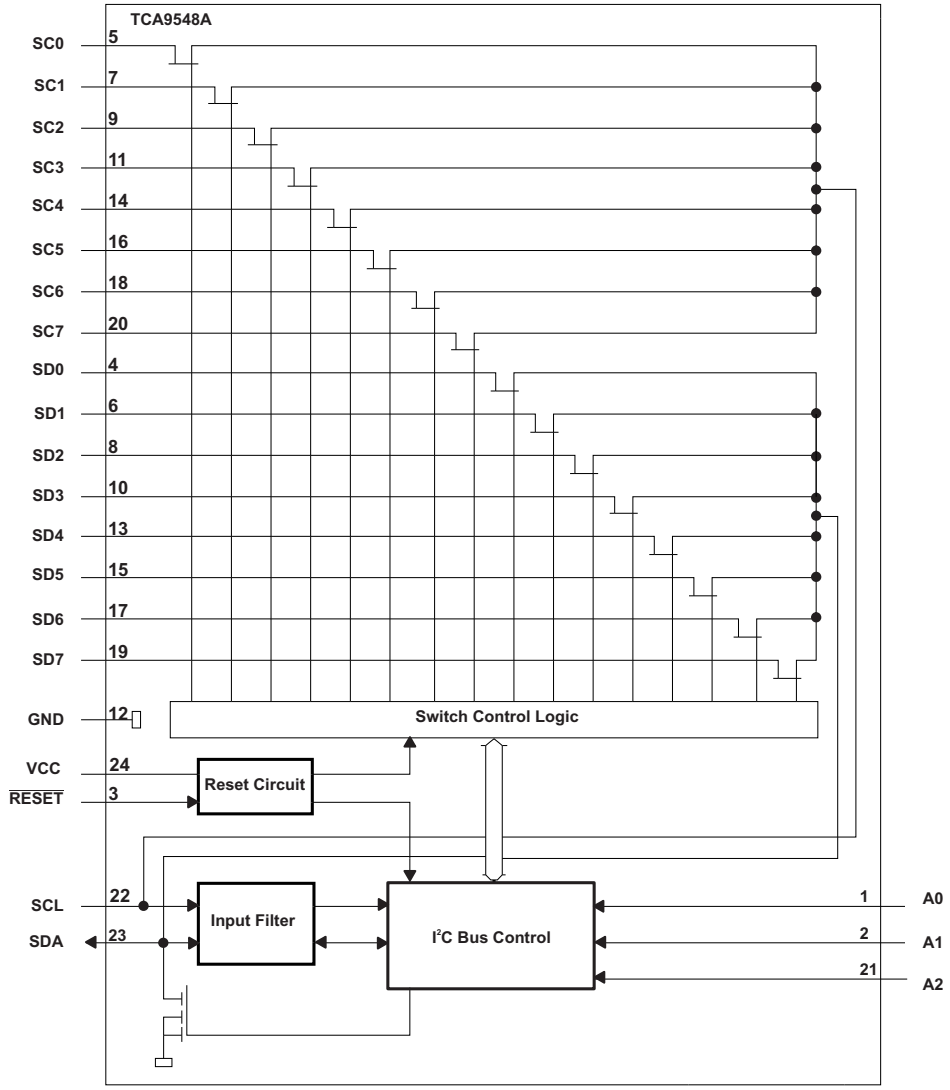

9.3 Feature Description

The TCA9548A is an 8-channel, bidirectional translating switch for I^2C buses that supports Standard-Mode (100 kHz) and Fast-Mode (400 kHz) operation. The TCA9548A features I^2C control using a single 8-bit control register in which each bit controls the enabling and disabling of one of the corresponding 8 switch channels for I^2C data flow. Depending on the application, voltage translation of the I^2C bus can also be achieved using the TCA9548A to allow 1.8-V, 2.5-V, or 3.3-V parts to communicate with 5-V parts. Additionally, in the event that communication on the I^2C bus enters a fault state, the TCA9548A can be reset to resume normal operation using the $\overline{\text{RESET}}$ pin feature or by a power-on reset which results from cycling power to the device.

9.4 Device Functional Modes

9.4.1 $\overline{\text{RESET}}$ Input

The $\overline{\text{RESET}}$ input is an active-low signal that may be used to recover from a bus-fault condition. When this signal is asserted low for a minimum of t_{WL}, the TCA9548A resets its registers and I^2C state machine and deselects all channels. The $\overline{\text{RESET}}$ input must be connected to V_{CC} through a pull-up resistor.

9.4.2 Power-On Reset

When power is applied to the VCC pin, an internal power-on reset holds the TCA9548A in a reset condition until V_{CC} has reached V_{PORR}. At this point, the reset condition is released, and the TCA9548A registers and I^2C state machine are initialized to their default states, all zeroes, causing all the channels to be deselected. Thereafter, V_{CC} must be lowered below V_{PORF} to reset the device.

9.5 Programming

9.5.1 I^2C Interface

The bidirectional I^2C bus consists of the serial clock (SCL) and serial data (SDA) lines. Both lines must be connected to a positive supply through a pull-up resistor when connected to the output stages of a device. Data transfer may be initiated only when the bus is not busy.

I^2C communication with this device is initiated by a master sending a start condition, a high-to-low transition on the SDA input/output while the SCL input is high (see Figure 7). After the start condition, the device address byte is sent, most significant bit (MSB) first, including the data direction bit (R/$\overline{\text{W}}$).

After receiving the valid address byte, this device responds with an acknowledge (ACK), a low on the SDA input/output during the high of the ACK-related clock pulse. The address inputs (A0–A2) of the slave device must not be changed between the start and the stop conditions.

On the I^2C bus, only one data bit is transferred during each clock pulse. The data on the SDA line must remain stable during the high pulse of the clock period, as changes in the data line at this time are interpreted as control commands (start or stop) (see Figure 8).

A stop condition, a low-to-high transition on the SDA input/output while the SCL input is high, is sent by the master (see Figure 7).

Any number of data bytes can be transferred from the transmitter to receiver between the start and the stop conditions. Each byte of eight bits is followed by one ACK bit. The transmitter must release the SDA line before the receiver can send an ACK bit. The device that acknowledges must pull down the SDA line during the ACK clock pulse so that the SDA line is stable low during the high pulse of the ACK-related clock period (see Figure 9). When a slave receiver is addressed, it must generate an ACK after each byte is received. Similarly, the master must generate an ACK after each byte that it receives from the slave transmitter. Setup and hold times must be met to ensure proper operation.

A master receiver signals an end of data to the slave transmitter by not generating an acknowledge (NACK) after the last byte has been clocked out of the slave. This is done by the master receiver by holding the SDA line high. In this event, the transmitter must release the data line to enable the master to generate a stop condition.

Programming (continued)

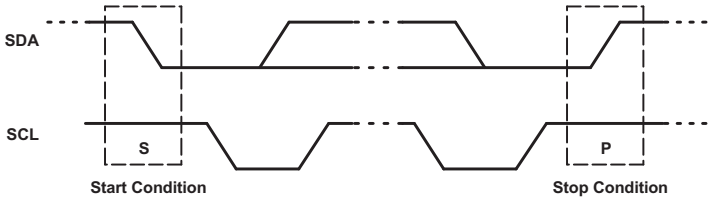

Figure 7. Definition of Start and Stop Conditions

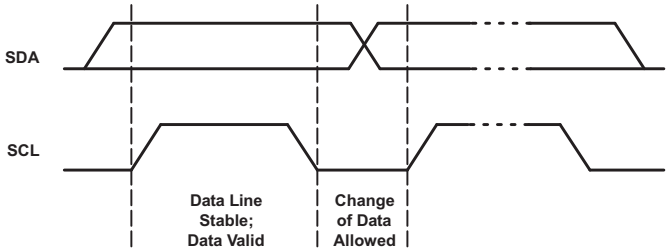

Figure 8. Bit Transfer

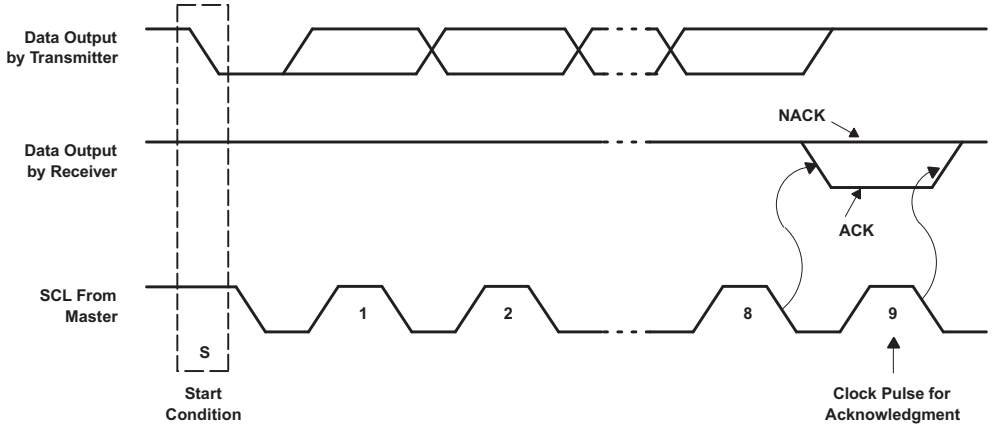

Figure 9. Acknowledgment on I^2C Bus

9.5.2 Device Address

Figure 10 shows the address byte of the TCA9548A.

Programming (continued)

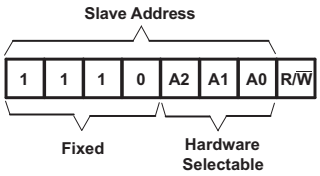

Figure 10. TCA9548A Address

The last bit of the slave address defines the operation (read or write) to be performed. When it is high (1), a read is selected, while a low (0) selects a write operation.

Table 1. Address Reference

INPUTS			I^2C BUS SLAVE ADDRESS
A2	A1	A0	
L	L	L	112 (decimal), 70 (hexadecimal)
L	L	H	113 (decimal), 71 (hexadecimal)
L	H	L	114 (decimal), 72 (hexadecimal)
L	H	H	115 (decimal), 73 (hexadecimal)
H	L	L	116 (decimal), 74 (hexadecimal)
H	L	H	117 (decimal), 75 (hexadecimal)
H	H	L	118 (decimal), 76 (hexadecimal)
H	H	H	119 (decimal), 77 (hexadecimal)

9.5.3 Control Register

Following the successful acknowledgment of the address byte, the bus master sends a command byte that is stored in the control register in the TCA9548A (see Figure 11). This register can be written and read via the I^2C bus. Each bit in the command byte corresponds to a SCn/SDn channel and a high (or 1) selects this channel. Multiple SCn/SDn channels may be selected at the same time. When a channel is selected, the channel becomes active after a stop condition has been placed on the I^2C bus. This ensures that all SCn/SDn lines are in a high state when the channel is made active, so that no false conditions are generated at the time of connection. A stop condition always must occur immediately after the acknowledge cycle. If multiple bytes are received by the TCA9548A, it saves the last byte received.

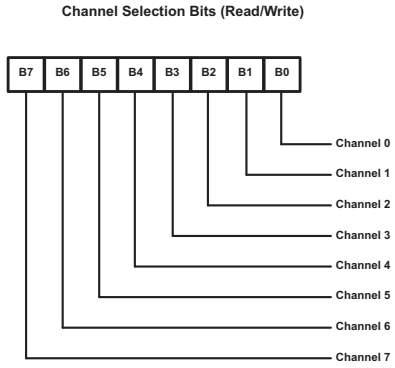

Figure 11. Control Register

Table 2. Command Byte Definition

CONTROL REGISTER BITS								COMMAND
B7	B6	B5	B4	B3	B2	B1	B0	
X	X	X	X	X	X	X	0	Channel 0 disabled
							1	Channel 0 enabled
X	X	X	X	X	X	0	X	Channel 1 disabled
						1		Channel 1 enabled
X	X	X	X	X	0	X	X	Channel 2 disabled
					1			Channel 2 enabled
X	X	X	X	0	X	X	X	Channel 3 disabled
				1				Channel 3 enabled
X	X	X	0	X	X	X	X	Channel 4 disabled
			1					Channel 4 enabled
X	X	0	X	X	X	X	X	Channel 5 disabled
		1						Channel 5 enabled
X	0	X	X	X	X	X	X	Channel 6 disabled
	1							Channel 6 enabled
0	X	X	X	X	X	X	X	Channel 7 disabled
1								Channel 7 enabled
0	0	0	0	0	0	0	0	No channel selected, power-up/reset default state

9.5.4 $\overline{\text{RESET}}$ Input

The $\overline{\text{RESET}}$ input is an active-low signal that may be used to recover from a bus-fault condition. When this signal is asserted low for a minimum of t_{WL}, the TCA9548A resets its registers and I^2C state machine and deselects all channels. The $\overline{\text{RESET}}$ input must be connected to V_{CC} through a pull-up resistor.

9.5.5 Power-On Reset

When power (from 0 V) is applied to V_{CC}, an internal power-on reset holds the TCA9548A in a reset condition until V_{CC} has reached V_{POR}. At that point, the reset condition is released and the TCA9548A registers and I^2C state machine initialize to their default states. After that, V_{CC} must be lowered to below V_{POR} and then back up to the operating voltage for a power-reset cycle.

9.5.6 Bus Transactions

Data is exchanged between the master and TCA9548A through write and read commands.

9.5.6.1 Writes

Data is transmitted to the TCA9548A by sending the device address and setting the least-significant bit (LSB) to a logic 0 (see Figure 10 for device address). The command byte is sent after the address and determines which SCn/SDn channel receives the data that follows the command byte (see Figure 12). There is no limitation on the number of data bytes sent in one write transmission.

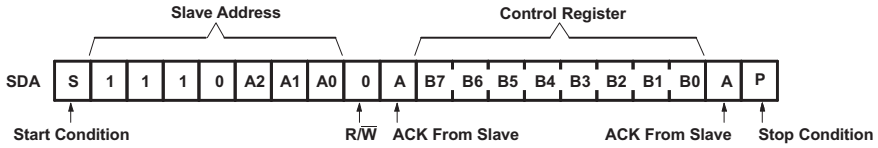

Figure 12. Write to Control Register

9.5.6.2 Reads

The bus master first must send the TCA9548A address with the LSB set to a logic 1 (see Figure 10 for device address). The command byte is sent after the address and determines which SCn/SDn channel is accessed. After a restart, the device address is sent again, but this time, the LSB is set to a logic 1. Data from the SCn/SDn channel defined by the command byte then is sent by the TCA9548A (see Figure 13). After a restart, the value of the SCn/SDn channel defined by the command byte matches the SCn/SDn channel being accessed when the restart occurred. Data is clocked into the SCn/SDn channel on the rising edge of the ACK clock pulse. There is no limitation on the number of data bytes received in one read transmission, but when the final byte is received, the bus master must not acknowledge the data.

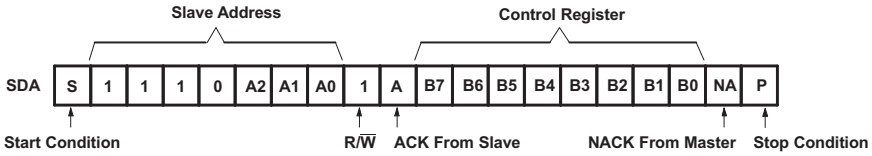

Figure 13. Read From Control Register

10 Application and Implementation

NOTE

Information in the following applications sections is not part of the TI component specification, and TI does not warrant its accuracy or completeness. TI's customers are responsible for determining suitability of components for their purposes. Customers should validate and test their design implementation to confirm system functionality.

10.1 Application Information

Applications of the TCA9548A will contain an I^2C (or SMBus) master device and up to eight I^2C slave devices. The downstream channels are ideally used to resolve I^2C slave address conflicts. For example, if eight identical digital temperature sensors are needed in the application, one sensor can be connected at each channel: 0-7. When the temperature at a specific location needs to be read, the appropriate channel can be enabled and all other channels switched off, the data can be retrieved, and the I^2C master can move on and read the next channel.

In an application where the I^2C bus will contain many additional slave devices that do not result in I^2C slave address conflicts, these slave devices can be connected to any desired channel to distribute the total bus capacitance across multiple channels. If multiple switches will be enabled simultaneously, additional design requirements must be considered (see *Design Requirements* and *Detailed Design Procedure*).

10.2 Typical Application

Figure 14 shows an application in which the TCA9548A can be used.

Typical Application (continued)

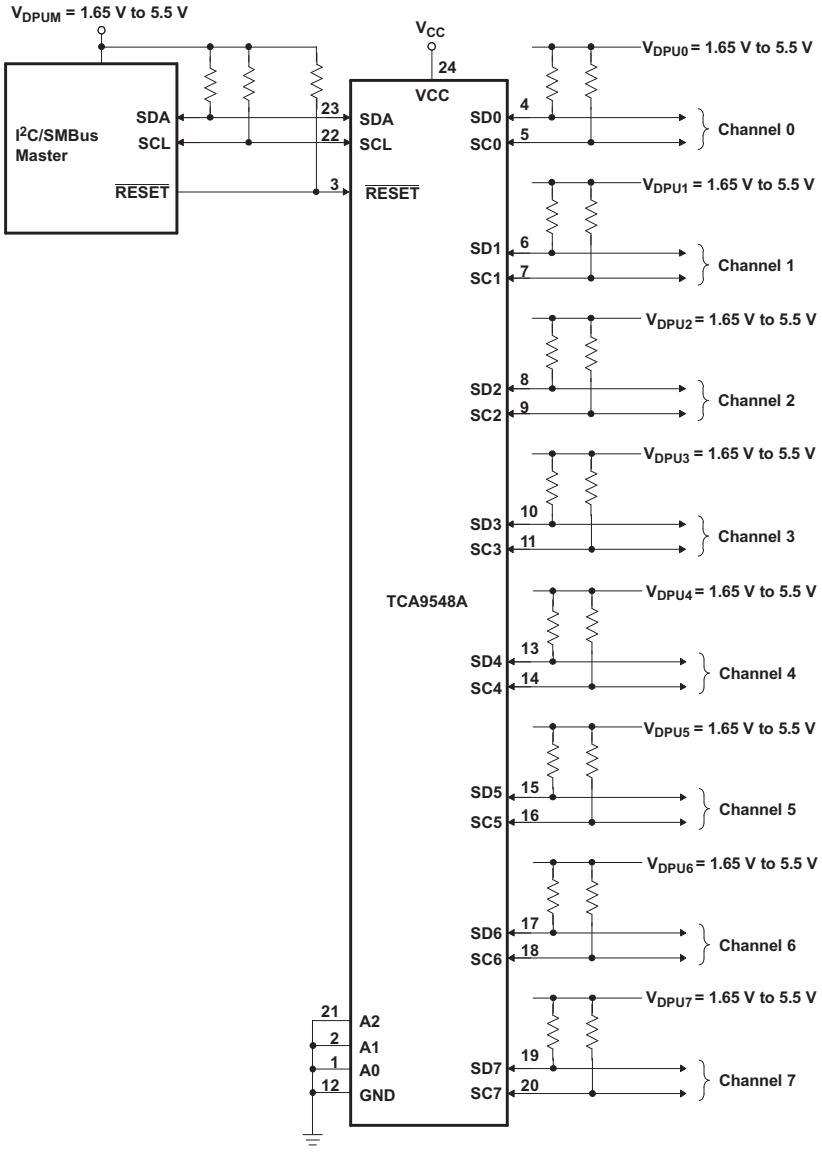

A. Pin numbers shown are for the PW package.

Figure 14. Typical Application Schematic

Typical Application (continued)

10.2.1 Design Requirements

A typical application of the TCA9548A will contain one or more data pull-up voltages, V_{DPUX}, one for the master device (V_{DPUM}) and one for each of the selectable slave channels (V_{DPU0} – V_{DPU7}). In the event where the master device and all slave devices operate at the same voltage, then V_{DPUM} = V_{DPUX} = VCC. In an application where voltage translation is necessary, additional design requirements must be considered to determine an appropriate V_{CC} voltage.

The A0, A1, and A2 pins are hardware selectable to control the slave address of the TCA9548A. These pins may be tied directly to GND or V_{CC} in the application.

If multiple slave channels will be activated simultaneously in the application, then the total I_{OL} from SCL/SDA to GND on the master side will be the sum of the currents through all pull-up resistors, R_p.

The pass-gate transistors of the TCA9548A are constructed such that the V_{CC} voltage can be used to limit the maximum voltage that is passed from one I^2C bus to another.

Figure 15 shows the voltage characteristics of the pass-gate transistors (note that the graph was generated using data specified in *Electrical Characteristics*). In order for the TCA9548A to act as a voltage translator, the V_{pass} voltage must be equal to or lower than the lowest bus voltage. For example, if the main bus is running at 5 V and the downstream buses are 3.3 V and 2.7 V, V_{pass} must be equal to or below 2.7 V to effectively clamp the downstream bus voltages. As shown in Figure 15, $V_{pass(max)}$ is 2.7 V when the TCA9548A supply voltage is 4 V or lower, so the TCA9548A supply voltage could be set to 3.3 V. Pull-up resistors then can be used to bring the bus voltages to their appropriate levels (see Figure 14).

10.2.2 Detailed Design Procedure

Once all the slaves are assigned to the appropriate slave channels and bus voltages are identified, the pull-up resistors, R_p, for each of the buses need to be selected appropriately. The minimum pull-up resistance is a function of V_{DPUX}, $V_{OL,(max)}$, and I_{OL}:

$$R_{p(min)} = \frac{V_{DPUX} - V_{OL(max)}}{I_{OL}} \quad (1)$$

The maximum pull-up resistance is a function of the maximum rise time, t_r (300 ns for fast-mode operation, f_{SCL} = 400 kHz) and bus capacitance, C_b:

$$R_{p(max)} = \frac{t_r}{0.8473 \times C_b} \quad (2)$$

The maximum bus capacitance for an I^2C bus must not exceed 400 pF for fast-mode operation. The bus capacitance can be approximated by adding the capacitance of the TCA9548A, $C_{io(OFF)}$, the capacitance of wires/connections/traces, and the capacitance of each individual slave on a given channel. If multiple channels will be activated simultaneously, each of the slaves on all channels will contribute to total bus capacitance.

Typical Application (continued)

10.2.3 Application Curves

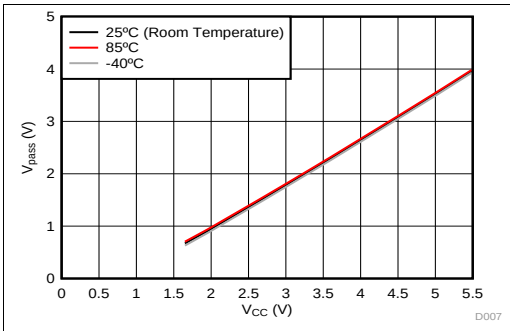

Figure 15. Pass-Gate Voltage (V_{pass}) vs Supply Voltage (V_{CC}) at Three Temperature Points

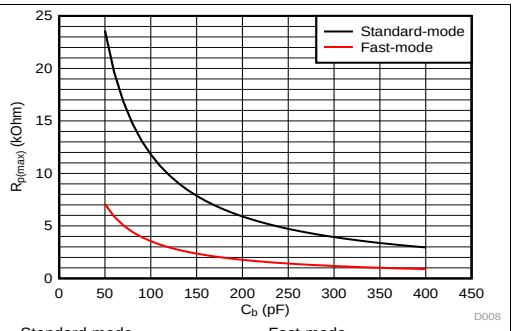

Standard-mode (f_{SCL}= 100 kHz, t_r = 1 µs)

Fast-mode (f_{SCL}= 400 kHz, t_r= 300 ns)

Figure 16. Maximum Pull-Up Resistance ($R_{p(max)}$) vs Bus Capacitance (C_b)

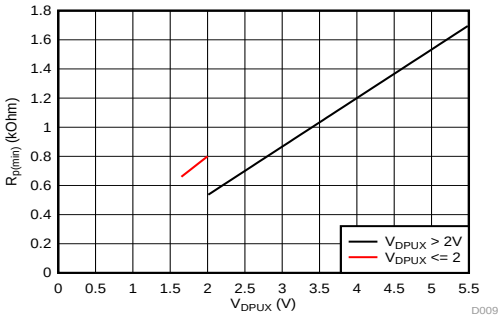

V_{OL} = 0.2*V_{DPUX}, I_{OL} = 2 mA when V_{DPUX} ≤ 2 V

V_{OL} = 0.4 V, I_{OL} = 3 mA when V_{DPUX} > 2 V

Figure 17. Minimum Pullup Resistance ($R_{p(min)}$) vs Pullup Reference Voltage (V_{DPUX})

11 Power Supply Recommendations

The operating power-supply voltage range of the TCA9548A is 1.65 V to 5.5 V applied at the VCC pin. When the TCA9548A is powered on for the first time or anytime the device must be reset by cycling the power supply, the power-on reset requirements must be followed to ensure the I^2C bus logic is initialized properly.

11.1 Power-On Reset Requirements

In the event of a glitch or data corruption, TCA9548A can be reset to its default conditions by using the power-on reset feature. Power-on reset requires that the device go through a power cycle to be completely reset. This reset also happens when the device is powered on for the first time in an application.

A power-on reset is shown in Figure 18.

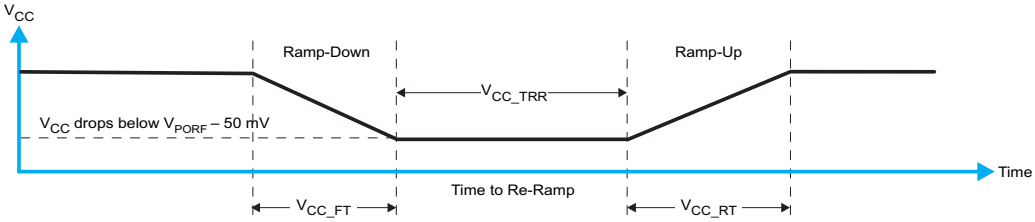

Figure 18. V_{CC} is Lowered Below the POR Threshold, Then Ramped Back Up to V_{CC}

Table 3 specifies the performance of the power-on reset feature for TCA9548A for both types of power-on reset.

Table 3. Recommended Supply Sequencing and Ramp Rates(1)

PARAMETER			MIN	TYP	MAX	UNIT
V_{CC_FT}	Fall time	See Figure 18	1		100	ms
V_{CC_RT}	Rise time	See Figure 18	0.1		100	ms
V_{CC_TRR}	Time to re-ramp (when V_{CC} drops below $V_{PORF(min)}$ – 50 mV or when V_{CC} drops to GND)	See Figure 18	40			µs
V_{CC_GH}	Level that V_{CC} can glitch down to, but not cause a functional disruption when V_{CC_GW} = 1 µs	See Figure 19			1.2	V
V_{CC_GW}	Glitch width that will not cause a functional disruption when V_{CC_GH} = 0.5 × V_{CC}	See Figure 19			10	µs

(1) All supply sequencing and ramp rate values are measured at T_A = 25°C

Glitches in the power supply can also affect the power-on reset performance of this device. The glitch width (V_{CC_GW}) and height (V_{CC_GH}) are dependent on each other. The bypass capacitance, source impedance, and device impedance are factors that affect power-on reset performance. Figure 19 and Table 3 provide more information on how to measure these specifications.

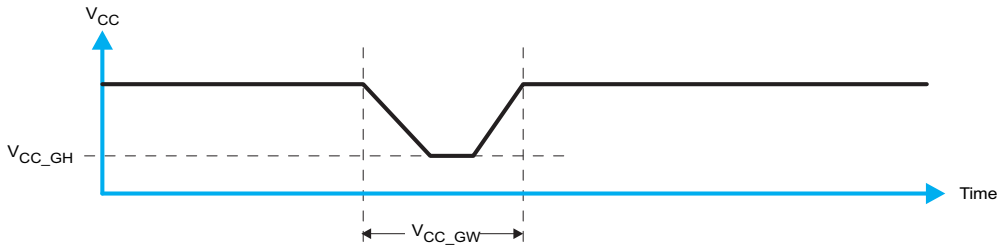

Figure 19. Glitch Width and Glitch Height

V_{POR} is critical to the power-on reset. V_{POR} is the voltage level at which the reset condition is released and all the registers and the I^2C/SMBus state machine are initialized to their default states. The value of V_{POR} differs based on the V_{CC} being lowered to or from 0. Figure 20 and Table 3 provide more details on this specification.

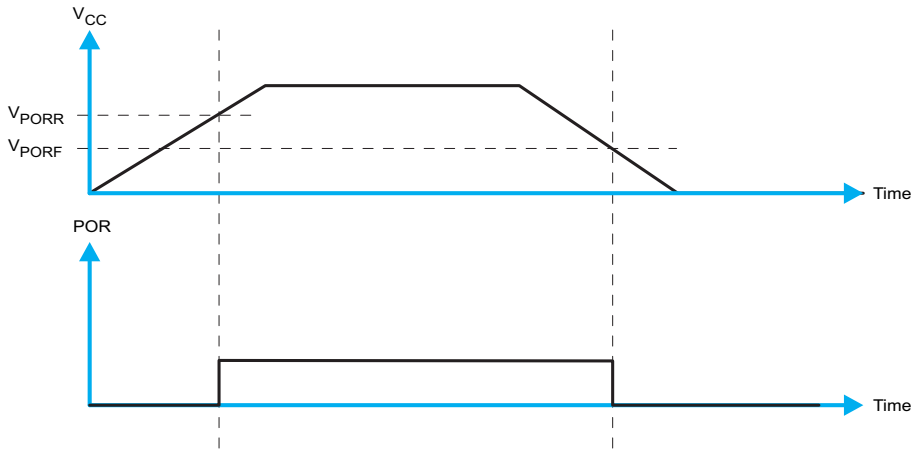

Figure 20. V_{POR}

12 Layout

12.1 Layout Guidelines

For PCB layout of the TCA9548A, common PCB layout practices should be followed but additional concerns related to high-speed data transfer such as matched impedances and differential pairs are not a concern for I^2C signal speeds. It is common to have a dedicated ground plane on an inner layer of the board and pins that are connected to ground should have a low-impedance path to the ground plane in the form of wide polygon pours and multiple vias. By-pass and de-coupling capacitors are commonly used to control the voltage on the VCC pin, using a larger capacitor to provide additional power in the event of a short power supply glitch and a smaller capacitor to filter out high-frequency ripple.

In an application where voltage translation is not required, all V_{DPUX} voltages and V_{CC} could be at the same potential and a single copper plane could connect all of pull-up resistors to the appropriate reference voltage. In an application where voltage translation is required, V_{DPUM} and V_{DPU0}-V_{DPU7}, may all be on the same layer of the board with split planes to isolate different voltage potentials.

To reduce the total I^2C bus capacitance added by PCB parasitics, data lines (SCn and SDn) should be a short as possible and the widths of the traces should also be minimized (e.g. 5-10 mils depending on copper weight).

12.2 Layout Example

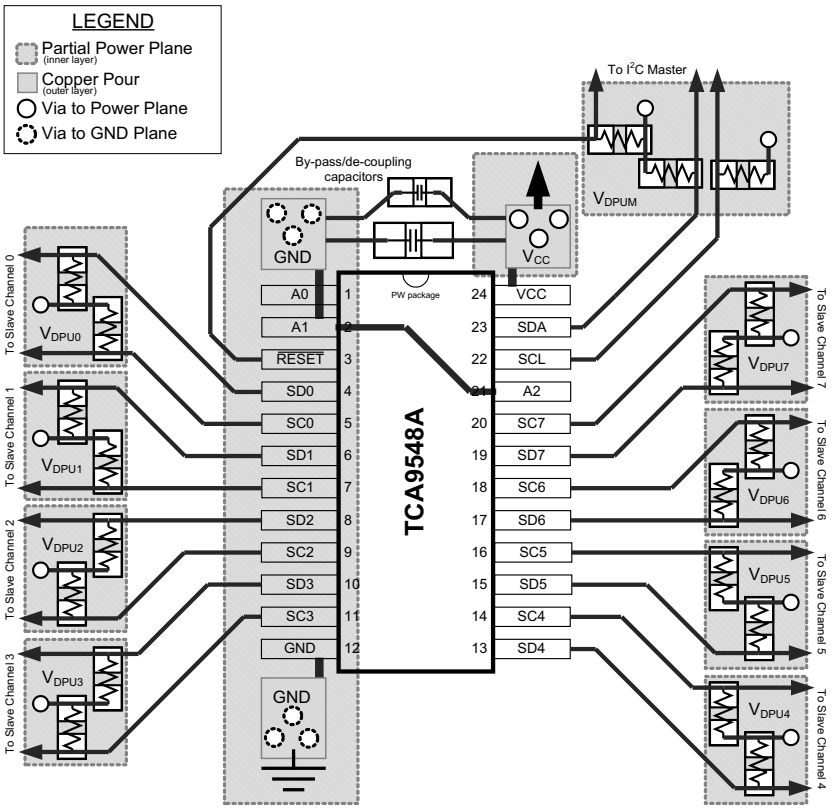

Figure 21. Layout Schematic

13 Device and Documentation Support

13.1 Trademarks

All trademarks are the property of their respective owners.

13.2 Electrostatic Discharge Caution

These devices have limited built-in ESD protection. The leads should be shorted together or the device placed in conductive foam during storage or handling to prevent electrostatic damage to the MOS gates.

13.3 Glossary

SLYZ022 — *TI Glossary*.

This glossary lists and explains terms, acronyms, and definitions.

14 Mechanical, Packaging, and Orderable Information

The following pages include mechanical, packaging, and orderable information. This information is the most current data available for the designated devices. This data is subject to change without notice and revision of this document. For browser-based versions of this data sheet, refer to the left-hand navigation.

PACKAGING INFORMATION

Orderable Device	Status (1)	Package Type	Package Drawing	Pins	Package Qty	Eco Plan (2)	Lead/Ball Finish (6)	MSL Peak Temp (3)	Op Temp (°C)	Device Marking (4/5)	Samples
TCA9548APWR	ACTIVE	TSSOP	PW	24	2000	Green (RoHS & no Sb/Br)	CU NIPDAU	Level-1-260C-UNLIM	-40 to 85	PW548A	Samples
TCA9548ARGER	ACTIVE	VQFN	RGE	24	3000	Green (RoHS & no Sb/Br)	CU NIPDAU	Level-2-260C-1 YEAR	-40 to 85	PW548A	Samples

(1) The marketing status values are defined as follows:
ACTIVE: Product device recommended for new designs.
LIFEBUY: TI has announced that the device will be discontinued, and a lifetime-buy period is in effect.
NRND: Not recommended for new designs. Device is in production to support existing customers, but TI does not recommend using this part in a new design.
PREVIEW: Device has been announced but is not in production. Samples may or may not be available.
OBSOLETE: TI has discontinued the production of the device.

(2) Eco Plan - The planned eco-friendly classification: Pb-Free (RoHS), Pb-Free (RoHS Exempt), or Green (RoHS & no Sb/Br) - please check http://www.ti.com/productcontent for the latest availability information and additional product content details.
TBD: The Pb-Free/Green conversion plan has not been defined.
Pb-Free (RoHS): TI's terms "Lead-Free" or "Pb-Free" mean semiconductor products that are compatible with the current RoHS requirements for all 6 substances, including the requirement that lead not exceed 0.1% by weight in homogeneous materials. Where designed to be soldered at high temperatures, TI Pb-Free products are suitable for use in specified lead-free processes.
Pb-Free (RoHS Exempt): This component has a RoHS exemption for either 1) lead-based flip-chip solder bumps used between the die and package, or 2) lead-based die adhesive used between the die and leadframe. The component is otherwise considered Pb-Free (RoHS compatible) as defined above.
Green (RoHS & no Sb/Br): TI defines "Green" to mean Pb-Free (RoHS compatible), and free of Bromine (Br) and Antimony (Sb) based flame retardants (Br or Sb do not exceed 0.1% by weight in homogeneous material)

(3) MSL, Peak Temp. - The Moisture Sensitivity Level rating according to the JEDEC industry standard classifications, and peak solder temperature.

(4) There may be additional marking, which relates to the logo, the lot trace code information, or the environmental category on the device.

(5) Multiple Device Markings will be inside parentheses. Only one Device Marking contained in parentheses and separated by a "~" will appear on a device. If a line is indented then it is a continuation of the previous line and the two combined represent the entire Device Marking for that device.

(6) Lead/Ball Finish - Orderable Devices may have multiple material finish options. Finish options are separated by a vertical ruled line. Lead/Ball Finish values may wrap to two lines if the finish value exceeds the maximum column width.

In no event shall TI's liability arising out of such information exceed the total purchase price of the TI part(s) at issue in this document sold by TI to Customer on an annual basis.

TAPE AND REEL INFORMATION

REEL DIMENSIONS

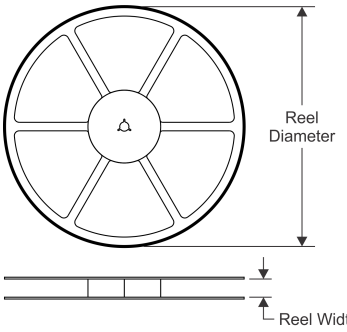

TAPE DIMENSIONS

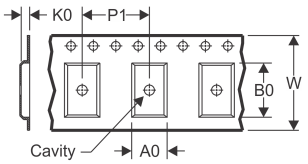

A0	Dimension designed to accommodate the component width
B0	Dimension designed to accommodate the component length
K0	Dimension designed to accommodate the component thickness
W	Overall width of the carrier tape
P1	Pitch between successive cavity centers

QUADRANT ASSIGNMENTS FOR PIN 1 ORIENTATION IN TAPE

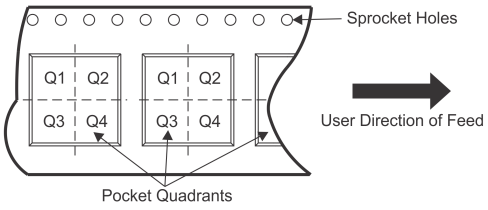

*All dimensions are nominal

Device	Package Type	Package Drawing	Pins	SPQ	Reel Diameter (mm)	Reel Width W1 (mm)	A0 (mm)	B0 (mm)	K0 (mm)	P1 (mm)	W (mm)	Pin1 Quadrant
TCA9548ARGER	VQFN	RGE	24	3000	330.0	12.4	4.25	4.25	1.15	8.0	12.0	Q2

TAPE AND REEL BOX DIMENSIONS

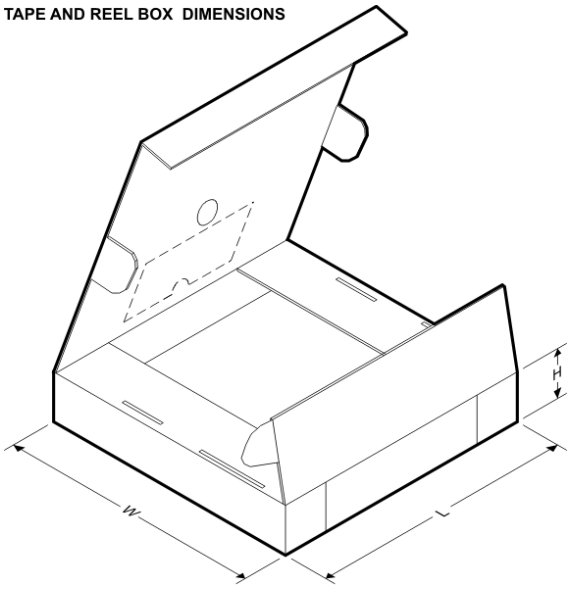

*All dimensions are nominal

Device	Package Type	Package Drawing	Pins	SPQ	Length (mm)	Width (mm)	Height (mm)
TCA9548ARGER	VQFN	RGE	24	3000	367.0	367.0	35.0

PW (R–PDSO–G24) PLASTIC SMALL OUTLINE

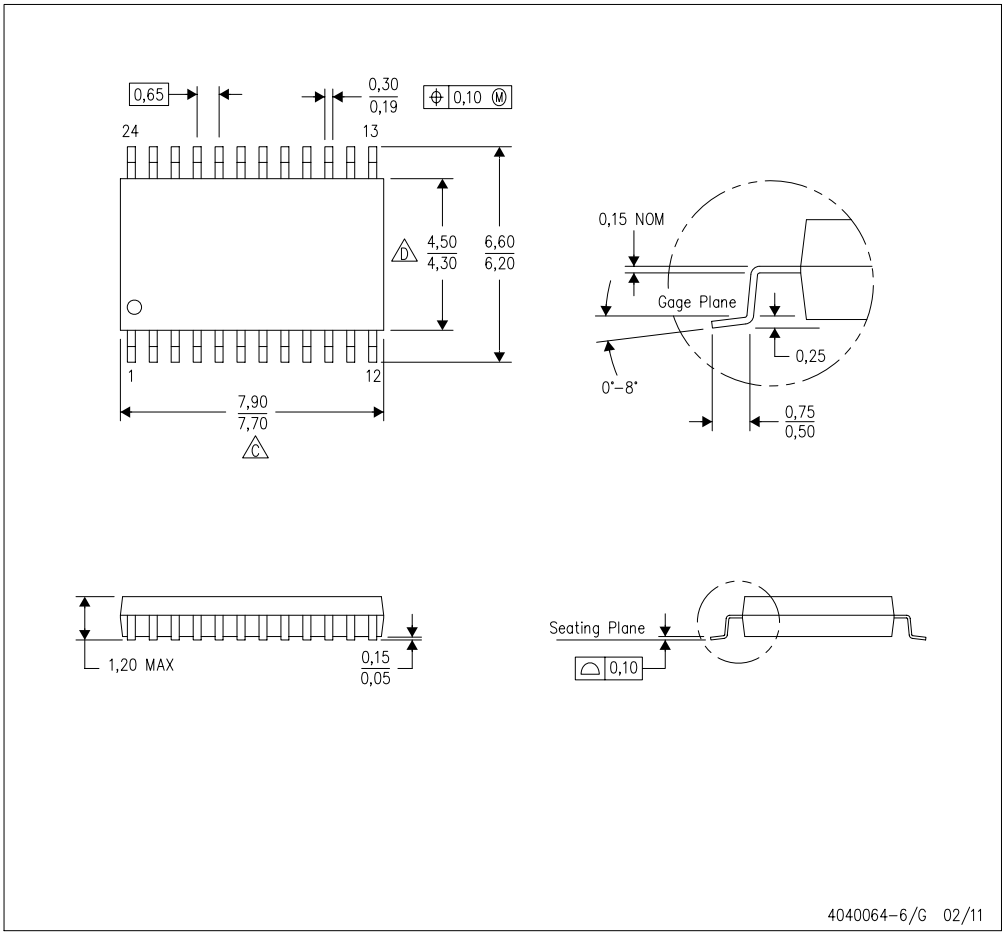

NOTES:
A. All linear dimensions are in millimeters. Dimensioning and tolerancing per ASME Y14.5M–1994.
B. This drawing is subject to change without notice.
C. Body length does not include mold flash, protrusions, or gate burrs. Mold flash, protrusions, or gate burrs shall not exceed 0,15 each side.
D. Body width does not include interlead flash. Interlead flash shall not exceed 0,25 each side.
E. Falls within JEDEC MO–153

PW (R–PDSO–G24) PLASTIC SMALL OUTLINE

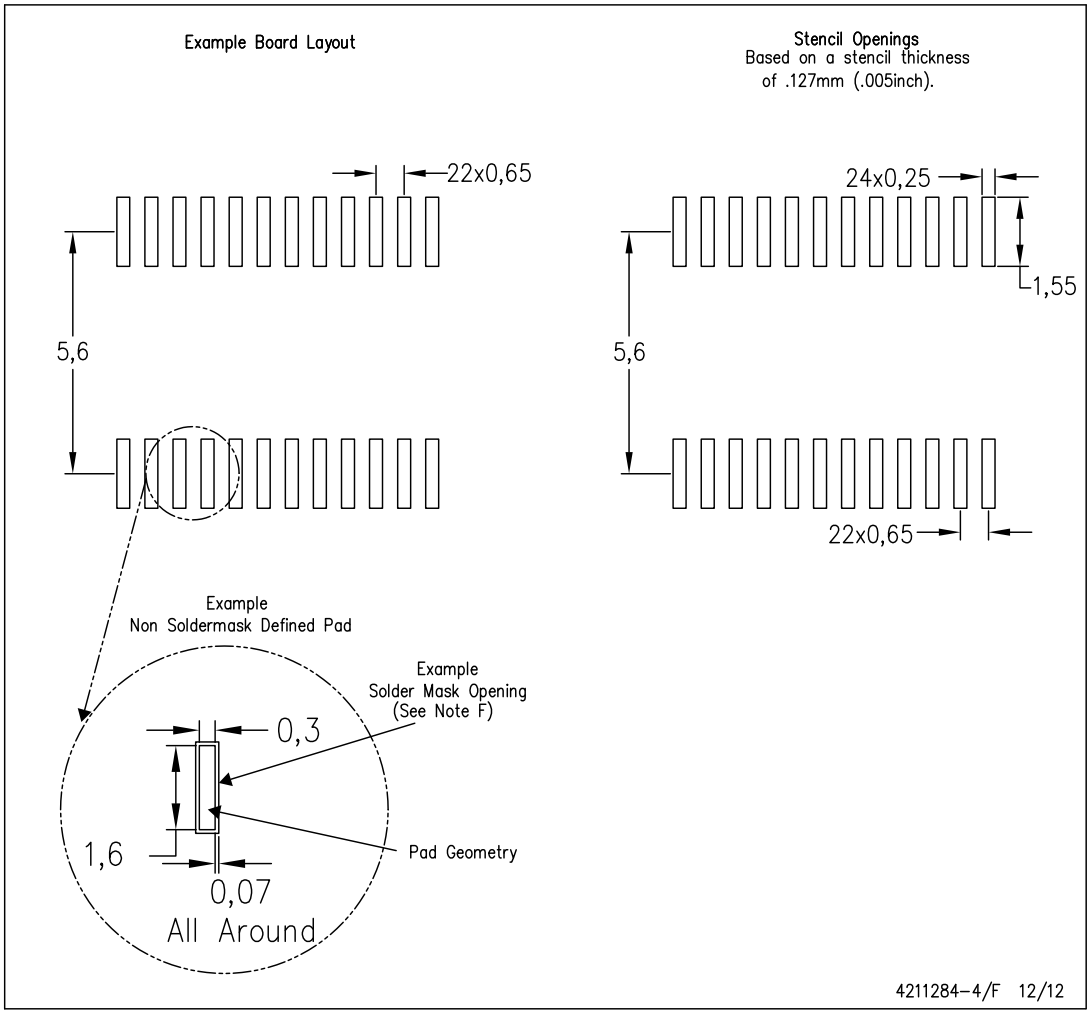

NOTES:
A. All linear dimensions are in millimeters.
B. This drawing is subject to change without notice.
C. Publication IPC–7351 is recommended for alternate design.
D. Laser cutting apertures with trapezoidal walls and also rounding corners will offer better paste release. Customers should contact their board assembly site for stencil design recommendations. Refer to IPC–7525 for other stencil recommendations.
E. Customers should contact their board fabrication site for solder mask tolerances between and around signal pads.

RGE (S–PVQFN–N24) PLASTIC QUAD FLATPACK NO–LEAD

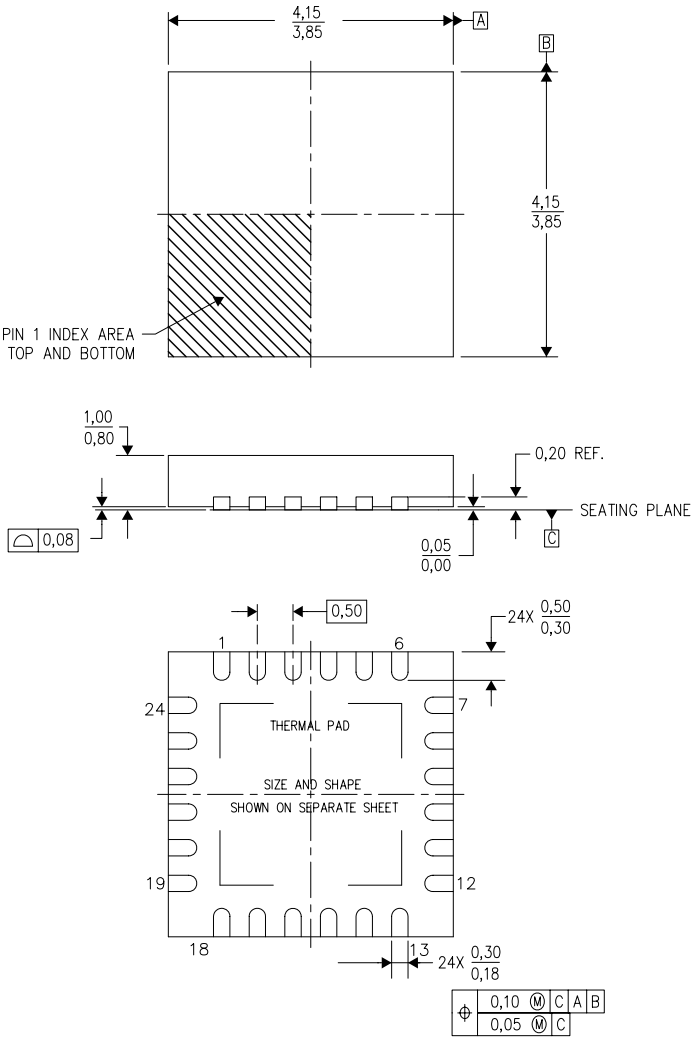

NOTES:
A. All linear dimensions are in millimeters. Dimensioning and tolerancing per ASME Y14.5M–1994.
B. This drawing is subject to change without notice.
C. Quad Flatpack, No–Leads (QFN) package configuration.
D. The package thermal pad must be soldered to the board for thermal and mechanical performance.
E. See the additional figure in the Product Data Sheet for details regarding the exposed thermal pad features and dimensions.
F. Falls within JEDEC MO–220.

RGE (S–PVQFN–N24) PLASTIC QUAD FLATPACK NO–LEAD

THERMAL INFORMATION

This package incorporates an exposed thermal pad that is designed to be attached directly to an external heatsink. The thermal pad must be soldered directly to the printed circuit board (PCB). After soldering, the PCB can be used as a heatsink. In addition, through the use of thermal vias, the thermal pad can be attached directly to the appropriate copper plane shown in the electrical schematic for the device, or alternatively, can be attached to a special heatsink structure designed into the PCB. This design optimizes the heat transfer from the integrated circuit (IC).

For information on the Quad Flatpack No–Lead (QFN) package and its advantages, refer to Application Report, QFN/SON PCB Attachment, Texas Instruments Literature No. SLUA271. This document is available at www.ti.com.

The exposed thermal pad dimensions for this package are shown in the following illustration.

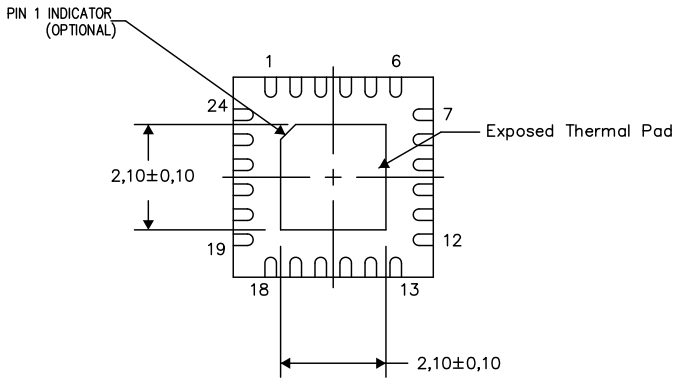

Bottom View

Exposed Thermal Pad Dimensions

4206344–6/AH 08/14

NOTES: A. All linear dimensions are in millimeters

RGE (S–PVQFN–N24) PLASTIC QUAD FLATPACK NO–LEAD

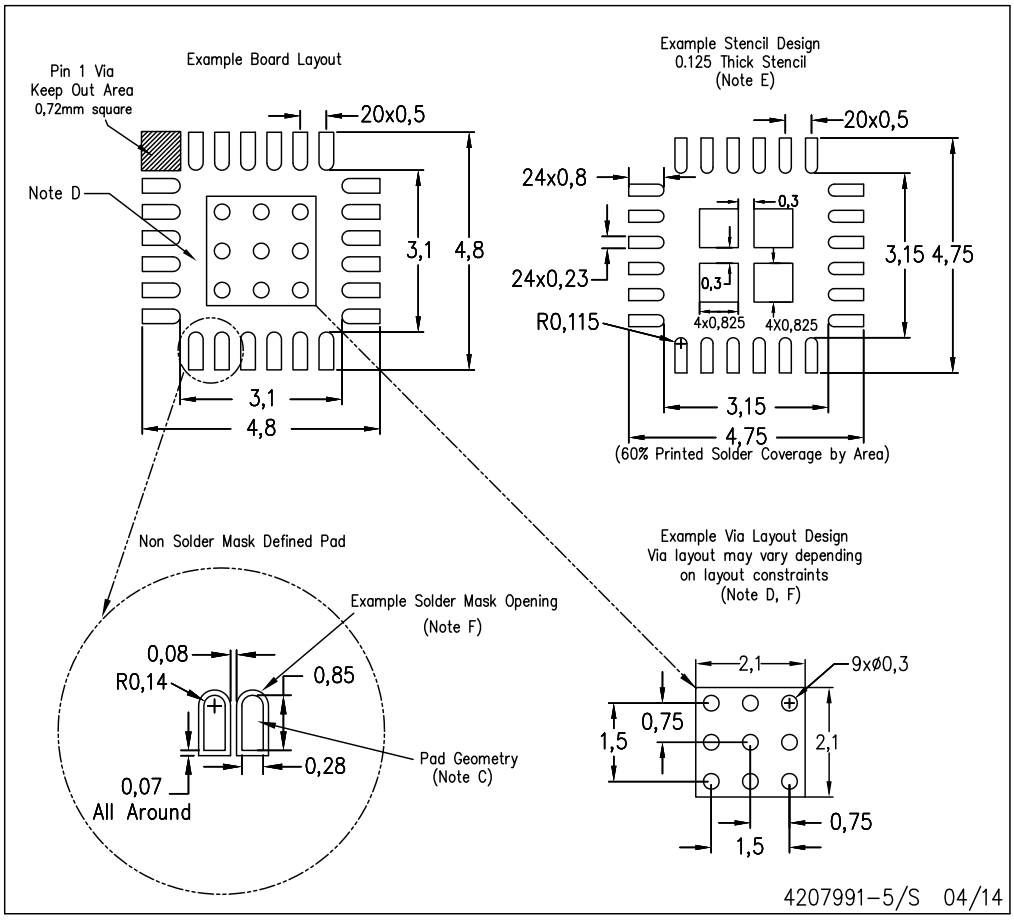

NOTES:
A. All linear dimensions are in millimeters.
B. This drawing is subject to change without notice.
C. Publication IPC–7351 is recommended for alternate designs.
D. This package is designed to be soldered to a thermal pad on the board. Refer to Application Note, Quad Flat–Pack Packages, Texas Instruments Literature No. SLUA271, and also the Product Data Sheets for specific thermal information, via requirements, and recommended board layout. These documents are available at www.ti.com <http://www.ti.com>.
E. Laser cutting apertures with trapezoidal walls and also rounding corners will offer better paste release. Customers should contact their board assembly site for stencil design recommendations. Refer to IPC 7525 for stencil design considerations.
F. Customers should contact their board fabrication site for recommended solder mask tolerances and via tenting recommendations for vias placed in the thermal pad.

IMPORTANT NOTICE

Texas Instruments Incorporated and its subsidiaries (TI) reserve the right to make corrections, enhancements, improvements and other changes to its semiconductor products and services per JESD46, latest issue, and to discontinue any product or service per JESD48, latest issue. Buyers should obtain the latest relevant information before placing orders and should verify that such information is current and complete. All semiconductor products (also referred to herein as “components”) are sold subject to TI’s terms and conditions of sale supplied at the time of order acknowledgment.

TI warrants performance of its components to the specifications applicable at the time of sale, in accordance with the warranty in TI’s terms and conditions of sale of semiconductor products. Testing and other quality control techniques are used to the extent TI deems necessary to support this warranty. Except where mandated by applicable law, testing of all parameters of each component is not necessarily performed.

TI assumes no liability for applications assistance or the design of Buyers’ products. Buyers are responsible for their products and applications using TI components. To minimize the risks associated with Buyers’ products and applications, Buyers should provide adequate design and operating safeguards.

TI does not warrant or represent that any license, either express or implied, is granted under any patent right, copyright, mask work right, or other intellectual property right relating to any combination, machine, or process in which TI components or services are used. Information published by TI regarding third-party products or services does not constitute a license to use such products or services or a warranty or endorsement thereof. Use of such information may require a license from a third party under the patents or other intellectual property of the third party, or a license from TI under the patents or other intellectual property of TI.

Reproduction of significant portions of TI information in TI data books or data sheets is permissible only if reproduction is without alteration and is accompanied by all associated warranties, conditions, limitations, and notices. TI is not responsible or liable for such altered documentation. Information of third parties may be subject to additional restrictions.

Resale of TI components or services with statements different from or beyond the parameters stated by TI for that component or service voids all express and any implied warranties for the associated TI component or service and is an unfair and deceptive business practice. TI is not responsible or liable for any such statements.

Buyer acknowledges and agrees that it is solely responsible for compliance with all legal, regulatory and safety-related requirements concerning its products, and any use of TI components in its applications, notwithstanding any applications-related information or support that may be provided by TI. Buyer represents and agrees that it has all the necessary expertise to create and implement safeguards which anticipate dangerous consequences of failures, monitor failures and their consequences, lessen the likelihood of failures that might cause harm and take appropriate remedial actions. Buyer will fully indemnify TI and its representatives against any damages arising out of the use of any TI components in safety-critical applications.

In some cases, TI components may be promoted specifically to facilitate safety-related applications. With such components, TI’s goal is to help enable customers to design and create their own end-product solutions that meet applicable functional safety standards and requirements. Nonetheless, such components are subject to these terms.

No TI components are authorized for use in FDA Class III (or similar life-critical medical equipment) unless authorized officers of the parties have executed a special agreement specifically governing such use.

Only those TI components which TI has specifically designated as military grade or “enhanced plastic” are designed and intended for use in military/aerospace applications or environments. Buyer acknowledges and agrees that any military or aerospace use of TI components which have ***not*** been so designated is solely at the Buyer's risk, and that Buyer is solely responsible for compliance with all legal and regulatory requirements in connection with such use.

TI has specifically designated certain components as meeting ISO/TS16949 requirements, mainly for automotive use. In any case of use of non-designated products, TI will not be responsible for any failure to meet ISO/TS16949.

Products		**Applications**	
Audio	www.ti.com/audio	Automotive and Transportation	www.ti.com/automotive
Amplifiers	amplifier.ti.com	Communications and Telecom	www.ti.com/communications
Data Converters	dataconverter.ti.com	Computers and Peripherals	www.ti.com/computers
DLP® Products	www.dlp.com	Consumer Electronics	www.ti.com/consumer-apps
DSP	dsp.ti.com	Energy and Lighting	www.ti.com/energy
Clocks and Timers	www.ti.com/clocks	Industrial	www.ti.com/industrial
Interface	interface.ti.com	Medical	www.ti.com/medical
Logic	logic.ti.com	Security	www.ti.com/security
Power Mgmt	power.ti.com	Space, Avionics and Defense	www.ti.com/space-avionics-defense
Microcontrollers	microcontroller.ti.com	Video and Imaging	www.ti.com/video
RFID	www.ti-rfid.com		
OMAP Applications Processors	www.ti.com/omap	**TI E2E Community**	e2e.ti.com
Wireless Connectivity	www.ti.com/wirelessconnectivity		

Mailing Address: Texas Instruments, Post Office Box 655303, Dallas, Texas 75265

VELOCIMETER

Vector - 300 m

Sample 3D velocity at up to 64 Hz for small-scale research in coastal areas

The Vector is a high-accuracy single-point current meter that is capable of acquiring 3D velocity in a very small volume at rates up to 64 Hz. It is widely used for sediment transport applications, small-scale turbulence measurements and coastal engineering studies. It has an excellent track record of delivering outstanding data quality in a variety of applications. This version is suitable for use down to a depth of 300 m. The Vector's titanium version is suitable for investigating deep- water currents.

VELOCIMETER

Vector - 300 m

Highlights

- ✓ Small-scale turbulence
- ✓ Sampling up to 64 Hz
- ✓ Small sampling volume for measurements close to boundaries

Applications

- ✓ Wave orbital studies
- ✓ Studies of bottom boundary layers
- ✓ Ocean engineering projects
- ✓ Coastal studies
- ✓ River turbulence
- ✓ Low flow measurements
- ✓ Flux measurements

VELOCIMETER

Vector - 300 m

Technical specifications

⟶ Water velocity measurements	
Maximum profiling range	N/A
Distance from probe	0.15 m
Sampling volume diameter	15 mm
Sampling volume height (user-selectable)	5-20 mm
Cell size	N/A
Velocity range	±0.01, 0.1, 0.3, 1, 2, 4, 7 m/s (software-selectable)
Adaptive ping interval	N/A
Accuracy	±0.5% of measured value ±1 mm/s
Velocity precision	typ. 1% of velocity range (at 16 Hz)
Sampling rate (output)	1-64 Hz
Internal sampling rate	100-250 Hz
⟶ Distance measurements	
Minimum range	N/A
Maximum range	N/A
Cell size	N/A
Accuracy	N/A
Sampling rate	N/A
⟶ Echo intensity	
Acoustic frequency	6 MHz
Resolution	0.45 dB
Dynamic range	90 dB
⟶ Sensors	
Temperature:	Thermistor embedded in end bell
Temp. range	-4 to +40 °C

VELOCIMETER

Vector - 300 m

⟶ Sensors	
Temp. accuracy/resolution	0.1 °C/0.01 °C
Temp. time response	10 min
Compass:	Magnetometer
Accuracy/resolution	2º/0.1º for tilt < 20°
Tilt:	Liquid level
Accuracy/resolution	0.2°/0.1°
Maximum tilt	30°
Up or Down	Automatic detect
Pressure:	Piezoresistive
Standard range	0-20 m (inquire for options)
Accuracy/precision	0.5% FS / Better than 0.005% of full scale
⟶ Analog inputs	
No. of channels	2
Supply voltage to analog output devices	Three options selectable through firmware commands:1) Battery voltage/500 mA, 2) +5 V/250 mA, 3) +12 V/100 mA
⟶ Data recording	
Capacity (standard):	9 MB, can add 4/16 GB
Data record (Standard)	24 bytes at sampling rate + 28 bytes/second
Data record (IMU)	72 bytes at sampling rate
⟶ Real-time clock	
Accuracy	±1 min/year
Backup in absence of power	4 weeks
⟶ Data communications	
I/O	RS-232 or RS-422
Communication baud rate	300-115 200 Bd
Recorder download baud rate	600/1200 kBd for both RS-232 and RS-422

VELOCIMETER

Vector - 300 m

⟶ Data communications	
User control	Handled via ”Vector” software, ActiveX® function calls, or direct commands.
Analog outputs	3 channels standard, one for each velocity component or two velocities and pressure.
Output range	0–5 V, scaling is user-selectable.
Synchronization	TTL (5V tolerant) sync in/sync out, start on sync, sample on sync
⟶ Connectors	
Bulkhead (Impulse)	MCBH-8-FS
Cable	PMCIL-8-MP on 10 m polyurethane cable
⟶ Software	
Functions	Deployment planning, instrument configuration, data retrieval and conversion (for Windows®).
⟶ Multi unit operation	
Software	N/A
I/O	N/A
⟶ Power	
DC input	9-15V DC
Maximum peak current	3 A
Max. consumption	1.5 W at 64 Hz
Typical consumption, 4 Hz	0.6 - 1 W
Sleep consumption	< 100 µA
Transmit power	2 adjustable levels
⟶ Batteries	
Battery capacity	50 Wh (alkaline or Li-ion),165 Wh (lithium), single or dual
New battery voltage	13.5 V DC (alkaline)
Data collection capacity	Refer to planning section in software

VELOCIMETER

Vector - 300 m

→ Environmental	
Operating temperature	-4 to +40 °C

VELOCIMETER

Vector - 300 m

⟶ Environmental	
Storage temperature	-20 to +60 °C
Shock and vibration	IEC 721-3-2
Depth rating	300m
⟶ Materials	
Standard model	POM housing, titanium probe and fasteners
⟶ Dimensions	
Maximum diameter	75 mm
Maximum length	468 mm (housing only), 246 mm (fixed stem) add 110 mm for double battery
⟶ Weight	
No batteries	Weight in air: 2.32 kg, in water: buoyant
2 batteries	Weight in air: 3.20 kg, in water: 0.54 kg
⟶ Options	
Probe mounted on fixed stem or on 2 m cable	
Vertical or horizontal probes	
Alkaline, lithium or Li-ion external batteries	
IMU - Inertial Measurement Unit	